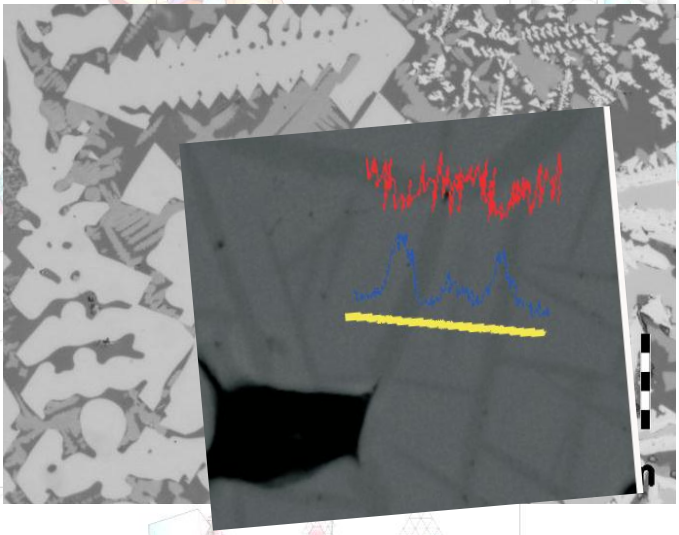

The Effect of Minor Oxide Components on Reduction of Iron Ore Agglomerates

Timo Paananen

Doctoral Thesis

University of Oulu

Department of Process and Environmental Engineering

Laboratorio of Process Metallurgy

DOCTORAL THESIS

The Effect of Minor Oxide Components on Reduction of Iron Ore Agglomerates

Timo Paananen

Laboratory of Process Metallurgy

The Department of Process and Environmental Engineering

University of Oulu

ACADEMIC DISSERTATION

to be presented with the assent of the Faculty of Technology, University of Oulu, for public discussion in Auditorium L10 on Linnanmaa on February 8th, 2013, at 12:00

Principal supervisor

Prof. Timo Fabritius, University of Oulu, Finland

Supervisor

PhD Kyösti Heinänen, Raahe, Finland

Pre-examiners

PhD Lena Sundqvist, Swerea MEFOS, Sweden

PhD Andrey Karasev, KTH Stockholm, Sweden

Opponent

Prof. Lauri Holappa, Aalto University, Espoo, Finland

ISBN 978-952-93-1814-8 (nid.)

ISBN 978-952-93-1815-5 (PDF)

Printed by Erweko Oy

OULU 2013

PREFACE

The research collected for this thesis started in 2001 in the laboratory of Process Metallurgy at the University of Oulu. I started the research work regarding this thesis while working for one year on a project named "Reduction of Iron Oxides" which was funded by Academy of Finland. When the project ended, I had an opportunity to continue part time research work as a research engineer for Corporate R&D at Rautaruukki Oyj on a fixed-term contract for another year. In the beginning of 2003, research work was temporarily interrupted until June 2003, when I received a position as an assistant in the laboratory of process metallurgy at the University of Oulu. Teaching while participating in an industrial project promoted the work and allowed me to continue my research at the same time. Stara Project (Stabilized hot metal production, 2005 – 2007) funded by the Finnish Funding Agency for Technology and Innovation (TEKES) and Rautaruukki Oyj gave an extra push to publish research results in international publications and to continue my PhD studies. Furthermore, financial support in the form of a personal scholarship from the Finnish Foundation for Technology Promotion (TES) prompted the writing of my doctoral thesis. I completed all post graduate courses and made experimental research during I worked in the laboratory of process metallurgy. However, publication of the planned supplements was incomplete. A new job as a development engineer in Rautaruukki Oyj, Ruukki production as of February 2008 demanded a lot of extra effort and after that preparation of my theses proceeded slowly, but

proceed it did with the encouragement of Rautaruukki – as long as the main work was not too much disturbed. I would like to thank Rautaruukki Oyj, TEKES, TES and Academy of Finland for their financial support during my post graduate studies.

I think the most important and crucial point in gaining PhD and completing the thesis has been the continuous encouragement and spurring by my supervisor PhD Kyösti Heinänen. I highly appreciate him for giving motivation for research work and providing excellent advice and co-operation for over 10 years. I acknowledge Professor Jouko Härkki who encouraged me to start my postgraduate studies, gave me an opportunity to do research work and to learn process metallurgy by teaching a number of courses. For professor Timo Fabritius I am grateful for his valuable advice, spurring and excellent guidance during the writing of this thesis. Pre-examiners PhD Lena Sundqvist and PhD Andrey Karasev are acknowledged for their valuable comments and advice during my pre-examination work.

I would like to thank my many colleagues for clarifying, stimulating and supportive discussions when I was working at the University of Oulu. Especially the scientific value-added discussions I have had with Pekka Tanskanen on mineralogy and Olli Mattila on a variety of natural science topics. In addition to discussions with Eetu Heikkinen on teaching co-operation and his advice on thermodynamics and PhD Jyrki Heino at "the school of life" on industrial ecology, many practical issues concerning co-

operation with industry, teaching and the preparation of doctoral thesis. I want to thank Esa Virtanen for teaching of argumentation in number of interesting discussions. Commonly I wish to express thanks to everybody in the laboratory of Process Metallurgy worked with me between 2000 - 2008. I would like to express my special thanks to Kimmo Kinnunen for excellent co-operation when I was working at the University of Oulu and later as a colleague in Rautaruukki Oyj. Also the colleagues who worked or are presently working in my team and who encouraged me to complete my studies, Rauno Hurme, Miika Sihvonen, Tuija Nevalainen, Rita Kallio, Riku Kanniala and Kari Helelä, I would like to thank them all warmly. My superiors at Rautaruukki, Juha Heikkinen and Jarmo Lilja I would like to thank for their positive attitude to the preparation of my doctoral thesis.

I would also like to thank technicians Jouko Virkkala, Jarmo Murto and Jorma Penttinen and M.Sc.Tech. Matti Nauha for their technical, mechanical and experiment-related support of my work. I would like to give special thanks to Tommi Kokkonen and Riku Mattila for unselfish and diligent work at all times when I was processing the experimental part of the research in the laboratory of process metallurgy. They both always had the means to convert many impossible things to possible ones. The analysis was a very important part of the research. My sincerest thanks are due to Olli Taikina-Aho for his advice on operating the XRD and SEM analysis equipment at the University of Oulu as well as Juha Kovalainen, Kari Kastelli and Anja Maaninka for the same work as well as the excellent preparation of samples

and polished sections at Rautaruukki. I would also thank Johanna Vielma for careful proofreading of my thesis.

Finally, I would like to warmly thank my parents, brothers and sisters and in-laws for spurring and supporting me to complete my PhD degree. I wish to express special thanks to my children and especially to my wife, Ansku, who has encouraged and spurred me on all these years and arranged time to concentrate on PhD studies and the preparation of this thesis. Her support and encouragement has been the most important and effective motivator for going ahead and achieving my goal.

ABSTRACT

The major part of iron in the world is produced using a blast furnace process. The blast furnace process refers to a shaft furnace in which agglomerated iron ore and coke are charged alternately from the top and blast air with additional carbon containing injection material is blown from numerous tuyeres on the lower level of the furnace.

Agglomerated iron ore charge material undergoes high mechanical, thermal and chemical stress in the blast furnace. Stress factors affect simultaneously when iron ore burden material is reduced, warmed up and been subject to pressure affected by high and heavy burden from above with particle flow erosion. In spite of all the stress factors and in order to have high permeability in the charged bed, iron ore burden material should remain unbroken until softened and melted down on a cohesive zone. The higher the reduction degree of iron oxides in burden achieved before the cohesive zone, the more efficient and energy efficient is the blast furnace operation.

In this research, the focus is on the impurities analyzed in the phases in the burden materials with measured content. The minor oxide components, such as CaO, MnO, MgO, and especially TiO_2 and Al_2O_3, were studied in this thesis. TiO_2 and Al_2O_3 were chosen because the correlation with reducibility and reduction strength was discussed but not explained. The aim of the research was to find the phenomena behind the degrading of the burden

material during reduction reactions. The aim of the thorough analysis of the laboratory scale reduction and oxidation tests was to deepen the understanding of the reduction disintegration phenomenon. Especially the effect of the impurity element or minor oxide component solid solution in iron oxides on expansion/shrinking of the crystal lattice was studied in this thesis. The main attention was focused on crystal and lattice boundaries.

According to the results, impurity elements dissolved in iron oxide lattice structure can have a considerable effect on the reduction rate of iron oxides and reduction strength of iron burden material of the blast furnace. They have also a clear effect on the oxidation rate and degree of iron oxides during the sintering process. Minor oxide components in solid solution with iron oxides have an effect on the lattice volume of the iron oxides. Volumetric (or dimensional) expansion or shrinking of lattices in proportion to one another can generate high tensile forces on the grain boundary of hematite-magnetite or magnetite-wüsite. The phenomenon has a substantial effect on the momentary strength and the reducibility of the iron burden material in the blast furnace process.

Keywords: Blast furnace, iron oxide, hematite, magnetite wüstite, impurity element, crystal lattice, TiO_2, Al_2O_3, MgO, MnO, CaO

SUPPLEMENTS

The present thesis is based on the following supplements:

Supplement 1:

Paananen T, Heinänen K & Härkki J: Degradation of Iron Oxide Caused by Alumina during Reduction from Magnetite, ISIJ International, 43(2003)5, pp. 597 - 605.

Supplement 2:

Paananen, T: Effect of Impurity Element on Reduction Behaviour of Magnetite, Steel research international, 78(2007)2, pp. 91 - 95.

Supplement 3:

Paananen, T & Kinnunen K: The Effect of Titanium on Reduction Degradation of Iron Ore Agglomerates, In proceedings: Iron Ore Conference 2007, Perth, WA, 20.-22.8.2007, pp. 361 - 368.

Supplement 4:

Paananen T, Heikkinen E-P, Kokkonen, T & Kinnunen K: Preparation of mono-, di and hemicalcium ferrite phases via melt for the reduction kinetics investigations, Steel research international, 80(2009)6, pp. 402 - 407. (Presented also in Scanmet III conference, 2008)

Supplement 5:

Paananen, T & Kinnunen, K: Effect of TiO2-content on Reduction of Iron Ore Agglomerates, Steel research international, 80(2009)6, pp. 408 - 414. (Presented also in Scanmet III conference, 2008)

Supplement 6:

Tanskanen P, Kinnunen K & Paananen T: Significant mineralogical differences between basic test and production iron ore sinters with equal chemical composition, In proceedings: VIII International conference on Molten slags fluxes and salts, 18.-21.1.2009 Santiago, Chile, pp. 947 - 956.

The contributions by the author to the different supplements of the thesis:

Supplement 1:

Main part of literature survey, main part in definition of research problem, experimental work, major part of writing

Supplement 2:

Main part of literature survey, main part in definition of research problem, major part of experimental work, writing

Supplement 3:

Part of literature survey, part in definition of research problem, laboratory scale experimental work, part of writing, presentation in conference (Iron ore conference, Austalia, Perth 2007)

Supplement 4:

Main part of literature survey, main part in definition of research problem, part of experimental work, part of writing, part of presentation preparation (SCANMET III, international conference, Luleå 2008)

Supplement 5:

Part of literature survey, main part in definition of research problem, laboratory scale experimental work, part of writing, presentation in conference (SCANMET III, international conference, Luleå 2008)

Supplement 6:

Part of literature survey, part in definition of research problem, part of experimental work, minor part of writing

TABLE OF CONTENTS

ABBREVIATIONS

ARUL	Advanced reduction test under load
B_2	Slag bacisity (CaO/SiO_2)
DR_{INT}	Reduction rate between 800 - 900 °C (%/min), (ARUL-test)
EDS	Energy dispersive spectrometer
LOM	Light optical microscope
LTB	Low temperature break down
LTD	Low temperature disintegration
R_{EXT}	Reduction extend at 1000 °C (ARUL-test)
RDI	Reduction degradation index
RUL	Reduction test under load
SEM	Scanning electron microscope
TDP_{20}	Temperature at the stage when pressure drop over the test burden is 20 mbar (ARUL-test)
TGA	Thermo gravimetric analyzer
TI	Tumble index
TK_{50}	Temperature at the stage when test burden has been compressed 50 % (ARUL-test)
XRD	X-ray diffraction
XRF	X-ray fluorescence
HOSIM	A dynamic reduction test - (blast furnace simulation test) where the sample is reduced to the endpoint of gas–reduction in a furnace

Burghard test	Metallurgical test developed to investigate softening and melting of iron burden materials under load during reduction
SFCA	Silico-ferrite of calcium and aluminium

1 INTRODUCTION

The major part of iron in the world is produced using a blast furnace process. The blast furnace process refers to a shaft furnace in which agglomerated iron ore and coke are charged alternately from the top and blast air with additional carbon containing injection material are blown from numerous tuyeres on the lower level of the furnace. Oxygen in blast air reacts with carbon originated from coke and the injection material producing reduction gas includes CO and H_2. Reaction gas flows through the material bed reducing iron oxides and warming up the burden material. Whilst the burden material descends, it is warmed up, reduced to metallic iron, and melt down. Melt hot metal and slag are tapped out regularly via a drilled hole located in the wall near the bottom of the furnace.

In order to have stabile operation and effective reduction in the process, sufficient permeability is essential in the blast furnace shaft. Thus the grain size of burden material, charged from the top of the blast furnace, has to be coarse enough to enable gas flow through the bed. However, the major part of iron ores as well as coking coals have to be ground to fines for enrichment and therefore have to be agglomerated before charging to the blast furnace. The coking process is used as an agglomeration method for the coal and sintering process for iron ore fines. Iron fines can also be pelletized before the sintering process. Use of sinter or pellets as a single iron burden material

is possible, but mostly they are used as a mixture. Also lumpy iron ore is used mainly as an additive to the iron burden material.

The burden material has to endure high mechanical, thermal and chemical stress in the blast furnace. Stress factors affect simultaneously when iron ore burden material is reduced, warmed up and been subject to pressure affected by a high and heavy burden above with particle flow erosion. In spite of the stress and in order to have high permeability in the charged bed, the iron ore burden material should remain unbroken until it is softened and melted down on cohesive zone. The higher the reduction degree of iron oxides in the burden is achieved before the cohesive zone the more efficient and energy efficient is the blast furnace operation.

In order to guarantee the quality of iron ore agglomerates various standardized tests and indexes have been developed for testing reducibility (reducibility index RI), cold strength (crushing strength test[1], tumbler index TI[2]), reduction strength (reduction degradation index RDI, low temperature degradation index LTD[3, 4]) and softening and melting properties (Burghard test, Reduction under load test RUL) of iron ore agglomerates. The optimal iron ore agglomerate has a good reducibility, sufficient cold and low temperature reduction strength and it begins to melt at a high temperature. Crystal structure and the formed phase association are essential parts of the factor to achieve good properties in iron ore agglomerate[5]. Also the chemical composition of each phase, even as a minor content, can have a remarkable

effect on the properties, especially in reduction or reduction strength. The high quality of iron ore agglomerates enables high and efficient operation of the blast furnace, in other words, high oxygen enrichment of the blast and a high injection rate of the additive reducing agent.

High injection rate (oil/pulverized coal) increases the significance of reduction strength due to a decrease in the coke rate. In order to improve blast furnace efficiency, i.e. high productivity or low consumption of the reducing agent, reduction strength of the burden material is emphasized. Practical experiments show that improvement in the reduction degradation property of sinter enables higher oil injection rate, higher productivity and lower consumption of reducing agents [6, 7, 8].

Although correlation of different impurities on RDI and LTD index is well-known, the phenomena behind the correlation, however, have not been discussed in many papers. The purpose of this study is to examine the individual crystal phase of the burden material with certain impurities under the conditions corresponding to the cooling stage of the sintering process as well as those corresponding to the blast furnace shaft. The research focuses on the impurities analyzed from the phases in the burden material with measured content. The aim of the research is to find the phenomena which are degrading the burden material during reduction reactions. The minor components of CaO, MnO, MgO, and especially TiO_2 and Al_2O_3 are discussed in this thesis.

The aim of the thorough analysis of the test sinters and laboratory scale reduction and oxidation tests was to deepen the understanding of the reduction disintegration phenomenon.

2 BACKGROUND

2.1 Iron oxides properties

Iron cation exists as two different valences (Fe^{2+}, Fe^{3+}) in oxides forming three different iron oxides, i.e. hematite, magnetite and wüstite in descending order of oxidation. Stoichiometric compositions in weight percentages as well as the non-stoichiometry of each iron oxide is presented in Figure 1. In addition to hematite, Fe_2O_3 has also another crystalline form called maghemite (γ-Fe_2O_3), but that form is very unstable[9].

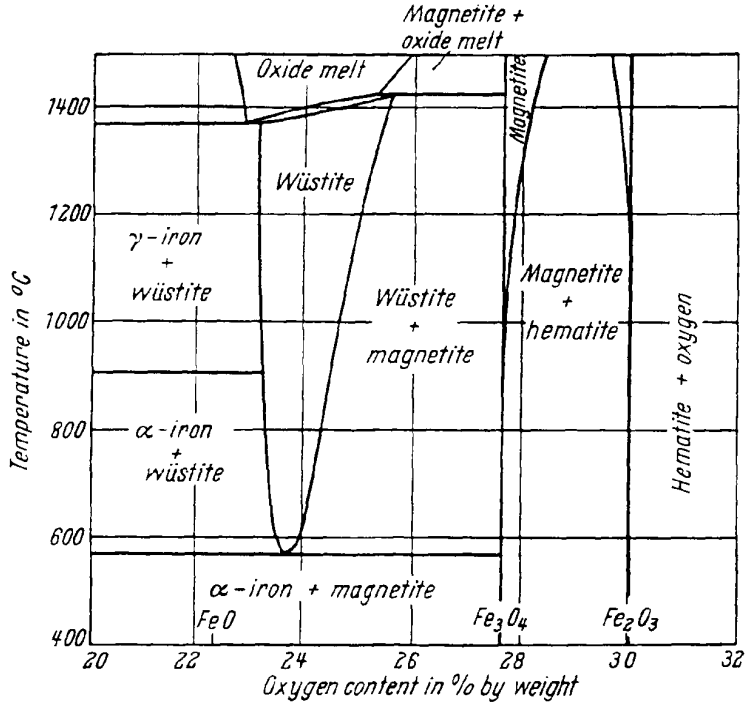

Figure 1. Fe-O phase diagram[10].

Because of a considerable difference in oxygen and iron ions (Figure 2), iron oxides consist of a crystal lattice formed by oxygen anions in which iron cations are located in octahedral or tetrahedral cells. Each iron oxide has its characteristic structure of crystal lattice as presented in chapters 2.1.1 - 2.1.3.

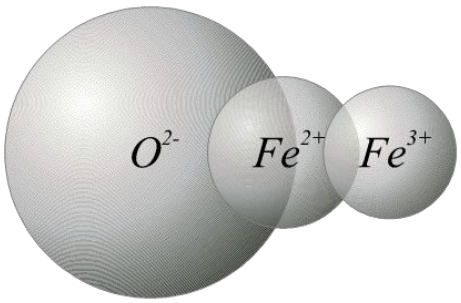

Figure 2. Oxygen anion and iron cations in relative sizes O^{2-} 0,136 nm, Fe^{2+} 0,078 nm and Fe^{3+} 0,065 nm. The illustration is based on Klein et al[11].

2.1.1 Hematite

Hematite (Fe_2O_3) rhombohedral structure is based on hexagonally stacked close-packing series of oxygen anions (ABAB...) in which trivalent iron cations are located in the middle of octahedrons in stoichiometric hematite (Figure 3)[11, 12, 13]. The non-stoichiometry of hematite typically exists as a lack of anions, when charging equilibrium is compensated with divalent instead of trivalent iron cations.

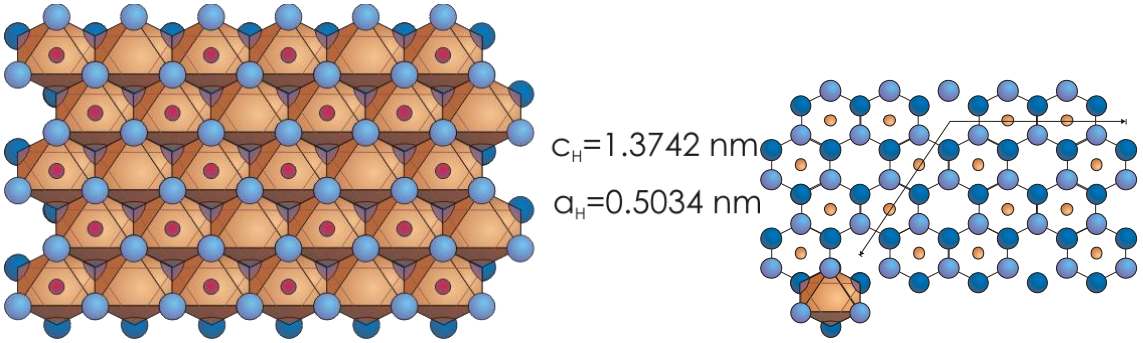

Figure 3. Structure of stoichiometric hematite in which two sequential layers (AB…) of oxygen anions are presented as blue spheres. Red spheres represent iron cations in the octahedron. The illustration is based on Klein et al[11].

2.1.2 Magnetite

Magnetite ($FeO{\cdot}Fe_2O_3$) is a mineral of cubic crystal system and it belongs to a group of spinel sturcture minerals. Magnetite consists of three different layers of oxygen anions (ABCABC…) in which iron exists as divalent and trivalent cations in oxygen forming a tetrahedron and octahedron with respectively (Figure 4) [11,12]. Stoichiometric magnetite consists of 2/3 of trivalent cations and 1/3 of divalent cations. Non-stoichiometry typically

exists as a lack of cations when charge balance is compensated with extra trivalent cations.

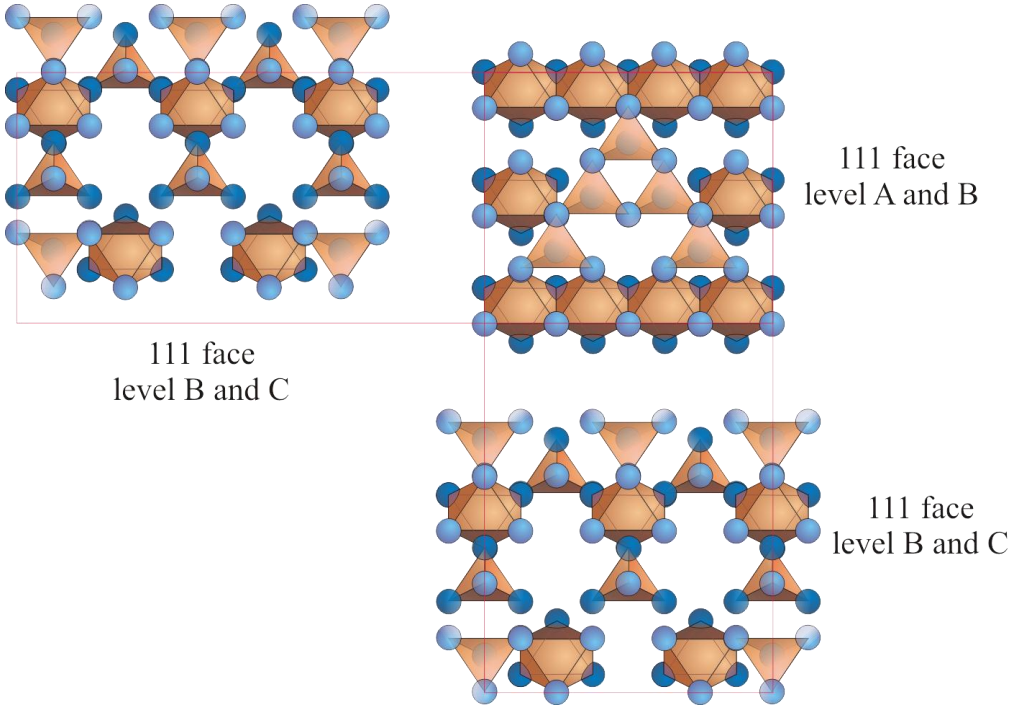

Figure 4. Magnetite levels presented on 111 face in which blue spheres are oxygen cations and the placement of iron cations Fe^{2+} and Fe^{3+} are presented as tetrahedrons and octahedrons respectively. The illustration is based on Klein et al[11, 12].

2.1.3 Wüstite

Wüstite has also a cubic crystal structure in which oxygen anions locate in a formation of the face centred cupic and iron cations are in the middle of the formed octahedron in the stoichiometric structure (Figure 5). Non-stoichiometry exists as a lack of cations resulting in a pair of Fe^{3+}-cations per every cation vacancy. Fe^{3+}-cations are located in the middle of the tetrahedron.

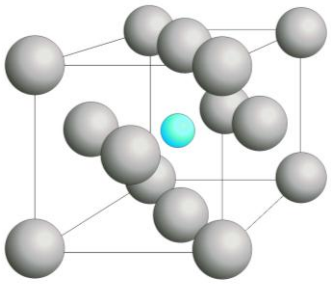

Figure 5. Crystal lattice of stoichiometric wüstite. The illustration is based on Waychunas[9].

2.2 Reduction thermodynamic of iron oxides

Equilibrium diagram with stability area under different H_2/H_2O and CO/CO_2 gas conditions for iron oxides is presented in Figure 6. Gasification of carbon in accordance with the Boudouard reaction

$$CO_2\,(g) + C(s) \Leftrightarrow 2\,CO\,(g) \qquad \text{(Eq. 1)}$$

is presented as a curve in the same illustration. The curve indicates the equilibrium limit in which solid carbon formation from CO gas as well as gasification of carbon are possible. In all presented CO/CO_2 gas atmospheres, the partial pressure of oxygen (p_{O2}) is so low that hematite is not stabile under those conditions.

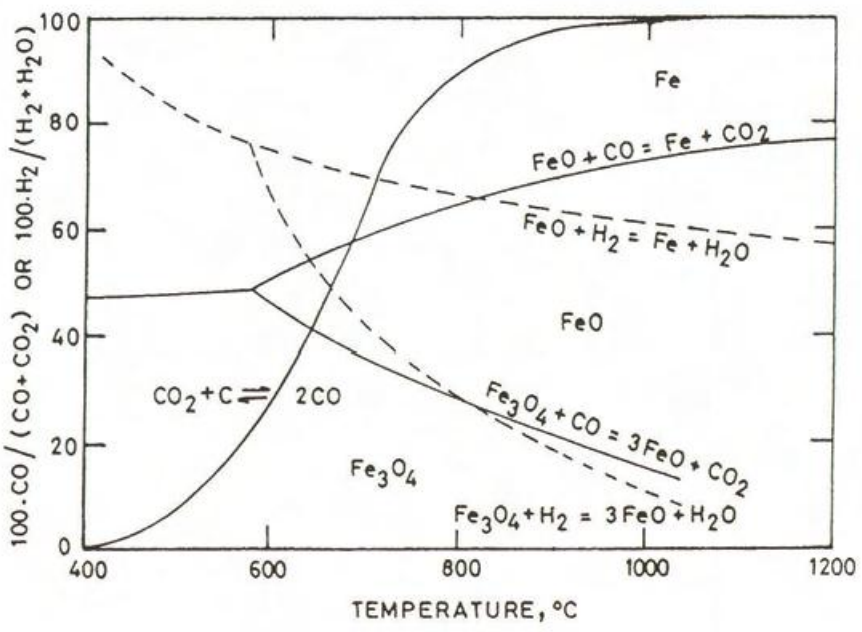

Figure 6. Equilibrium curves of Fe-O with H_2/H_2O and CO/CO_2-gas connected with the Boudouard curve.[14]

Impurity elements in solid solution with iron oxides change stability of iron oxides (Figure 7).

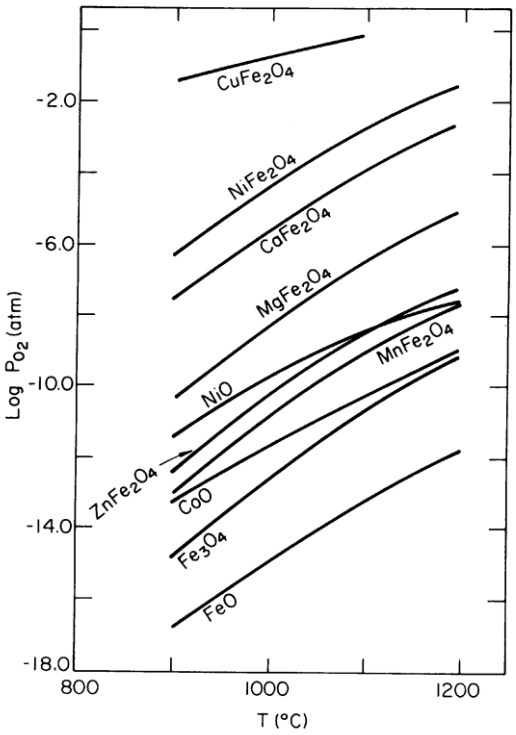

Figure 7. Effect of impurities on stability of iron oxides. [15]

2.3 Reduction of iron oxides

Gaseous reduction of iron oxides can be presented in CO/CO_2 and H_2/H_2O atmospheres as the following reactions (Eq. 2-7):

$$3Fe_2O_3 + CO \Leftrightarrow 2Fe_3O_4 + CO_2 \quad \textbf{(Eq. 2)}$$

$$3Fe_2O_3 + H_2 \Leftrightarrow 2Fe_3O_4 + H_2O \quad \textbf{(Eq. 3)}$$

$$Fe_3O_4 + CO \Leftrightarrow 3FeO + CO_2 \quad (T > 570°C) \quad \textbf{(Eq. 4)}$$

$$Fe_3O_4 + H_2 \Leftrightarrow 3FeO + H_2O \quad (T > 570°C) \quad \textbf{(Eq. 5)}$$

$$FeO + CO \Leftrightarrow Fe + CO_2 \quad (T > 570°C) \quad \textbf{(Eq. 6)}$$

$$FeO + H_2 \Leftrightarrow Fe + H_2O \quad (T > 570°C) \quad \textbf{(Eq. 7)}$$

As a consequence, wüstite is unstable below 570 °C magnetite reaction

straight to iron exists below 570 °C as presented in following reactions (Eq. 8-9):

$$Fe_3O_4 + 4CO \Leftrightarrow 3Fe + 4CO_2 \quad (T < 570°C) \quad \textbf{(Eq. 8)}$$

$$Fe_3O_4 + 4H_2 \Leftrightarrow 3Fe + 4H_2O \quad (T < 570°C) \quad \textbf{(Eq. 9)}$$

2.4 Compatibility of iron oxide lattice surfaces

In order to an iron oxide to reduce to another iron oxide, a new phase has to form on the surface of the host oxide with its characteristic lattice structure. The formation favours a certain face of the host phase and orientation in proportion to host phase (Figure 8). Compatibility depends on the lattice structures and size of the host and the oxide formed.

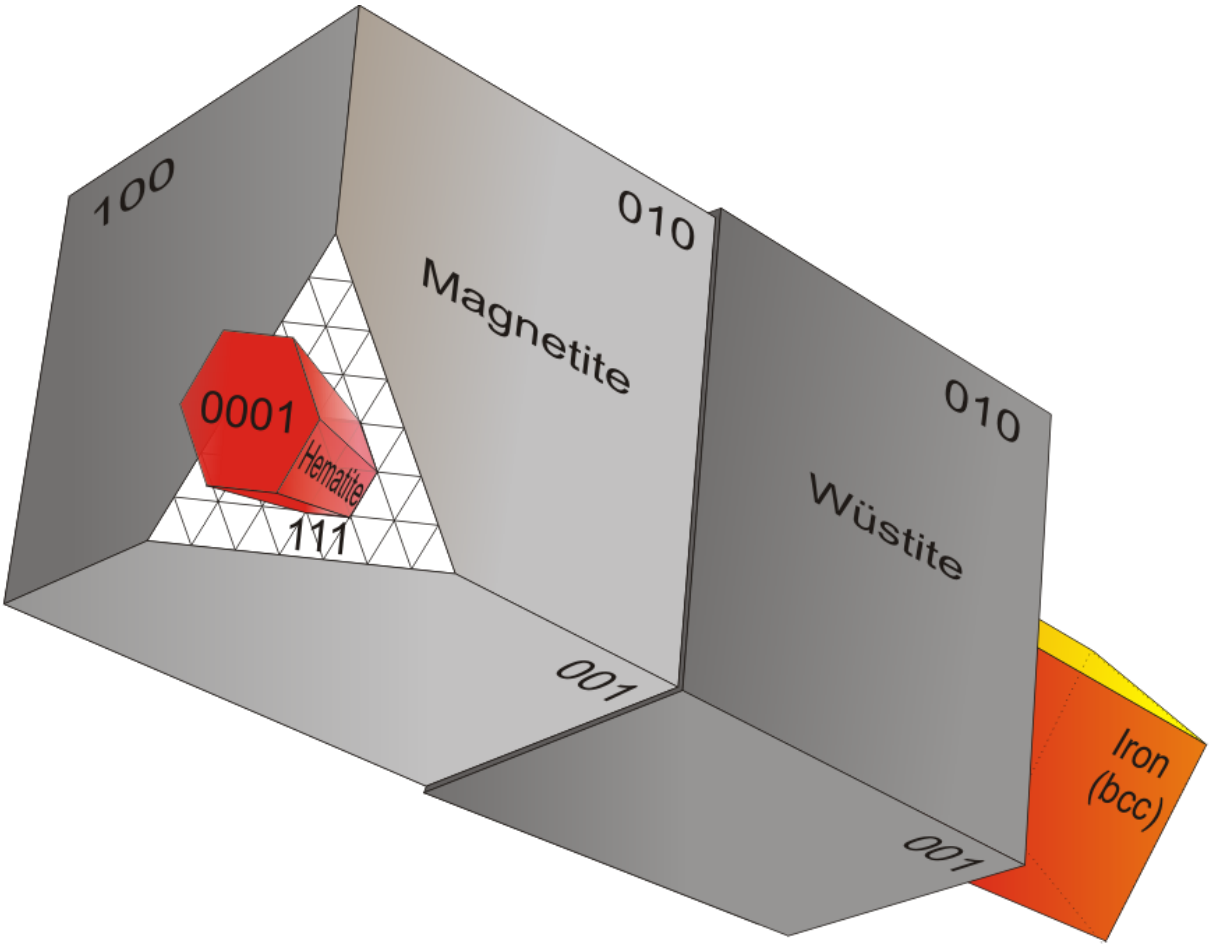

Figure 8. Schematic illustration of the favourable orientation of iron oxides. The calculated lattice volumes of wüstite and magnetite are in right proportions in the illustration.

Epitaxy of hematite and magnetite during reduction is, according to previous publications, as presented in the Figure 8, in which the surface 111 of the formed magnetite is parallel with the 0001 surface of hematite. Goodness of fit as well as volumetric difference between hematite and magnetite is schematically presented in Figure 9. The volumetric shrinking of lattices from hematite to magnetite is discussed[16], but the two dimensional (surface area in the boundary) expansion in orientation of surface is about 40 %.

Expansion during the reduction is stated to be caused only by porous formation taking place simultaneously with lattice shrinking[21], but the comparison of contact surfaces with each other on the phase boundary results in expansion (Figure 9). This is proposed to be the main cause for swelling in the phase transformation from hematite to magnetite.

The orientation of magnetite and wüstite in proportion to each others during the reduction is, according to publications, a parallel in which both of the oxides have a cubic crystal structure. The volumetric expansion calculated for the lattices from magnetite to wüstite is about 6 %.

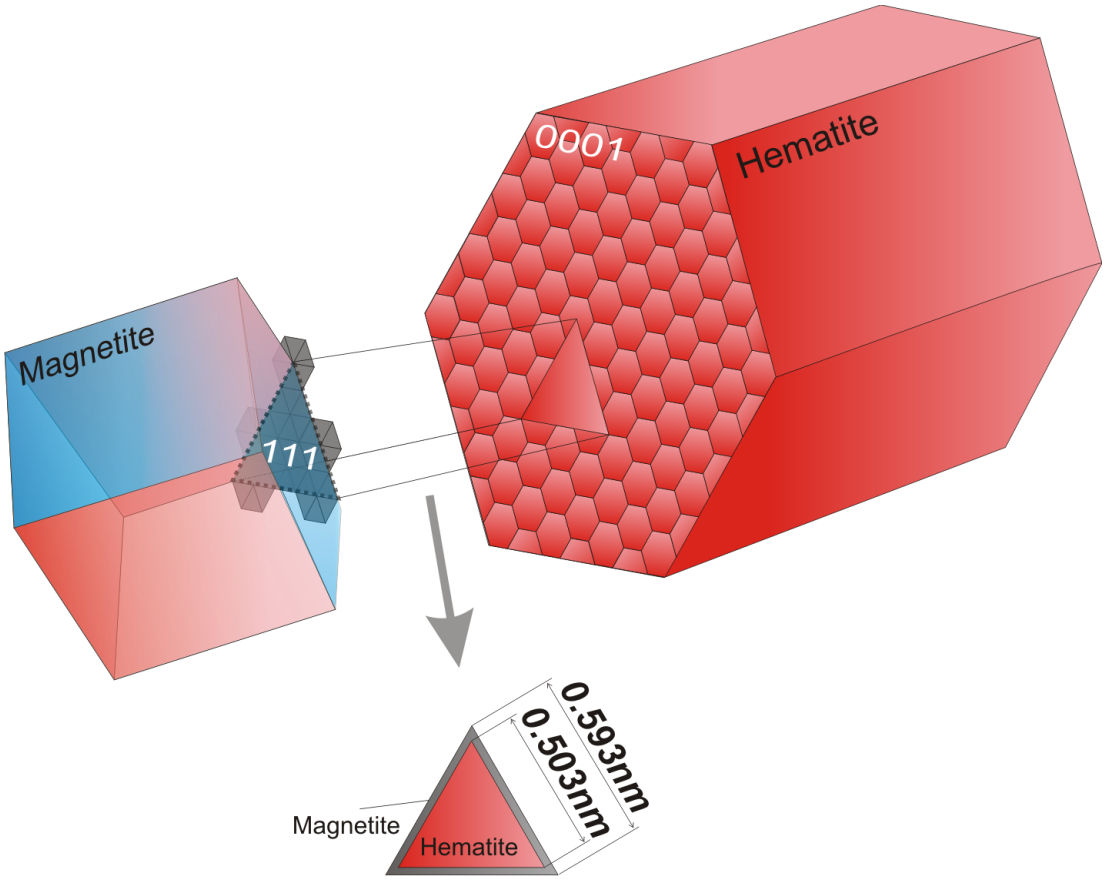

Figure 9. Compatibility and orientation of reduced magnetite on the surface of hematite with proportional calculated lattice volume.

The formation of iron on the surface of wüstite during reduction was studied and the results published by Sasaki et al[17]. Epitaxy of iron and orientation on the wüstite (100) face is presented in Figure 10. The lattice parameter values of α-iron (0.286 nm) and wüstite (0.428 nm) are presented in the graph as well as the distance of iron cations calculated from one another in the wüstite lattice (0.303 nm). The difference in distance of iron cations between wüstite and α-iron indicates the mismatch or shrinking of structures when wüstite reduces to α-iron.

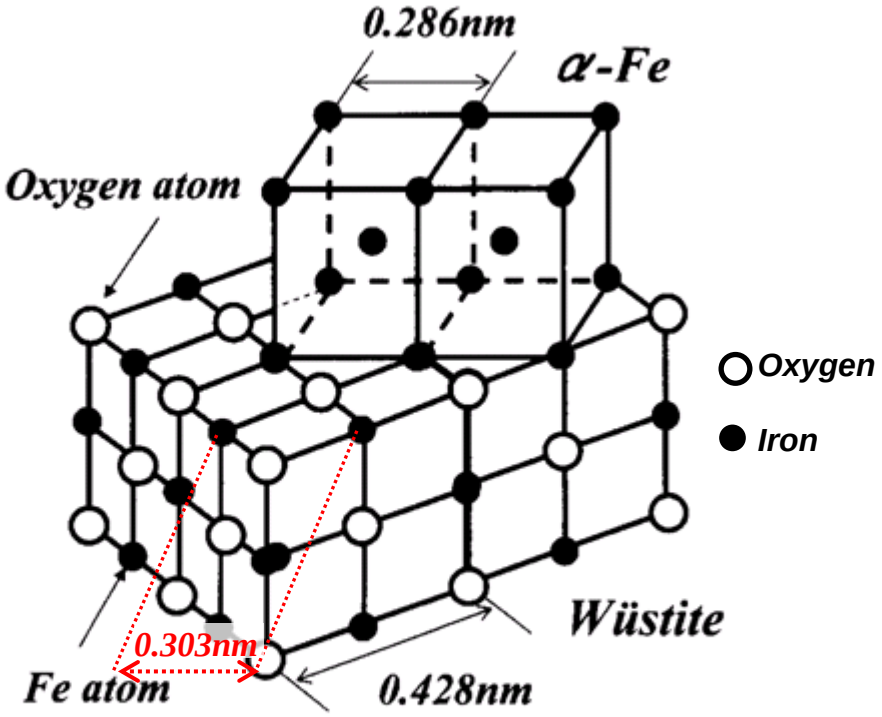

Figure 10. Epitaxy and orientation of iron on wüstite (100) face[17].

2.5 Research on impurities in iron ore agglomerates

The blast furnace burden material has to be agglomerated because the permeability of the burden bed must be sufficient for the reduction of gases to flow up from the low part of the furnace. The agglomeration is generally carried out by pelletizing or sintering the iron concentrate. In both cases, the material is warmed up to the temperature in which liquid eutectic phases can occur and cation and anion diffusion in solid phases are accelerated. The solid phases in a high temperature with initial melts enable changes in the composition phases in the solid state. Possible composition gradients are able to smoothen in high temperatures and ions solid solution in one phase may dissolve to another one. Gas composition changes simultaneously with

a temperature increase in the sintering process (both sinter and pellet sintering). In particular, changes in partial pressure of oxygen cause a rapid change of thermodynamic phasies and continuous disequilibrium among phases. The composition of phases aspires to equilibrium but it is kinetically limited when temperature is rapidly decreased during the cooling stage. The reduction behaviour of different phases depends on the stage after sintering. For example, a solid solution can be function of temperature; therefore synthetically prepared samples were used for the study of impurities on reduction behaviour of iron oxides in this study (*Supplement II*). The content levels of impurities in the solid solution with iron oxides were adjusted and based on analysed contents of iron oxides occurring in sinters or pellets.

The quality of sinter consists of two main factors, i.e. strength and reducibility that are partly opposite to each other. The effect of impurity on reducibility of iron oxides has been discussed in many papers. The cold strength and the reduction strength should be good with, however, a high level of reducibility. Since the sampling from the blast furnace process is difficult, the quality of the agglomerates is measured using such standard tests as the reducibility (HOSIM, RUL, ARUL, Burghard), the cold strength (Thumble test) and the reduction strength (LTB, LTD, RDI) test for ensuring good BF operation. Most of the minerals in BF agglomerates consist of iron oxides (hematite and magnetite), but also calcium ferrites, vitreous slag and crystallized slag. Hematite and magnetite are not pure iron oxides, but contain impurity elements in solid solution. Some impurities have a radical

effect on reduction kinetics and reduction strength via various mechanisms. The impurity elements can generate disintegration of oxide phases, accelerate reduction, enhance diffusion, increase gas-solid reaction surface area and have an influence on thermodynamic stability of oxides [18]. Deceleration or acceleration of reduction can occur, if impurity components cause the formation of new phases at the reaction front. The direction of the effect depends on the stoichiometry and the stability of the existing phases [19, 20]. The reduction step from wüstite to iron demands the thermodynamically most reducible gas among pure iron oxides and it is mostly the restrictive factor of the total reduction rate. However, previous reduction steps have a significant effect on the following step via morphology and surface area at the interface between the reduction gas and wüstite [21]. The dissolution of impurity elements or their insolubility in iron oxides has an important effect on the reducibility of iron oxides.

Even a small amount of Ca (0.05 – 0.2 mol. %) was observed to have a strong enhancing effect on the reducibility of wüstite [22]. The presence of MgO and CaO (2 wt. % and 5 wt. %) were found to promote the metallization of wüstite [23] and cause the formation of porous iron when reduced from wüstite in CO/CO_2-atmosphere [24]. The formation of pores can be caused by the precipitation of micro oxide particles at the interface of wüstite and iron phases [25]. Deceleration in reduction of iron oxides was observed when manganese content of magnetite was initially 1 wt. % (Supplement II).

According to Molenda et al., the electrical conductivity of mangano-wüstite was decreased when the content of manganese was increased [26].

2.6 Significance of reduction strength of iron ore agglomerates on the blast furnace operation

The oil replaces coke and relieves volumetric space inside the furnaces for iron burden reduction resulting in increased production capacity of hot metal. Murty et al.[7] reported that an improvement of sinter RDI by 6 % would lower the blast furnace coke rate by approximately 14 kilograms per ton of hot metal and increase blast furnace productivity by 3 %. Kim et al.[27] reported that the degradation of self fluxed sintered ore during low temperature reduction of iron bearing material increases the permeability resistance at the upper shaft of the blast furnace and the variation of gas flow exerting an unfavourable in-furnace upon stable operation. Lecomte et al.[28] reported of a test in which eight types of iron-rich sinters were charged into blast furnace. They found a clear correlation between burden permeability and blast furnace operation using different sinters with evaluated reduction strengths. Grebe et al.[29] reported on a magnitude of laboratory based quality tests versus production scale and basket sample experiments. They discovered that a real production scale atmosphere can smooth the effect of a considerable change in quality analyzed under laboratory conditions. For example, sulfur, alkalis, and chlorine compounds in gas have some unexpected effects on burden behavior. Nevertheless,

Grebe et al. observed a notable influence of fines rate on the deterioration of permeability in blast furnace.

The factors affecting sinter RDI have been discussed in a great number of papers. The parameters affecting the RDI can be categorized as sintering parameters, properties of raw materials, and the chemical composition of a sintering mix. For example, increasing the MgO content [5, 30, 31, 32], basicity [30, 31] (CaO/SiO_2), and fuel rate improves the reduction degradation property of the sinter. On the other hand, increasing the content of Al_2O_3 [32, 31, 33, 34, 35, 36] and TiO_2 [33, 35, 37, 38, 39] has a negative effect on RDI. Moreover, mineralogy of sinter is a significant factor of reduction strength. One controlling factor of mineralogy is the chemical composition, especially the CaO/SiO_2 ratio and even small changes in the content of minor components such as MgO, Al_2O_3 and TiO_2, have a clear effect on the sinter mineralogy. [32, 40] An increase in the alumina content has been shown to cause more calcium ferrites or SFCA-phase (silico-ferrite of calcium and aluminium) in sinter [5]. Similarly, MgO has been shown to stabilize magnetite in sinter [41].

The amount of hematite and secondary hematite in particularly is widely regarded the main cause of disintegration of sinter in low temperature reduction. However, the amount of hematite in sinter does not alone explain the RDI variation observed [5].

As mentioned earlier, the negative effect of titanium oxide on RDI has been

demonstrated previously in several papers. However, neither the degradative mechanism of TiO_2 nor the phase in which the phenomenon had an effect is unambiguous. This study focuses on the distribution of titanium oxide in sinter, and in particular on the effect of the titanium content on reduction degradation of hematite.

RDI presents reduction strength of sinter similarly to the LTD index being carried out for testing the pellet quality in this study.

3 PROCESS CONDITIONS AND DEMANDS FOR RAW MATERIAL IN IRON MAKING

Iron making process demands pretreatment of iron burden material before it is charged to the blast furnace. Process flow from iron ore to liquid steel is presented in Figure 11.

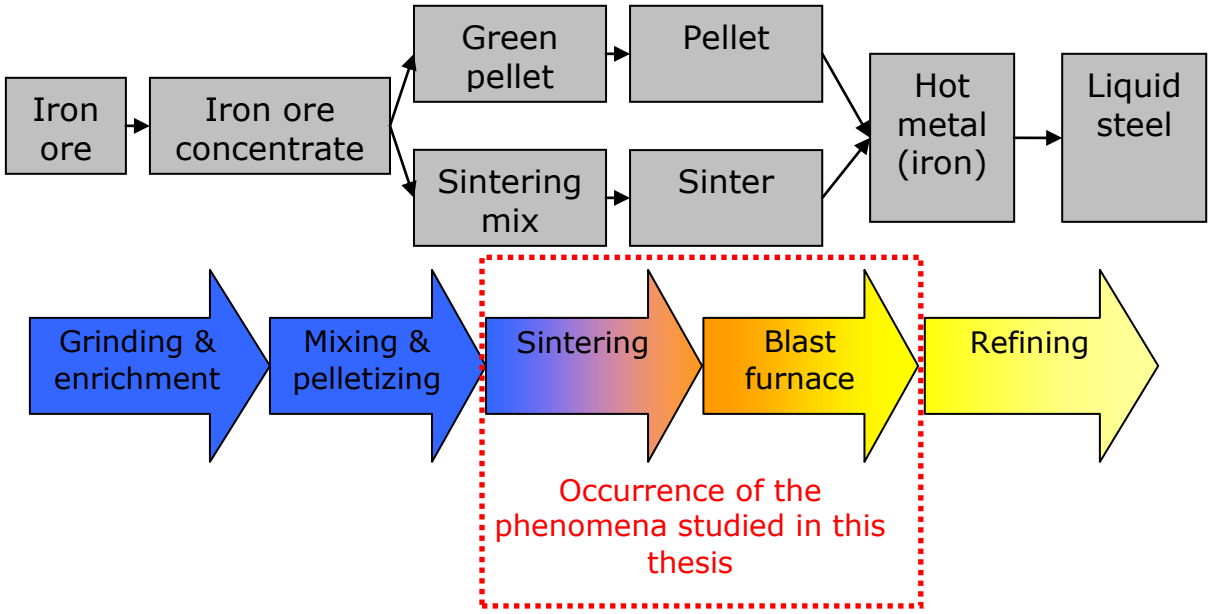

Figure 11. Schematic process flow chart about a process chain from iron ore to steel. Red dashed line represents the processes in which the phenomena studied in this thesis occur.

3.1 Iron oxide composition in ore

Iron ore always consists of iron ore minerals (as oxides or hydroxides etc.) and gangue minerals. Grinding and enrichment decrease fraction of gangue, but do not remove it. On this account, chemical analysis from enriched iron ore bulk does not represent composition of iron oxide phases. Impurity

components can be located in gangue but also in solid solution with iron oxide, in which case an iron cation is replaced with an impurity element in iron oxide lattice. The composition of magnetite and hematite is dependent of ore and the adjacent mineral phases have been in contact with iron oxide when ore has been generated. The chemical composition of different ore fines analyzed from magnetite and hematite phases are presented in Table 1 and

Table 2.

Table 1. Typical compositions of the magnetite in different iron ore fines such as MAF (Malmgerget A Fines), Olenogorsk, Rautuvaara and Mustavaara [5, 42].

	Magnetite (MAF)	Magnetite (Olenogorsk)	Magnetite (Rautuvaara)	Magnetite/ Mustavaara[42]
MgO	0.22	0.10	0.10	0.04
Al_2O_3	0.13	0.07	0.18	0.02
CaO	0.00	0.00	0.00	0.04
TiO_2	0.15	0.01	0.02	1.14
V_2O_3	N/A	N/A	N/A	1.4
MnO	0.02	0.10	0.09	0.03
Fe	71.4	71.3	71.1	68.5

Table 2. Typical compositions of the hematite in different iron ore fines (XF) and hematite in pellet such as Kostamus.

	Hematite (XF) (natural)	Hematite (Kostamus) (initial magnetite)
MgO	0.05	0.06
Al_2O_3	0.04	0.15
CaO	0.01	0.00
TiO_2	0.01	0.00
MnO	0.07	0.00
Fe	69.5	
V_2O_5	0.003	0.02
SiO_2	0.27	0.28
Na_2O	0.17	0.03

3.2 Sinter production

Iron ore fines are agglomerated at a high temperature and the resulting material is partly melted with the particles in the sinter feed are stuck together forming continuous uniform sinter cake on the sintering belt. The sinter cake is crushed in the end of the belt and cooled down in the rotary coolers.

The temperature of the material rapidly increases in the sintering bed as well as decreases after fuel, i.e. coke breeze is burnt out. Simultaneously with

temperature change, the gas composition also changes from reducing to oxidizing. Iron oxides are reduced from hematite and magnetite partly to wüstite until oxidized back to magnetite and partly to hematite (Figure 12). Iron oxides also reach with such fluxes as CaO, SiO_2, MgO, Al_2O_3, TiO_2 and other impurities, form for example different types of calcium ferrites, magnesioferrites and crystallized or vitreous slag. The effect of different factors on sinter mineralogy with magnetite based sinter at bacisity (B_2) of 1.5 - 1.85 has been studied by Heinänen[5].

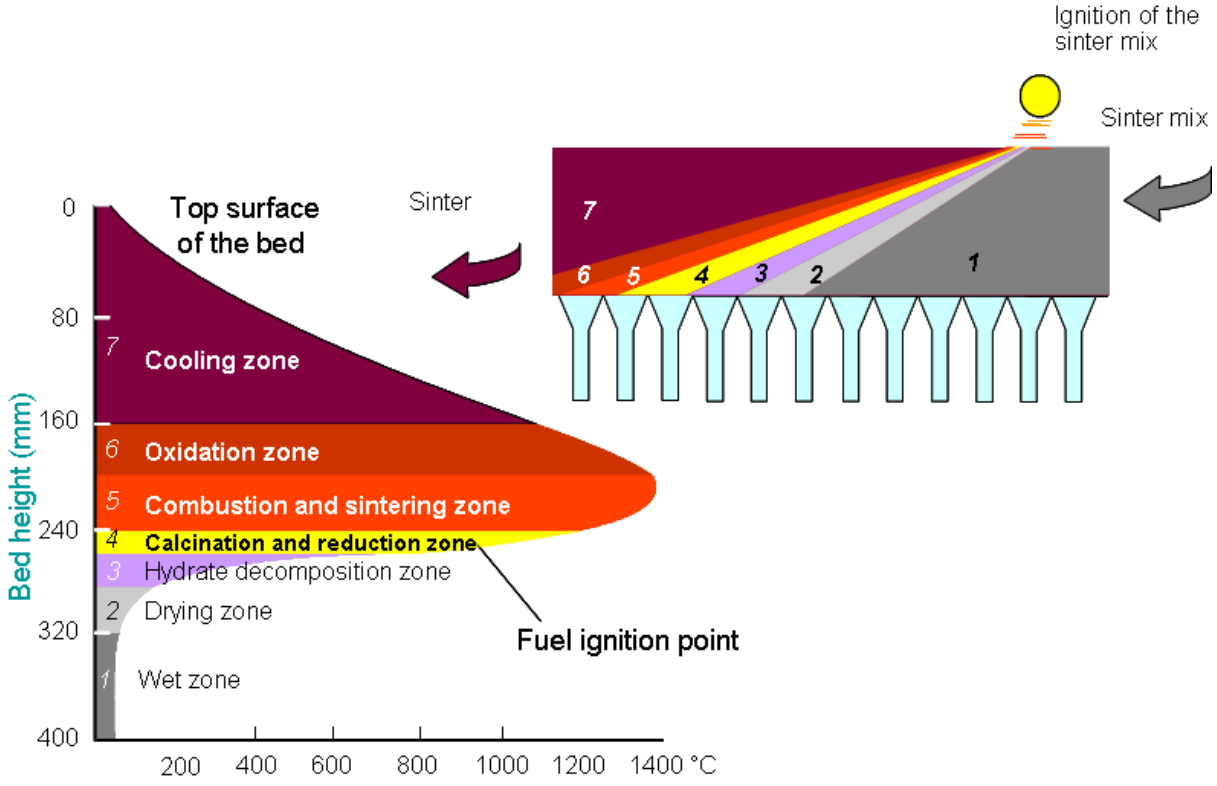

Figure 12. Reaction zones in sintering bed.[5]

In order to improve the quality of sinter and increase the amount of acid pellet with sinter in the blast furnace, higher burden bacisity of sinter is needed. The iron content of sinter varies usually between 56-58 wt. % in the

sintering plants in Central Europe and it used to be higher in magnetite based sinter in Northern Europe. A typical chemical composition of high bacisity magnetite based sinter (B_2 = 2.1 - 2.3) is presented in Table 3.

Table 3. Typical chemical composition of high bacisity sinter[43].

Fe	FeO	CaO	SiO_2	MgO	Al_2O_3	TiO_2	CaO/SiO_2
60.33	10.87	7.28	3.49	2.18	0.61	0.25	2.09
60.91	10.95	6.95	3.02	2.02	0.58	0.27	2.30

The structure of high bacisity sinter (B_2 = 2.1 - 2.3) consist of many minerals with their own chemical compositions. Typical mineral compositions of sinter are presented in Table 4.

Table 4. Mineral composition of high bacisity sinter (B_2 = 2.1-2.3).

Typical minerals in sinter with B_2 bacisity of 2.1 - 2.3		**Proportion**	
Magnetite	Fe_3O_4	50 - 54 %	*
Hematite	Fe_2O_3	17 - 19 %	*
Silicoferrite of calcium and aluminium (SFCA)		15 - 19 %	*
Hemi-calcium ferrite	$CaFe_2O_4$	< 5%	**
Larnite	Ca_2SiO_4	< 5%	**
Vitreous slag		9 -14 %	*
Dicalcium titanate-ferrite of silicon	$Ca_2(Si,Fe,Ti)O_4$	< 1%	**
Ilmenite	$FeTiO_3$	< 1%	**
Forsterite (Olivine)	$(Mg,Fe)_2FeO_4$	< 3%	**

* Typical analysis of LOM figure analysis determined for four phases

** Estimated content

The structure of sinter depends on initial mineralogy and chemical composition of minerals as well as sintering conditions. The reactions and change of chemical composition of an individual phase during sintering depends on the adjacent mineral phases. Certain mineral association produces characteristic compositions for the minerals depending on the adjacent minerals included in the association. Typical minerals and mineral associations in high bacisity sinter are presented in Figure 13.

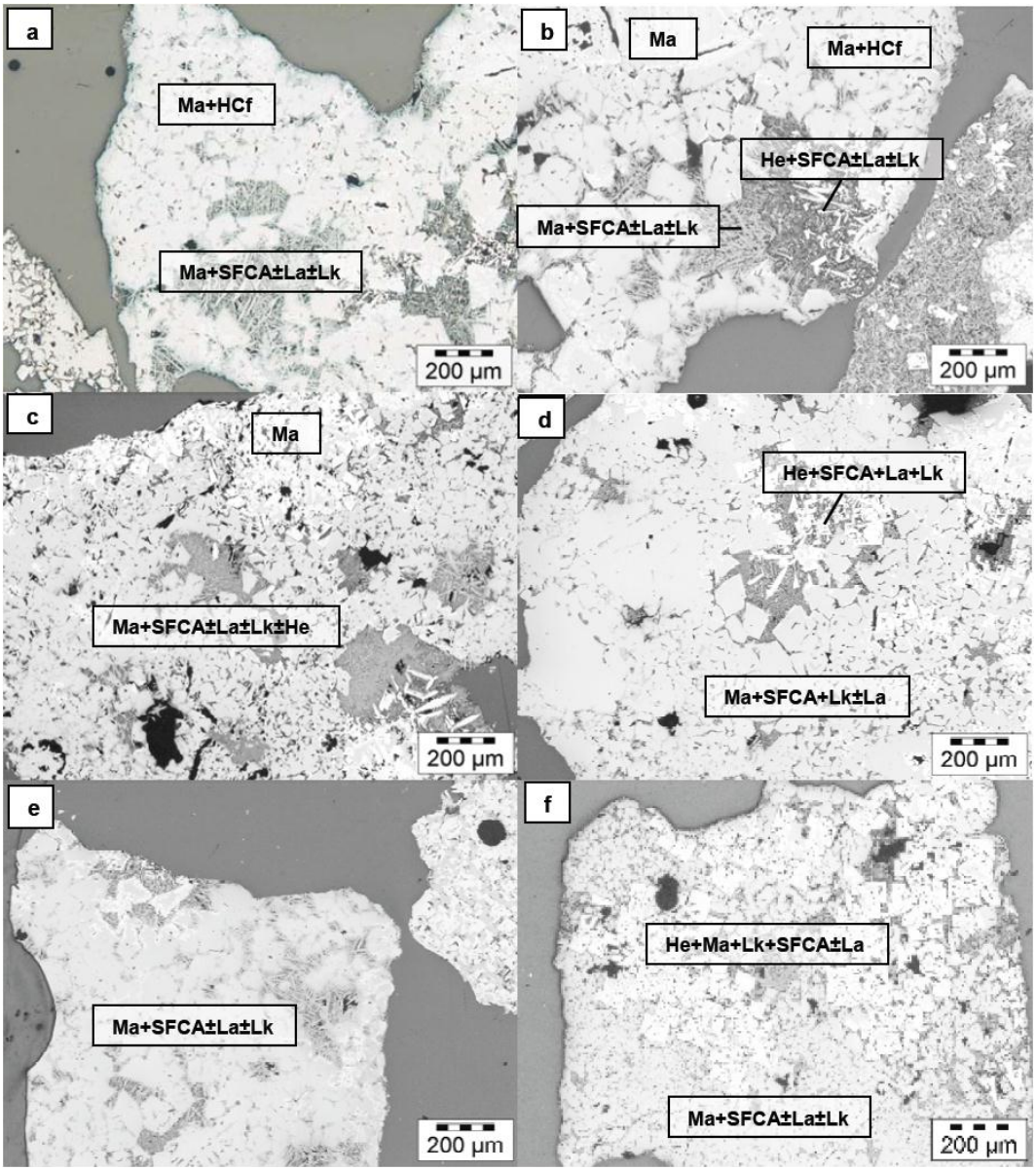

Figure 13. Different minerals and mineral groups in high bacisity sinter (CaO/SiO_2 = 2.1-2.3). Ma = magnetite, He = hematite, HCf = hemi calcium ferrite, SFCA = Silico-ferrite of calcium and aluminium, La = Larnite, Lk = vitreous slag. [43]

Different compositions of minerals analysed in the sinter are presented in Table 5.

Table 5. Typical composition of minerals with different phase associations in sinter.[5, 43, 50]

Mineral in sinter										
	FeO	Fe	MgO	CaO	SiO_2	TiO_2	Al_2O_3	V_2O_5	MnO	K_2O
Magnetite										
relic phase	85.08		0.22	0		0.15	0.13		0.02	
magnetite with in hematite			6 - 8	1.5-2.0					1.1	
crystallised into matrix	84.09		2.09	0.99			0.53			
Hematite										
lamellae with in magnetic relic	83.62			0		0				
crystallised hematite on magnetite periphery	85.60					0.5				
hematite HE1	81.95	63.7	0.37	0.81		7.39	1.08		0.21	
hematite in two-phase area between magnetite crystals	83.21			0.44	0	1.9	0.73			
SFCA-phase	62.88		0.53	15.59	8.29	0.63	1.64			
Hemi calcium ferrite	70.95			11.88	3.02		1.01			
Larnite	2.18			61.39	31.48	0		1.62		0
Vitreous Slag	10.8		0	38.36	31.02	3.19	0.61	0	6.3	0.99
Silicon titanium dicalcium ferrite										
Ti-rich phase	18.13		0	40.88	10.03	23.2	0.44	0		
Fe-rich phase	29.37		0	40.43	10.33	9.82	0.73	0.92		
Ilmenite	76.00					7.86		0.57		
Forsterite with its periphery										
Forsterite crystal	8.72		47.6	0	39.01	-	0			
Magnesioferrite corona	75.73		7.52	1.53	0	-	0.62			

3.3 Sintering of pellets

Concentrated iron oxide fines with selected additives are pelletized before sintering of pellets. Typical additives in the raw material mixture are quartzite (SiO_2), forsterite (Mg_2SiO_4), limestone ($CaCO_3$) and clay minerals such as bentonite. In order to increase mechanical strength of the pellets two different methods are commonly used in the sintering of pellets. The grate kiln sintering process with pre-treatment i.e. pelletizing process flow is presented in Figure 14.

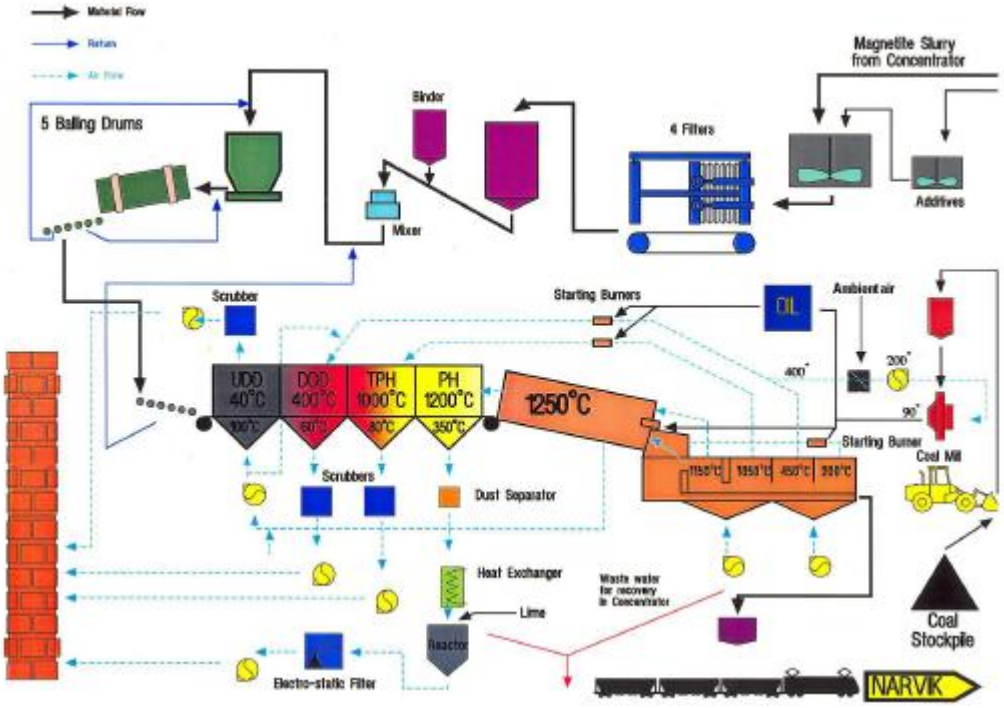

Figure 14. Grate kiln sintering process of pellets at Kiruna (KK3)[44].

The straight-grate sintering process is presented in Figure 15.

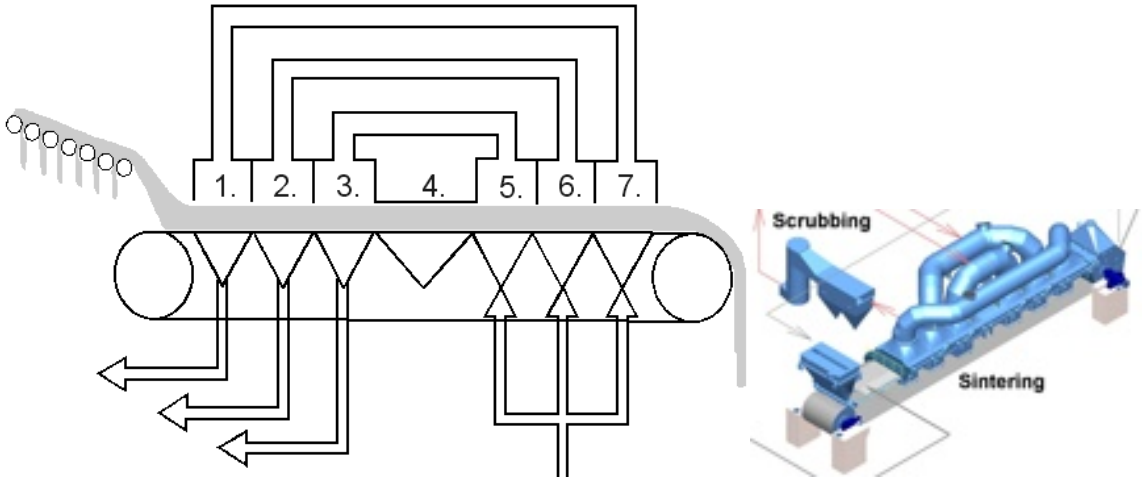

Figure 15. Straight-grate sintering process of pellets.[44]

The properties in the pellet sintering process are oxidizing with the maximum temperature of approximately 1,250 °C causing oxidation of

magnetite to hematite and forming a small amount of melt slag phase functions as a binder. The chemical composition of different pellets is presented in Table 6 and mineral composition in Table 7.

Table 6. Chemical composition of different pellet types[45, 46].

Pellet	Fe	FeO	CaO	SiO2	MgO	TiO2	Al2O3	CaO/SiO_2
Acid pellet I	65.1	1.4	0.41	5.98	0.14	0.01	0.30	0.07
Acid pellet II	66.9	0.4	0.55	2.6	0.52	0.18	0.23	0.21
Fluxed pellet	63.8	0.9	3.45	4.61	0.25	0.01	0.30	0.75
Olivine pellet I	66.6	0.5	0.46	2.1	1.4	0.18	0.23	0.22
Olivine pellet II	66.8	0.5	0.45	1.8	1.3	0.35	0.35	0.25

Table 7. Mineral composition of sintered olivine pellet[47] and acid pellet[48]

Typical minerals in olivine pellet	Mineral formula in olivine pellet	minerals in acid pellets (Kostamus)	Mineral formula in acid pellet
Hematite	Fe_2O_3	Hematite	Fe_2O_3
Magnetite	Fe_3O_4		
Forsterite	$(Mg,Fe)_2FeO_4$		
Vitreous slag			
Quartz	SiO_2	Quartz	SiO_2
Magnesioferrite	$(Mg,Fe)Fe_2O_4$		
Orthopyroxene	$(Mg,Fe)SiO_3$		

3.4 Hot metal production from iron ore agglomerates

Pelletized or sintered iron ore fines are charged into the blast furnace from the top alternately with coke agglomerated from coal. Preheated blast enriched with oxygen is blown via numerous tuyeres in the lower part of the blast furnace. Reaction of oxygen with carbon, originated from coke and injected oil or pulverized coal, generates heat in the process as well as carbon monoxide and hydrogen gas. The generated reduction gas flows through iron oxide burden materials and reduces iron oxides to metallic iron step-by-step from hematite to magnetite, from magnetite to wüstite and finally to metallic iron. Simultaneously charged burden material is heated up and finally smelted by hot reducing gas and exothermic reactions downstream from the tuyeres.

The iron blast furnace is divided into different zones which are the indirect reduction zone, thermal reserve zone, cohesive and direct reduction zone, dropping zone, "dead man" and hearth (Figure 16).

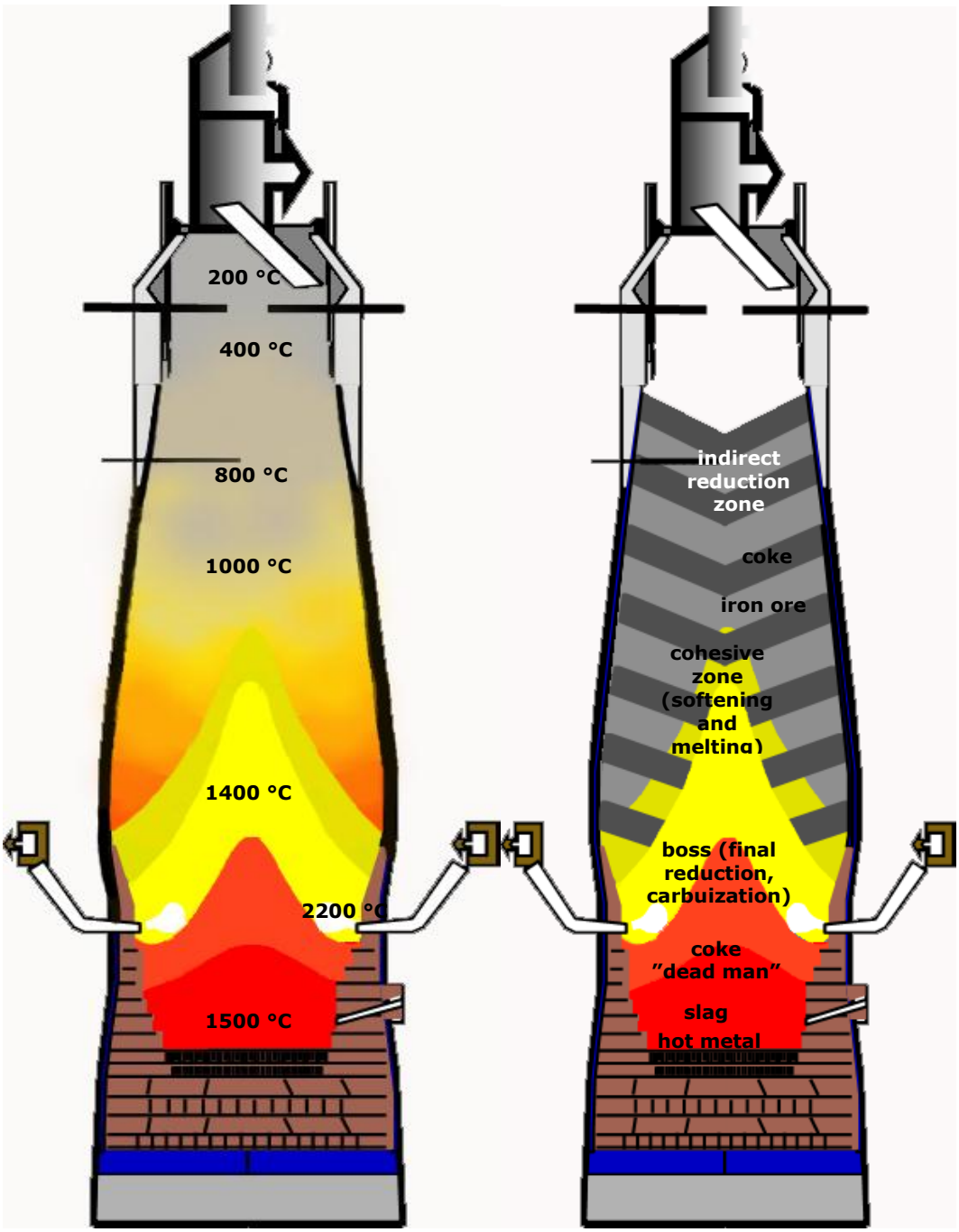

Figure 16. Blast furnace process[49].

Indirect reaction zone:

- is located below from the charging level down in the shaft, on the level in which hematite and magnetite are reduced to wüstite.
- iron oxides are reduced by the gas generated on raceway (downstream from the tuyeres)
- wüstite is partly reduced to metallic iron.
- regeneration of reducing gas is insignificant

Next down the indirect reaction zone is the chemical and thermal reserve zone in which

- reducibility and temperature are not strong enough to induce significant reduction from wüstite to iron, because the reduction gas is almost on phase equilibrium of with wüstite and iron
- temperature increases slowly being about 900 - 1000 °C and is too low for regeneration of reduction gas.

When the burden descends down in the shaft and the temperature increases up to about 1,100 °C, reduction gas becomes rapidly regenerated and wüstite is able to reduce to iron by strongly reductive gas. The regeneration of reduction gas is a strongly endothermic reaction called the Boudouard reaction or "solution loss reaction". The said reaction just mentioned occurs in the direct reduction zone.

The melt down of iron burden material starts in the cohesive zone and the permeability of ore layers decreases dramatically causing channelling of gas flows through the coke layers. The rest of the iron oxides are reduced to

metallic iron while melt slag begins to flow down to the dropping zone. Direct reduction is localized in the cohesive zone.

Melted slag and metallic iron flow towards the deadman and hearth of the blast furnace in dropping zone. While metal droplets flow down, carburization occurs in hot metal when it contacts carbon of coke or via high CO content and reductive gas. Simultaneously melted slag flows down to hearth and impurity oxides, ash of coke and sulphur is dissolves in slag forming the second slag composition.

"Dead man" consists of coke is not reached with anything. "Dead man" can float on hot metal and slag or lie in the bottom of the hearth. In general, the latter situation is unwanted.

Blast air enriched with oxygen is blown via numerous tuyeres into blast furnace with possible injection material such as pulverized coal (PC), oil, plastic or gas. Oxygen and carbon, from coke or injection material, are reached downstream of the tuyeres, in the area called raceway. The reaction produces reduction gas including CO gas from carbon and H_2-gas from injected hydrocarbon or vaporized water. The gas and heat produced in the raceway is utilized in the shaft in indirect reduction reactions. Gas containing CO and H_2 reduces iron oxides producing CO_2 and H_2O gas in the reduction reactions. The reducibility of gas is diminished while reduction gas flows up in the blast furnace shaft.

Both melted hot metal and slag accumulates in the hearth of the blast furnace and be regularly tapped from the blast furnace via a tap hole. The tap hole is drilled open for example every two hours being always closed for about 30 minutes between drillings. The length of the tapping period depends on the size of the blast furnace and production rate. Three or four tap holes can be used in bigger blast furnaces.

4 THESIS OBJECTIVES

The purpose of this thesis is to study the phenomena in which minor oxide components in solid solution with iron oxides have an effect on the reducibility and reduction strength of iron oxides and iron ore agglomerates. The reducibility of iron oxides and the reduction strength of iron ore agglomerates are connected because the phenomena reflect a real process as follows:

- Good reducibility of iron oxide agglomerate with good reduction strength enable effective operation of the blast furnace
- Good reducibility of iron oxide agglomerate because of an increased surface area on the reaction zone between the reduction gas and oxides caused by low reduction strength. This causes disturbances in the blast furnace process via low permeability of the shaft resulting in lower productivity and increased consumption of the reducing agent in the process.

- Low reducibility with good reduction strength requires increased consumption of the reducing agent in the process because indirect reduction is insufficient and the proportion of direct reduction increases and needs more reducing agent in the blast furnace hearth.

The objective of the research was to study the effect of minor oxide components as solid solution in iron oxides on

- Reducibility and reduction mechanism.
- Phenomena and mechanism behind reduction strength.

The minor components such as CaO, MnO, MgO, and especially TiO_2 and Al_2O_3 were studied in this thesis. TiO_2 and Al_2O_3 were chosen because correlations with reducibility and reduction strength have been discussed but not explained in other publications.

The aim of the thesis was to focus on the most essential factors among indirect reduction of iron oxides in the blast furnace from the aspect of minor oxide components solid solution in iron oxides. The phenomena occurring in the end of the sintering process (oxidizing of magnetite), low temperature reduction strength occurring in the upper shaft of the blast furnace (reduction of hematite to magnetite) and reducibility occurring in the whole shaft of the blast furnace (reduction of iron oxides to iron) are concerned in this thesis (Figure 17).

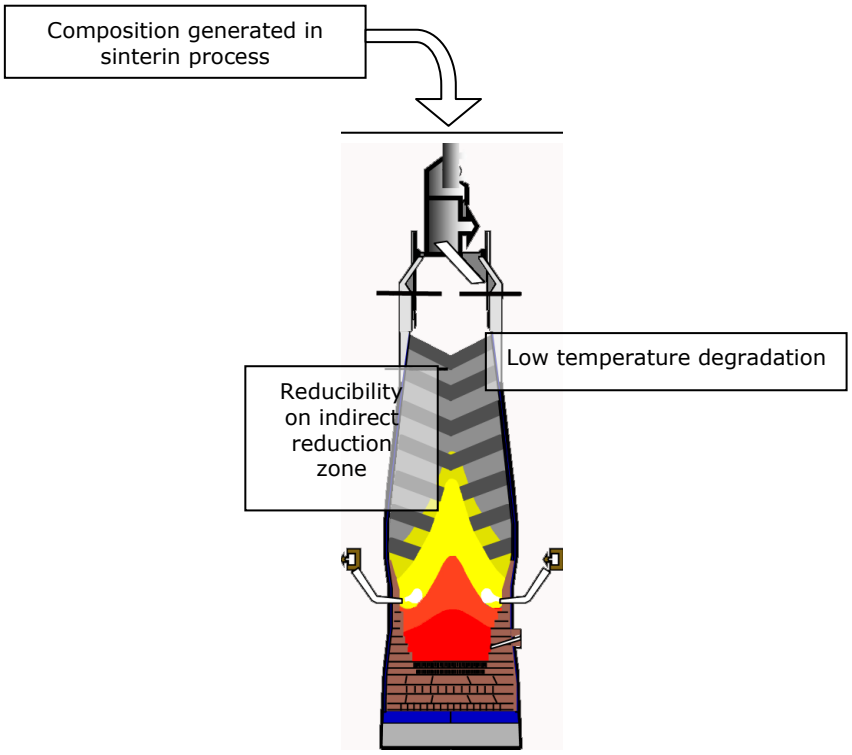

Figure 17. Occurrence of phenomena studied in the blast furnace process.

5 EXPERIMENTAL RESEARCH

The purpose of the experiments is to simulate an individual phenomenon in an individual structure caused by an impurity element and observed in the burden material of blast furnace. In order to prepare a certain structure with a certain impurity composition in the initial stage, controlled chemicals with right heat treatment are needed. When the initial stage is achieved and confirmed, the study of the reaction can be carried out under controlled conditions.

In this thesis, every test on the effect of impurity on reduction or oxidation behaviour consists of the experiment procedure with the following three main functions:

1. The preparation of samples is of the utmost importance, moreover, the initial state hast to be familiar and confirmed for main reaction tests.
2. Reaction test in which reduction or oxidation is executed in a selected temperature and gas atmosphere.
3. The analysis includes numeric results from the tests and an analysis of the samples. The numeric results consist of, e.g. values achieved in the reduction strength test, reducibility as well as reduction slopes. etc. The analysis of the samples includes the preparation of polished sections, powder samples for mineralogy and chemical analysis combined with the results from gravimetric data, optical and electron microscopy views and microanalysis.

In order to have results comparable with on another, especially with reference to the pure samples, reproducibility of the sample preparation and reaction tests is crucial. Tests on the reproducibility of the reduction experiments including sample preparation is presented in (Figure 18). Moreover, attempts were made to prepare samples identically for mineralogy and chemical analysis.

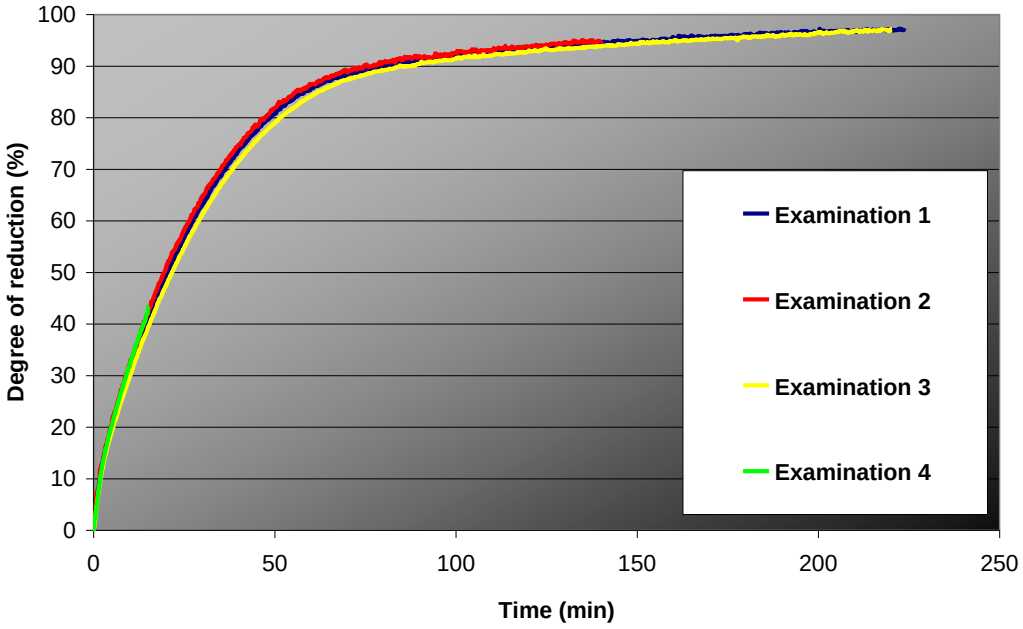

Figure 18. Reproducibility of reduction experiment (reference sample).

5.1 Solid gas reactions

In order to arrange comparable properties and reduction/oxidation tests for each sample, the aim was to adjust some variables:

- as a consequence of the sample height and diameter being constant, the macroscopic solid-gas surface area between sample and reaction gas was constant
- in order to achieve equal solid-gas surface area in micro scale the used sintering temperature was high for homogenous solid solution,
- experiments were static i.e. temperature and gas composition were constant
- starting and ending the experiments were carried out equally

- the cooling of the samples after the experiments were executed rapidly in argon atmosphere

5.2 Laboratory experiments

5.2.1 Materials

In order to research the selected phenomenon, commercial magnetite fines as well as synthetic iron oxides were used for sample preparation. Varying amounts of impurities such as Al_2O_3, TiO_2, MgO, CaO and MnO were added in into the initial iron oxides. More accurate details on the composition and quality of oxides used in the experiments are presented in *Supplements*.

5.2.2 Preparation of mixture

The powder mix, to which approximately 15 wt. % of purified ethyl alcohol had been added, was forced into the briquettes with the pressure of 50 MPa. The wet briquettes were dried at 110 ^{o}C for the minimum of two hours (e.g. *Supplements I - III*).

5.2.3 Preparation of sintered samples

In the sintering tests, the initial stage had been prepared and aimed for the reduction experiments. In this part of the test, the actual sintering process was not simulated but in order to get a solid solution of certain oxides, sufficiently high preparation temperature was required. During the sample preparation, the conditions have to be constant and within the stability area of the prepared iron oxides such as magnetite or hematite.

Pressed magnetite briquettes (diameter = 12 mm and height = 5 mm), as described earlier, were sintered in a 34 mm diameter tube furnace at 1300 ^{o}C for 5 hours in a CO/CO_2 atmosphere (CO/CO_2 = 5/95 and flow rate 1 l/min) for magnetite. The briquettes were quickly quenched in a copper chamber cooled by water and at argon atmosphere after sintering. After cooling, the briquettes were ready for the reduction experiment. The aim was to produce compact and dense briquettes for topochemical reaction during the reduction. Hematite briquettes were sintered in air at the same temperature and for the same duration as magnetite samples. (e.g. *Supplements I - III*).

5.2.4 Preparation of calcium ferrites via melt

Hemi-, mono- and dicalcium ferrites were prepared by melting hematite and calcium oxide in proportions to the homogenous melts and then crystallising them. The first attempt on the preparation of calcium ferrites was made by carrying it out in a solid state but no successful preparation of homogenous calcium ferrites was made. The more detailed preparation is presented in *Supplement IV.*

5.2.5 Reduction of the samples

The reduction of iron oxide in the blast furnace is a dynamic process in which temperature and reducibility of gas increases all the time. In order to

achieve the highest possible degree of identical repeatability in this study, the experiments were performed under static conditions.

Once prepared and sintered, the briquettes were reduced in the 34 mm diameter tube furnace, in a reducing gas mixture of N_2, H_2, CO, and CO_2 with a flow rate of 2 l/min.

Reduction experiments from hematite and magnetite were done with strong reducibility gas (CO/CO_2 = 90/10, 950 °C), but also some reduction experiments from hematite to magnetite were executed. In that case, the gas composition was the same as that of the RDI test and was kept constant during the experiments. The reduction temperature was maintained constant at 500 ^oC during the reduction. Before the reduction, the sample was first heated in an argon atmosphere to 500 ^oC for 5 minutes. The reduction period was 60 minutes. A more detailed description about the experiment is presented in *Supplements I, II, III and V*.

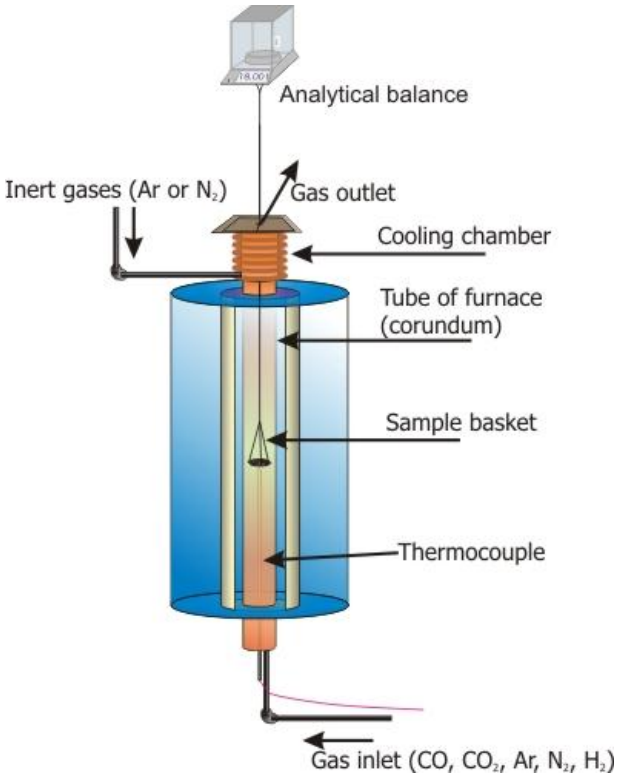

Figure 19. Thermo gravimetric analyzer equipment.

During the reduction test, the sample was in a platinum basket hanging on a gravimeter connected to a computer for data collecting. After the reduction, briquettes were rapidly cooled in a copper chamber at the argon atmosphere described earlier.

5.2.6 Oxidation of the samples

Four magnetite briquettes (0, 0.5, 2 and 5 wt. % doped with TiO_2), sintered as described earlier, were set on a platinum crucible at the same time. The briquettes were oxidized in a chamber furnace in air for 15 minutes and cooled at room temperature. The oxidation temperature of 950 ^{o}C was measured using thermo element placed in the centre point, on the same depth level as the samples. (*Supplement III*)

5.3 Pilot experiments

The effect of titanium content on the sinter RDI was studied using pot sintering tests. Raw materials and the test equipment were designed to resemble the production scale characteristics and materials as closely as possible. All of the materials with the exception of rutile have been in production scale use at Raahe Works of Ruukki. The coke breeze rate was adjusted to reach equilibrium with the return fines rate similarly to that of a production scale *Dwight-Lloyd*-type sintering process. The detailed experiment procedure and results are presented in *Supplement III, V* and *VI*.

Sinter was analysed very thoroughly by sieve analysis, tumbling tests (ISO 3271 1975 (E)), reduction degradation test, reducibility tests, mineralogical and chemical analysis. The reduction degradation index (RDI) equipment was constructed in total compliance with the international standard (ISO 4696-1). Reducibility, softening and melting properties were analysed using a method developed by Rautaruukki[50]. Other indexes were: *TI* (tumbler index <6.3 mm), *RDI* (reduction degradation index <3.15 mm), *REXT* (reduction extends at 1,000ºC, %), *DRINT* (reduction rate between 800 - 900ºC, %), *TK5*0 (softening index, 50% collapse in voidage ºC), *TDP20* (first melt formation temperature, 20 mbar pressure drop reached, ºC). Mineralogy was analysed by an optical light microscope by texture analysis. The analysis was capable of separating plastic, vitreous slag/silicate phases, calcium ferrites, magnetite and hematite. Reflectivity of some of the calcium

ferrite types and magnetite/magnesioferrite was partly overlapped which led to lower validity.

5.4 Analytical methods

The polished sections from the sintered, reduced and oxidized samples were examined optically and by a scanning electron microscope.

5.4.1 Light optical microscope examination

Olympus BX51 optical microscope was used for the optical examination. Reflected polarized/non-polarized light with 40, 100, 200 and 500 times magnitudes were possible to use. Phases were visually identified and confirmed using SEM-EDS and XRD analysis.

Figure 20. Olympus BX51 light optical microscope with camera was used in the study.

An example of a microscopy image of the sample is presented in Figure 21.

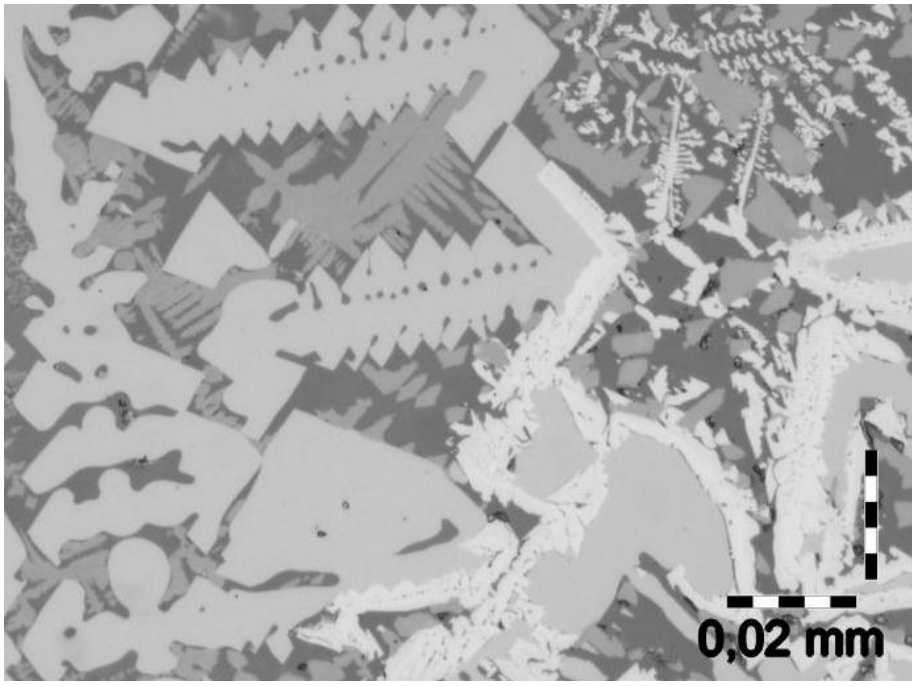

Figure 21. A light optical microscope view of synthetic crystallised sample prepared from Ca-Ti-Fe-O -melt[51].

5.4.2 Scanning electron microscopy - energy dispersive spectroscopy analysis (SEM-EDS)

Microprobe analyses were performed with a JEOL JSM-6400 scanning electron microscope using energy dispersive spectrometry. The equipment included a digital camera and Oxford Instruments Inca 3.03 software for the evaluation of the analyses. Back scattery image setting is used with SEM images in this thesis. Chemical analysis was executed using energy dispersive point analysis and line analysis. In order to achieve about 1-2 µm diameter analysis beam, an accelerating voltage of 15 kV and a beam current of 120 nA were used.

5.4.3 X-ray diffractometer analysis

Crystallographic analyses were made using a Philips X'Pert PW3040/00 X-ray powder diffractometer with a PW3376/00 Co LFF ceramic X-ray tube and Philips Data Collector 2.0c (2003). Phase identifications from the diffraction patterns were performed with the aid of PANanalytical X'Pert HighScore 1.0d software (2003).

5.4.4 Chemical analysis using X-ray fluorescence method

X-ray fluerescence method was used for the bulk chemical analysis using Philips PW 2404 equipment. The atoms of each chemical element in the sample are excited using high energy X-ray radiation causing removal of electrons from the outer shells. The free place thus generated is replaced by electrons from the outer shell and the excited state is discharged initiating energy release from the atoms. This release of energy is called as X-ray fluerescence radiation and is characteristics of each chemical element. The intensity of each characteristics radiation is measured by detectors. The content of chemical elements in a sample is determined based on the intensities. All of the chemical components were analysed using XRF-method with the exception of FeO content that was analysed chemically.

5.4.5 Iron content and valence analysis using titration method

In order to confirm proportion of Fe^{2+}- and Fe^{3+}-ions of iron oxides, complementary analysis were carried out using the titration method. Total

iron content as well as Fe^{2+} content were determined by titration and Fe^{3+} content was calculated to cover the rest.

Determination of the Fe^{2+}-content is suitable when FeO-content is 0.1 - 100 %. The method is disturbed by metallic iron, but could be corrected, if the metallic iron content is known. A pulverized sample is dissolved in HCl simultaneously warming up the sample. Oxidation of iron is prevented using carbon dioxide flow through the solution. Fe^{2+}-ion is oxidized after cooling of the solution by titration using potassium dichromate as the titration solution (Eq. 10).

$$\mathbf{6\ Fe^{2+} + Cr2O7^{2-} + 14\ H^{+} \rightarrow 6\ Fe^{3+} + 2Cr^{3+} + 7H_2O} \quad \textbf{(Eq. 10)}$$

Titration is carried out as potentiometer determination. [52]

Total iron analysis is an accredited method and applicable when iron content is 5 - 100 % Fe. The sample is dissolved in salt-fluorhydric acid mixture using microwave dissolution method. Iron is reduced by chromo sulphate solution after sulphur acid addition as in Eq. 11.

$$\mathbf{2\ Fe^{3+} + 2Cr^{2+} \rightarrow 2Fe^{2+} + 2\ Cr^{3+}} \quad \textbf{(Eq. 11)}$$

Reduced iron is titrated using potassium dichromate solution corresponding to the Fe^{2+} analysis mentioned earlier according to Eq. 10. Titration is carried out as potentiometer determination. [53]

6 RESULTS AND DISCUSSION

The detailed results from the study of minor oxide components and their effects on the reduction phenomena of iron oxides are presented in the *Supplements I - VI.* Five different impurity elements were studied from the aspect of their occurrence in the iron burden material of the blast furnace. Supplement numbers, in which different impurity elements and iron oxides are discussed are presented in Table 8.

Table 8. Supplements in which cations with different iron oxides are discussed.

	Al^{3+}	Ti^{4+}	Ca^{2+}	Mg^{2+}	Mn^{2+}
Hematite		III, V, VI	IV, V, VI		
Magnetite	I, II	III, V,VI	II, IV, V, VI	II	II
Wüstite	I, II	III, V, VI	II, IV, V	II	II
Iron	I, II	III, V	II	II	II

6.1 Sintering tests

In sintering tests initial stage have been prepared and achieved for reduction experiments. Analysis of each sample prepared for and achieved in the sintering tests and the composition of phases have been presented in *Supplements I - VI*.

6.2 Dissolution of TiO_2 into iron oxides

TiO_2, up to the maximum amount used in the experiment of 5 wt.% TiO_2, is completely solid solution in hematite and magnetite. Moreover, TiO_2 was uniformly distributed and according to the SEM-EDS analysis the content was practically constant. The XRD analysis of the hematite synthesis indicated only the alpha hematite phase in all the TiO_2 contents. However, a slight shift from peaks of hematite towards peaks of ilmenite with hematite doped with 5 wt. % TiO_2 could be observed. This is logical phenomena in two oxide solid solution in which different size of impurity cations have an effect on the lattice dimension of the host oxide. In the case in which hematite is the host phase the solid solution of Ti^{4+}-cation causes also reduction of Fe^{3+} -cation to Fe^{2+}-cation (supplement 5). Increasing the TiO_2 content from 0 wt.% to 5 wt.% increased the content of Fe^{2+}-cation from <0.1 to 3.0 wt.%. Considered on an atomic level, this means that each Ti^{4+}-cation caused reduction of one Fe^{3+}-cation to Fe^{2+}-cation.

6.3 Reduction

Minor oxide components in solid solution with host oxide have a clear effect on the reduction rate of iron oxides as shown in Figure 22. As presented in *Supplement II,* the impurities were prepared identically in order to get comparable samples and a solid solution with magnetite. However, a high amount of MgO and CaO did not form a homogenous solid solution with magnetite but also magnesio-ferrite and calcium ferrite phases occurred in the prepared samples.

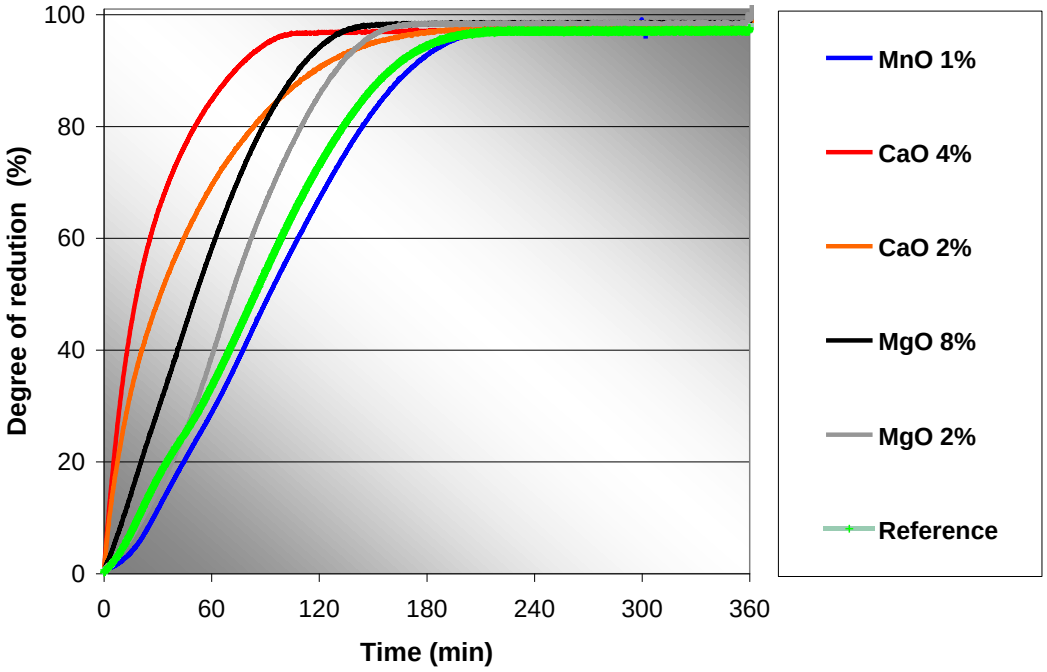

Figure 22. Results of reduction tests in TGA.

Reduction rate difference from the reference sample, i.e. undoped magnetite sample, can be seen for each impurity elements in Figure 23. In the graph, the reference curve has been diminished from every other curve to achieve a comparison for the impurity elements studied. MgO and especially CaO have a strongly accelerative effect on the reduction of magnetite. The higher the content the higher the effect was. Correspondingly, MnO decelerated reduction of magnetite when impurity content was only 1 wt. % as MnO.

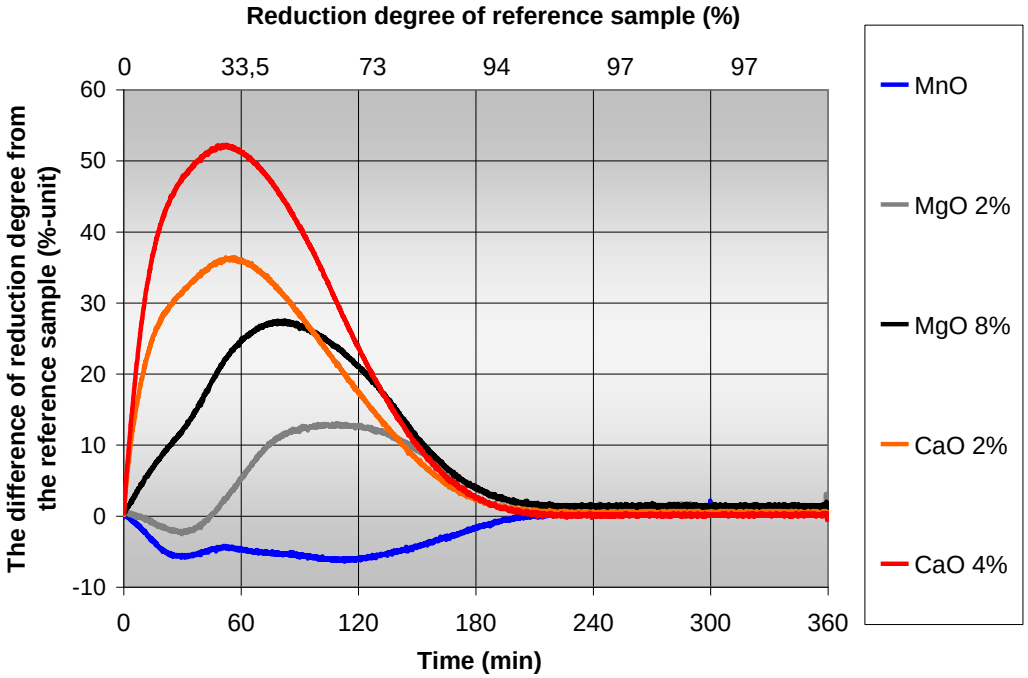

Figure 23. Comparison of reduction curves with impurity differences and with a reference sample (i.e. x-axis and value is readable form secondary x-axis)

TiO_2 has an irrelevant decelerating effect on the reduction of hematite to magnetite in the beginning of the reduction. However, angular coefficient of the reduction graph continuously rises with the experiments using the samples doped with 2 wt. % and 5 wt. % TiO_2 unlike the samples undoped and doped with 0.5 wt. %. One hour after initiating the test, the reduction process was interrupted in compliance with the standard RDI test. The results revealed that the degree of reduction exceeded 50 % with the samples doped with 2 wt. % and 5 wt. % and was approximately 20 % with samples undoped and doped with 0.5 wt. %.

6.4 Reduction of hematite to magnetite with impurities

Manufacture of iron ore agglomerate always involves thermal treatment as sintering of material. During sintering, solid diffusion occurs not only in iron oxide and foreign phases but also between them, although the treatment time is only 15 to 30 minutes. Contact of different phases and diffusion of ions are enhanced by eutectic melt between the solid phases. During sintering composition of iron oxide phases can be significantly changed and had effect on the reduction phenomena of iron ore agglomerate in the blast furnace. The solubility of different impurities on iron oxides is dependent on the properties of ions as electric charge and cation size compared with ferrications or ferrocations. When impurity cation is soluble in iron oxide, iron cation must be replaced in solid solution. In the stoichiometric iron oxides the cation replacement can be presented as follows:

In hematite

$$(Fe^{3+})_2\,(O^{2-})_3 + (Me^{3+}) \rightarrow (Fe^{3+},Me^{3+})_2\,(O^{2-})_3 \qquad \textbf{(Eq. 12)}$$

$$(Fe^{3+})_2\,(O^{2-})_3 + (Me^{4+}) \rightarrow (Fe^{3+}, Fe^{2+},Me^{4+})_2\,(O^{2-})_3 \qquad \textbf{(Eq. 13)}$$

In magnetite

$$(Fe^{3+})_2(Fe^{2+})\,(O^{2-})_4 + (Me^{3+}) \rightarrow (Fe^{3+},Me^{3+})_2(Fe^{2+})\,(O^{2-})_4 \qquad \textbf{(Eq. 14)}$$

$$(Fe^{3+})_2(Fe^{2+})\,(O^{2-})_4 + (Me^{2+}) \rightarrow (Fe^{3+},Fe^{3+})_2(Me^{2+})\,(O^{2-})_4 \qquad \textbf{(Eq. 15)}$$

In wüstite

$$(Fe^{2+})\,(O^{2-}) + (Me^{2+}) \rightarrow (Fe^{2+}, Me^{2+})\,(O^{2-}) \qquad \textbf{(Eq. 16)}$$

In the natural case all oxides are characteristically non-stoichiometric lacking anions or cations. In order to preserve charge equilibrium, vacancies are replaced by cations with higher or lower electric charge. In consequence, wüstite and magnetite have short of cations wüstite contains Fe^{3+} -cations while magnetite contains an excess of Fe^{3+} cations. Hematite contains also a small amount of Fe^{2+}, because it has short of anions. Non-stoichiometric structure can be presented with hematite:

$$\mathbf{(Fe^{3+})_2\,(O^{2+})_3 + Fe^{2+} \rightarrow (\,(1\text{-}2x)\cdot Fe^{3+},\ 2x\cdot Fe^{2+})_2\,(O^{2+})_{3-x}} \quad \textbf{(Eq. 17)}$$

and correspondingly with wüstite:

$$\mathbf{Fe^{2+}O^{2+} + Fe^{3+} \rightarrow (\,(1\text{-}2x)\cdot Fe^{2+},\ 2x\cdot Fe^{3+})_{1-x}\,O^{2+}} \quad \textbf{(Eq. 18)}$$

It is proposed that the charge equilibrium can also be preserved by impurity cation in each case.

The effect of impurities in the reduction of hematite to magnetite is dependent on the size and vacancy of impurity cation. The consequence of vacancy of impurity cation effect also on the vacancy of Fe-cation this has effect on stability of formed oxide as shown in Figure 7. In addition impurity cation has an effect on the lattice parameter value of the host mineral when impurity is dissolved in host phase. Börge et. al[54] have published a paper in

which the effect of different impurity cations in magnetite with lattice parameter has been studied. An equation for calculating the lattice parameter was the result of the publication (Eq. 19):

[841.1 - 0.30 wt. % (MgO) - 0.60 wt. % (Al_2O_3) + 0.36 wt. % (TiO_2) - 0.020 wt. % (V_2O_5) - 0.10 wt. % (Cr_2O_3) + 0.24 wt. %(MnO) - 0.17 wt. % (CoO) - I).33 wt. % (NiO) - 0.23 wt. % (Cu_2O) - 0.057 wt. % (ZnO)+ 0.52 wt. % (CdO)] pm (Eq. 19)

Expansion or shrinking of the crystal lattice, caused by impurity cation, initiates also change in the volume of crystal lattice. Comparison of volume changes of different spinel structure oxides and magnetite (belonging in spinel structure oxides) is presented in Figure 24.

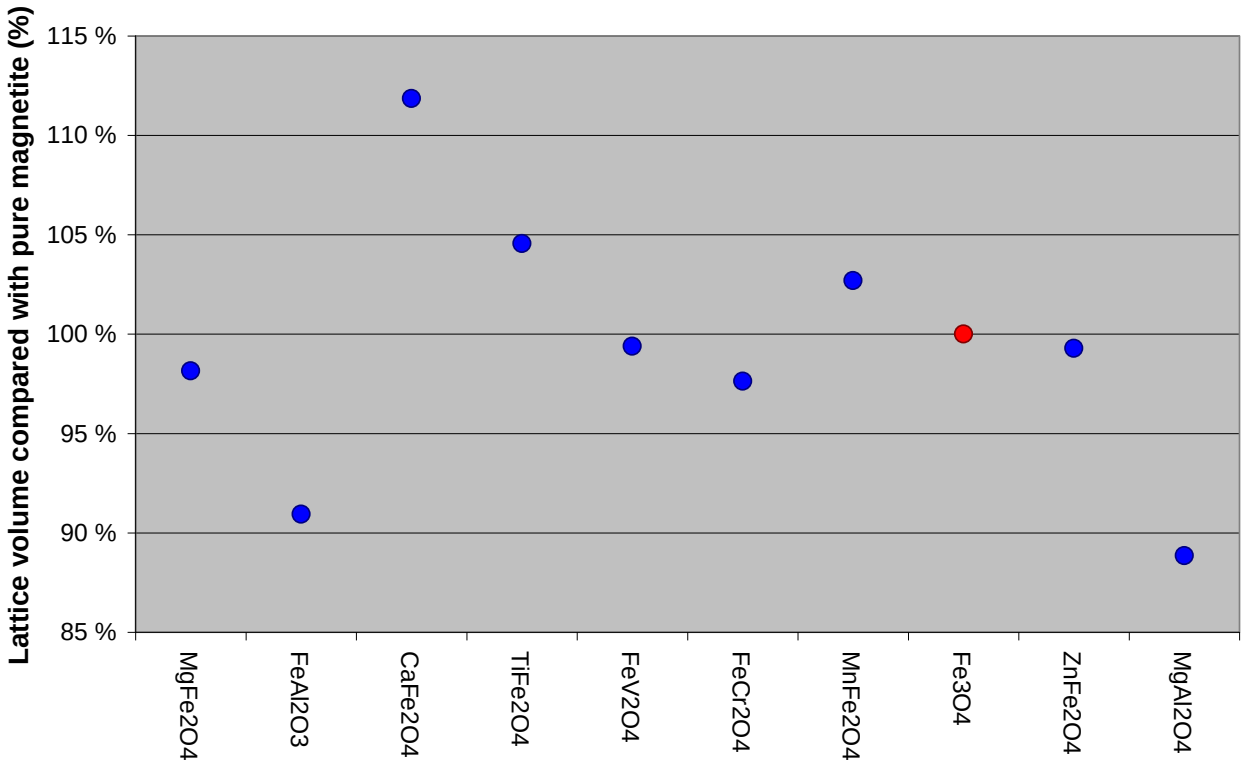

Figure 24. Lattice volume compared with magnetite based on the value of lattice parameters[54].

The volumetric changes with different "impurity"-iron solid solution oxides are mainly logical with cation sizes between iron cations and "impurity" cations (Figure 25). For example, replacing all Fe^{2+} -cations in magnetite with Ca^{2+}-cation, volumetric expansion is more than 10 %. The expansion can be forecast by comparing the cation size of Ca^{2+}- and Fe^{2+}-cations. The same logic can occur with Mg^{2+}, Mn^{2+} (Fe^{2+}) and with Al^{3+} (Fe^{3+}) -cations. Ti- cation is exception. Ti^{4+} is considerably smaller than Fe^{3+} which is replaced while spinel structure is expanded due to Ti. Ulvönspinel ($TiFe_2O_4$) is another structural exception when compared with other normal spinel structures including two divalent cations and having inverse spinel structure.

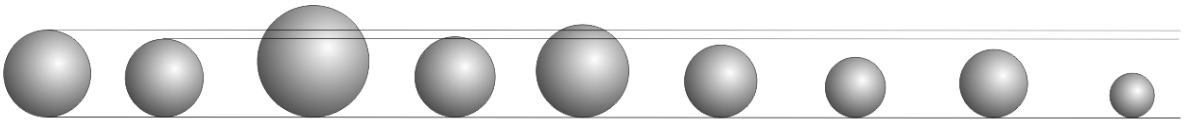

Fe^{2+} Fe^{3+} Ca^{2+} Mg^{2+} Mn^{2+} Mn^{3+} Al^{3+} Ti^{4+} Si^{4+}

Figure 25. Relative size of different cations[11, 12].

6.5 Degradation phenomena caused by low solubility of impurity in wüstite - case alumina

The presence of Al cations in magnetite induced swelling and cracking of the briquettes during reduction. Al cations have a low solubility in wüstite because of which Al cations have to diffuse in the magnetite away from the growing wüstite during the reduction (Figure 26). As the reduction process proceeds the average content of Al in magnetite increases approaching that of hercynite. This made the oxide structure shrink because the lattice volume of hercynite is smaller than that of magnetite. If the stoichiometry of wüstite is $Fe_{0.88}O$ and magnetite is pure, the structure expands about 6% during the reduction from magnetite to wüstite, but if the spinel structure is as hercynite the expansion is over 16 %. In the latter case high tensile forces are generated in the hercynite/magnetite solid solution at the interface with wüstite which presumably causes the fracturing of the structure during the reduction from hercynite/magnetite to wüstite.

Aluminium in magnetite promoted the reduction if the surface area became the limiting factor controlling the rate of reduction. The explanation for this difference is that Al cracked the structure of iron/iron oxide.

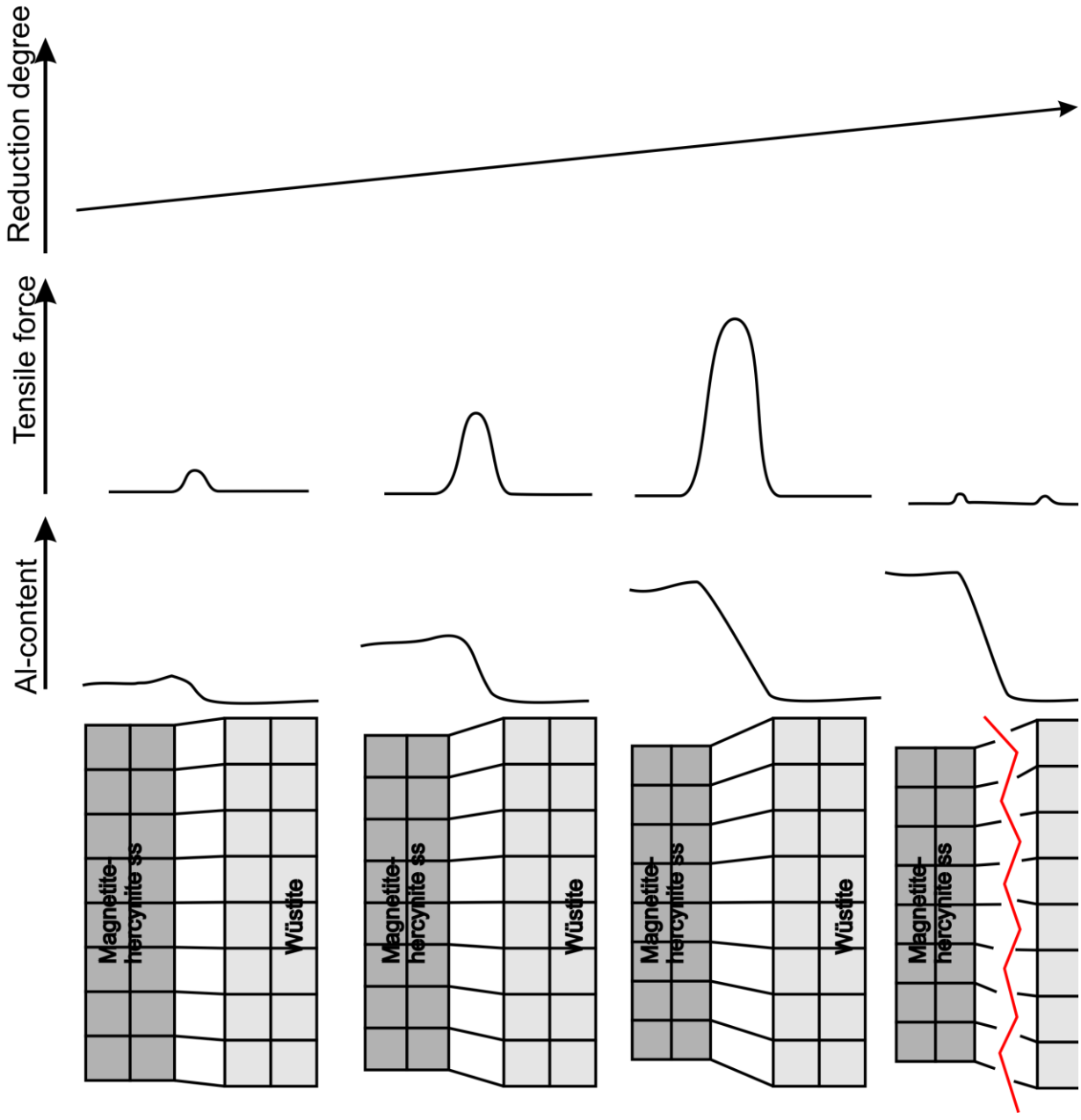

Figure 26. Schematic presentation of crack formation caused by low solubility of alumina on wüstite during reduction.

6.6 Case TiO2 - Solid solution of TiO_2 with iron oxides - Reduction and Oxidation

The effect of titanium oxide in solid solution in magnetite on the magnetite to hematite oxidation was separately studied in order to simulate the final stage of the sintering process. In the reduction experiments, hematite samples doped with various titanium oxide contents were studied using thermogravimeter under a controlled gas atmosphere ($CO/CO_2/H_2/N_2$) corresponding to the atmosphere used in RDI tests. The samples were studied using microscopy and SEM-EDS-analysis.

6.6.1 Reduction

The titanium oxide content of hematite has a clear effect on reduction degradation of the samples. The polished sections prepared from the samples reduced for 1 hour at the atmosphere corresponding to the RDI conditions are presented in Figure 27. The sharpness or front of the magnetite-hematite boundary changes less clearly when TiO_2 content of samples increases. Also the thickness of the magnetite layer on the surface of the sample is clearly wider in the samples containing more TiO_2. Magnetite layer on the undoped sample is a quite pure and no outstanding hematite relic phases can be observed contrary to the sample doped by 5 wt. % of TiO_2.

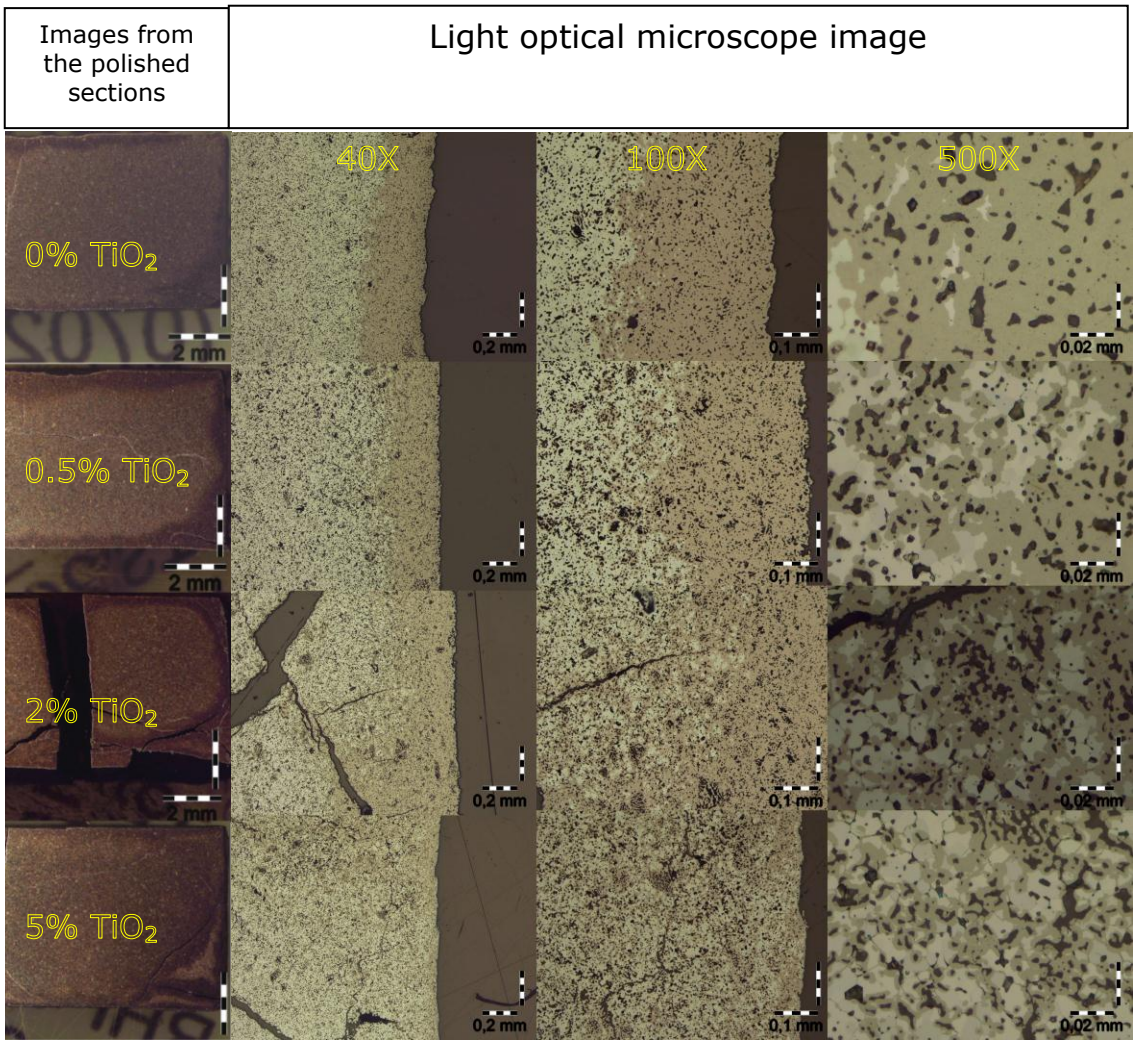

Figure 27. The polished sections prepared from the samples reduced for 1 hour at the atmosphere under conditions corresponding to those used in the RDI test.

SEM-EDS line analysis from the polished section indicates a constant Ti-content in the samples over the hematite and magnetite phases (Figure 28). Although Ti cation has been observed to favour hematite in certain cases, under the RDI conditions in which temperature is as low as 500°C, diffusion of Ti cation in magnetite is supposed to be so slow that it is not substantial.

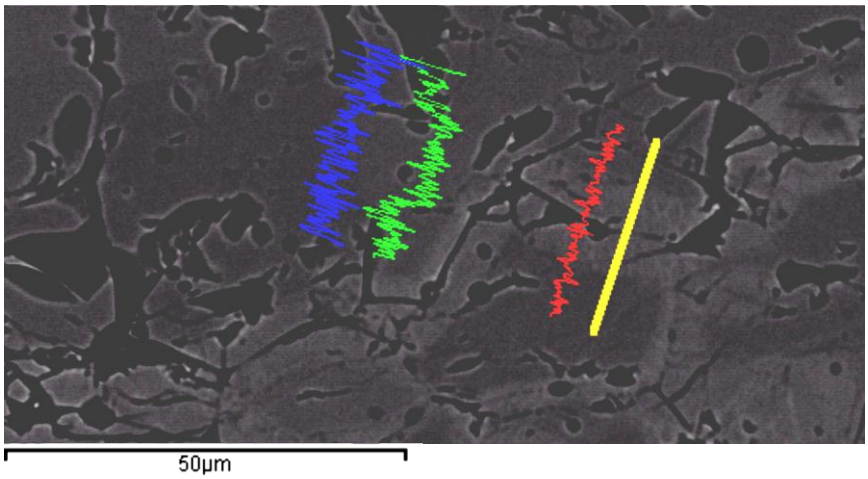

Figure 28. SEM-EDS line analysis from hematite (dark grey) grains with magnetite surface layers (light grey). The green curve represents O-content with proportional intensity, blue iron and red oxygen respectively.

6.6.2 Oxidation

Increasing titanium oxiden content in solid solution in magnetite radically accelerated the oxidation rate (Figure 29). The thickness of hematite layer after oxidation was about 5 µm in the samples doped with 0 wt. % and 0.5 wt. % TiO_2. The sample doped with 2 wt. % TiO_2 increase of hematite lamellae can be observed but significant acceleration of oxidation does not occur. The sample with 5 wt. % TiO_2 oxidation was dramatically accelerated. The layer of hematite was about 100 - 400 µm. On the other hand, the hematite layer was not a pure hematite phase but maybe includes some inclusions. Moreover, hematite lamellae can be observed.

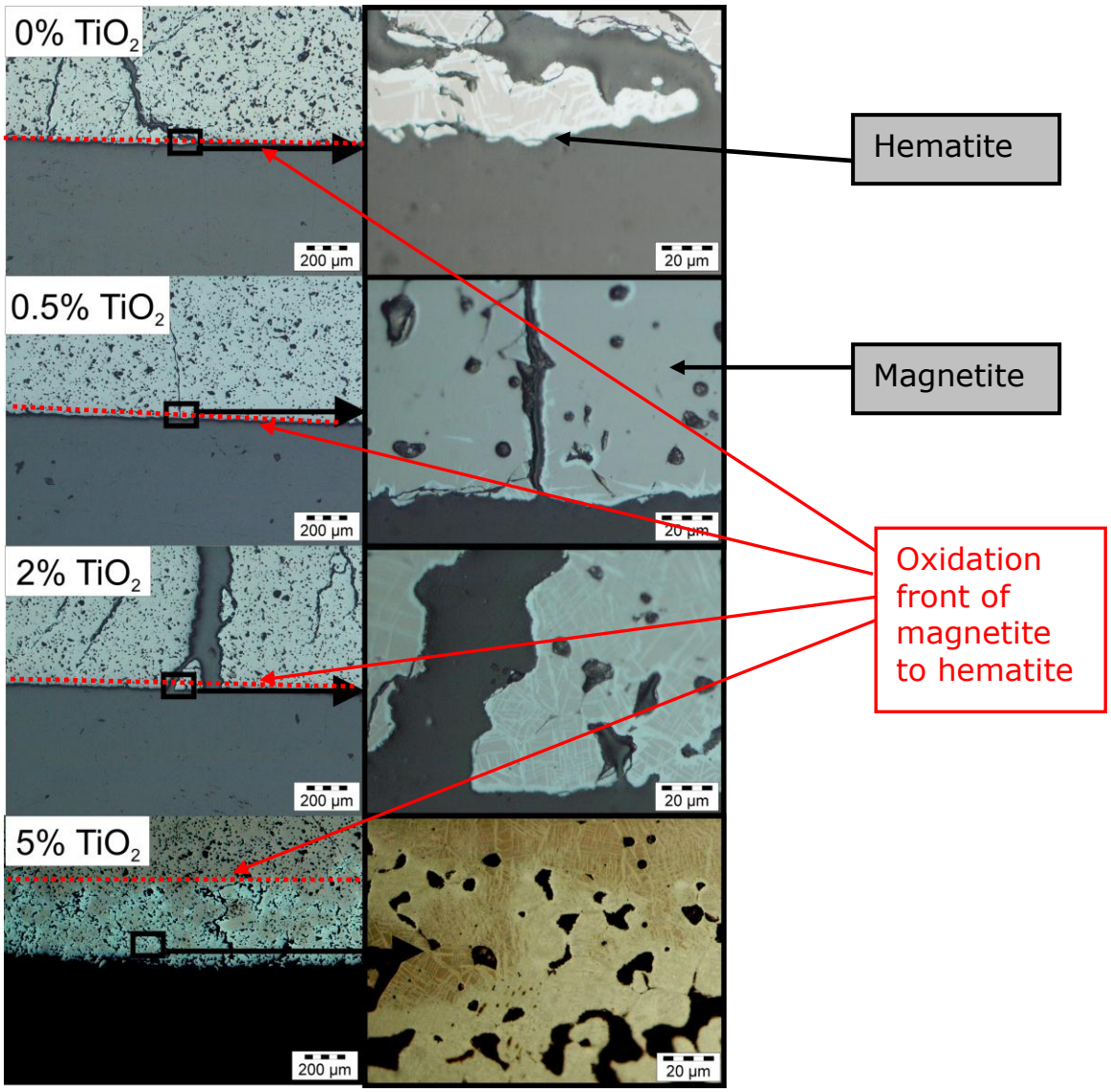

Figure 29. Comparison of microscope images from polished section prepared from magnetite samples with various TiO_2 content oxidized in 950 °C and interrupted after 15 minutes.

Being uniformly in solid solution with magnetite (5 wt. % as TiO_2) TiO_2 diffused immediately into newly formed hematite during oxidation. TiO_2 content increased from 5 wt. % up to 15 wt. % in hematite lamellae during 15 minute oxidation at 950 °C. Enrichment of TiO_2 can be seen in SEM-EDS line analysis in Figure 30 and SEM-EDS point analysis in Figure 31 in which dark grey hematite is lamellae and light grey magnetite

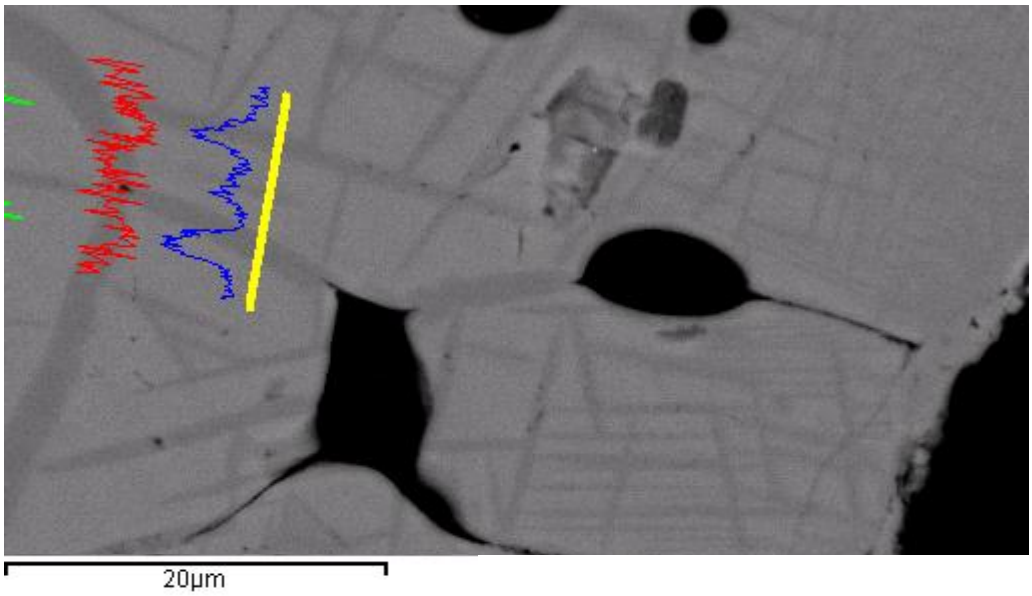

Figure 30. Increased titanium content in hematite lamellae formed in magnetite during 15 minute oxidation in 950 °C. SEM-EDS line analysis from hematite (dark grey) lamella in magnetite (light grey). The green curve represents the Ti-content with proportional intensity, blue iron and red oxygen respectively.

$$Fe^{3+}{}_2O_3 + 2\ Ti^{4+}O_2 \rightarrow 2\ Fe^{2+}Ti^{4+}O_3 + 1/2\ O_2(g) \qquad \text{(Eq. 20)}$$

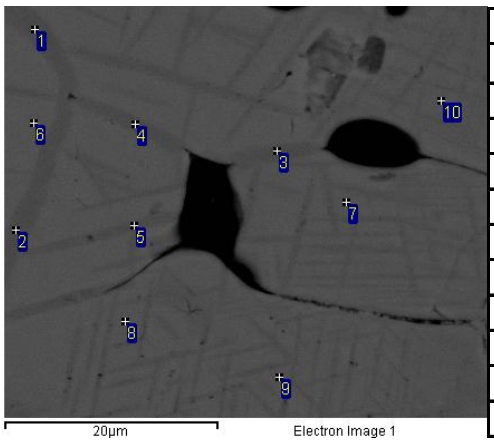

Analysed			Calculated as oxide			
Point	Ti	Fe	TiO_2	Fe_2O_3	Fe_3O_4	Sum
1	8.9	59.6	14.8	85.1		99.9
2	8.2	60.3	13.6	86.2		99.8
3	7.3	60.4	12.2	86.3		98.5
4	8.4	61.1	14.1	87.4		101.4
5	7.7	60.4	12.9	86.3		99.2
6	1.9	69.4	3.2		95.9	99.0
7	2.2	67.7	3.7		93.5	97.2
8	1.4	69.3	2.4		95.8	98.2
9	1.4	68.0	2.4		94.0	96.4
10	1.4	68.6	2.4		94.8	97.1

Figure 31. SEM-EDS analysis of hematite and magnetite phases of the sample with 5 wt. % TiO_2 doped, oxidized at 950 °C until interrupted after 15 minutes.

Inclusions smaller than 1 μm on the reaction front are presented in Figure 32.

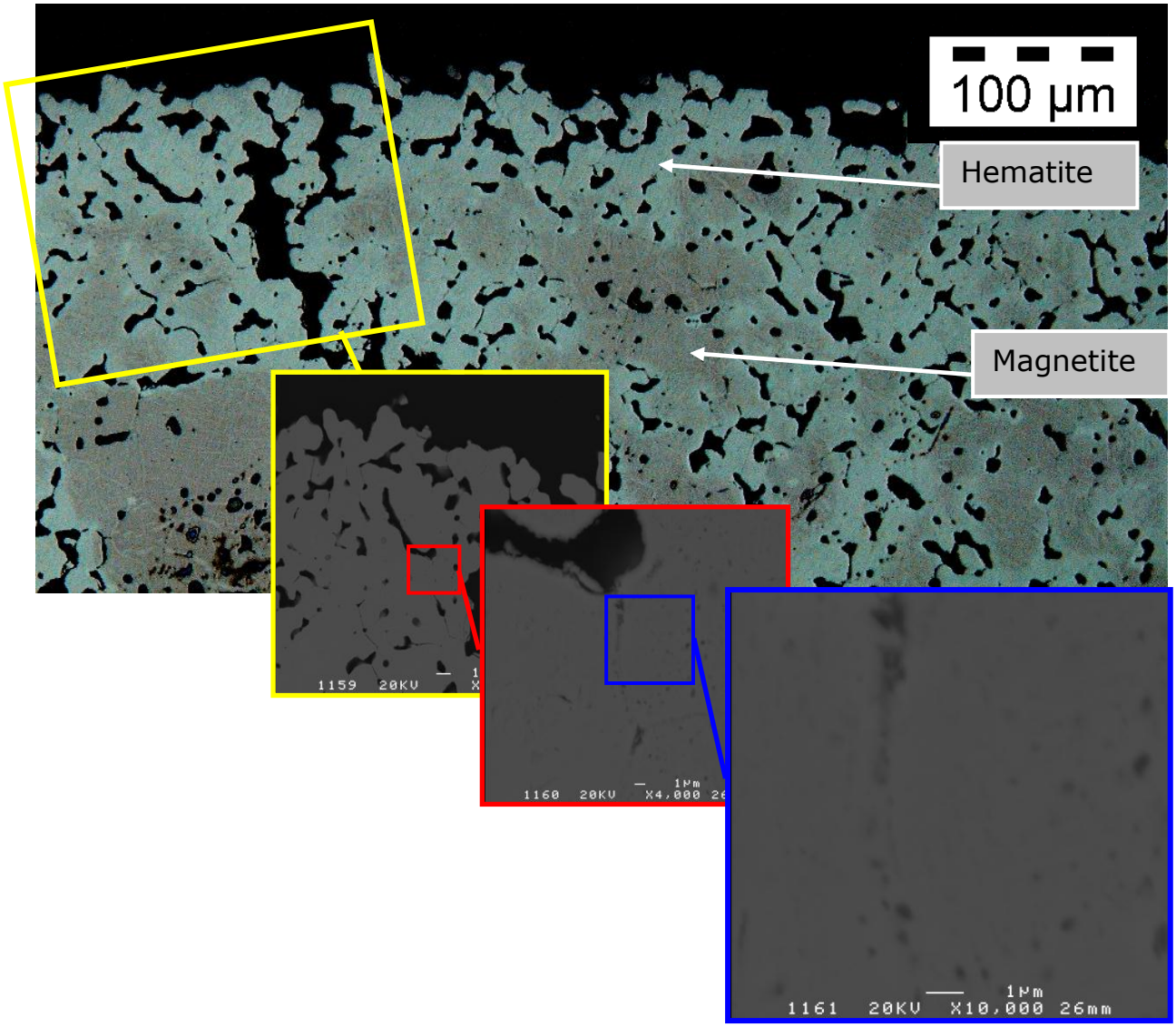

Figure 32. Light optical microscope image and SEM-images from the oxidation front in which tiny dark unknown phases within hematite can be observed.

7 CONCLUSIONS

7.1 Objectives achieved in this thesis

Modern and effective iron production makes demands for the charge material of in the blast furnace process such as pellet/sinter iron ore, coke and fluxes. The most important demands for iron burden material are high reducibility and sufficient reduction strength that enable effective reducibility of iron burden on a larger scale in the blast furnace shaft.

All iron burden materials contain impurity elements which have a significant effect on the reduction behaviour of iron oxides. The structure of the iron burden material and composition phases change as early as in the sintering process. The elements that have high solid solution with iron oxides can cause tension in the structure by changing the lattice volume of iron oxides already in the sintering stage. In the blast furnace during reduction comparability of iron oxides with an another, especially in the vicinity of lattice/grain boundary, as well as proportional volume of oxides (lattice volume), have a substantial effect on momentary strength and reducibility of the iron burden material in the blast furnace process.

Regardless of today’s advanced thermodynamic models comprehensive modelling of the reduction phenomena influenced by an impurity element is unfeasible to do. Although the effect on the thermodynamic equilibrium can

be modelled, the structural changes at various stages caused by different impurities are not known. Moreover, the changes in the material structure are essential for reduction strength and reducibility of the iron burden material.

In this thesis, the effect of an individual impurity element on reduction behaviour of iron oxides and iron burden material has been experimentally studied. The important thing to take into account experimental procedure is to produce reproducible of experiments, which include three factors:

- control of initial state as through composition, grain size, homogenity, porosity of prepared sample
- control of experimental properties such as temperature, gas composition, reproducibility, cooling
- control of analysis through preparation of samples for different analyses, interpretation of results.

A correlation between the concentration of dissolved alumina and the degree of degradation of iron oxides during reduction has been discussed in many papers. The fundamental mechanism behind the degradation was studied in this study.

The reduction degradation strength seems to have quite a clear but sometimes ambiguous impact on the blast furnace process. The RDI is

affected by several factors but variation in TiO_2 content was observed to be the most significant factor, while other variables were quite stable.

In the case of aluminium the degradation mechanism of iron oxides caused by alumina during reduction from magnetite to wüstite was studied with the conclusions are:

- The presence of Al cations in magnetite induced swelling and cracking of the briquettes during reduction.
- Because of the low solubility of Al cations in wüstite during the reduction of Al_2O_3 doped magnetite to wüstite Al cations have to diffuse in the magnetite in the opposite direction from the growing wüstite. As the reduction process proceeds the average content of Al in magnetite increases approaching that of hercynite.
- If the stoichiometry of wüstite is $Fe_{0.88}O$ and magnetite is pure, the structure expands about 6 % during the reduction from magnetite to wüstite, but if the spinel structure is that of hercynite the expansion is over 16 %. In the latter case, high tensile forces are generated in the hercynite/magnetite solid solution at the interface with the wüstite which presumably causes the fracturing of the structure during the reduction from hercynite/magnetite to wüstite.
- Aluminium in magnetite promoted the reduction, provided the surface area became the limiting factor controlling the rate of reduction. The explanation for this difference is that Al cracked the structure of iron/iron oxide.

The main results regarding TiO_2 in this study are:

- The increase in TiO_2-content deteriorates clearly the RDI index of test sinter using both rutile and crushed hematite pellets containing TiO_2 as additives although the change in the TiO_2 content was quite small.
- TiO_2 additions to test sinter mix increased the amount of hematite phase in sinter.
- The higher the TiO_2 content in doped hematite briquettes the more significant their disintegration which was detected visually and also by a microscope.
- Oxidation of TiO_2 doped magnetite briquettes showed that increase in the TiO_2 content of magnetite accelerated the oxidation of magnetite to hematite.

The degradation mechanism demands further study but the phenomenon seems to occur in the magnetite phase during low temperature reduction.

7.2 Recommendations for further research

Single component effect on reduction behaviour of iron oxides was investigated in the thesis. However some preliminary experiments were executed with two and three component systems (Figure 33 and Figure 34). Preliminary results showed that the results are unforeseen and therefore additional investigation is needed. One impurity with a poor and decelerating

effect can perhaps be compensated by another. It is also possible that two components, having one by one accelerative effect on the reduction, simultaneously together have a negative effect on the reduction.

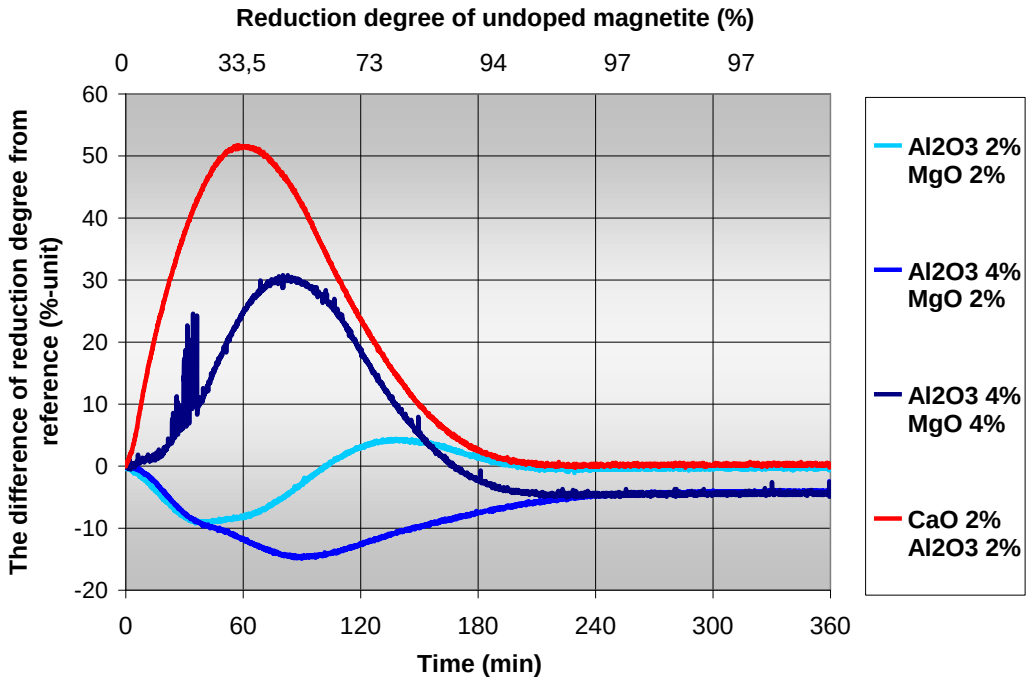

Figure 33. Effect of two impurities simultaneously on reduction of magnetite.

The important thing to take into account in the investigation, when sample for multi-component system is prepared, is that the initial stage of a sample is confirmed and identified. Also the preparation procedure and details mentioned in Chapter 4 should be considered.

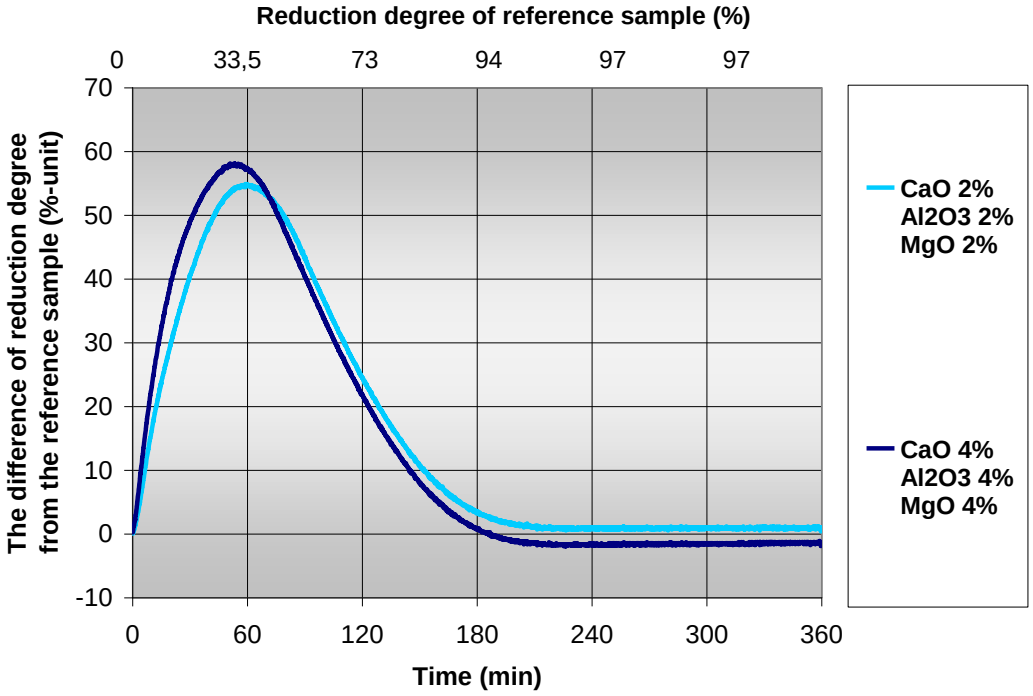

Figure 34. Effect of three impurities simultaneously on reduction of magnetite.

Degradation mechanism demands further study but the phenomenon seems to occur in the magnetite phase during low temperature reduction. However, other phases in some mineralogical structures may also react under the RDI test conditions and are capable of dissolving TiO_2. They, too, require further study.

A limitation to the research was the insufficient resolution and analysis accuracy of the scanning electron microscopy to identify small phases (under 100 nm diameter) on the grain boundary of hematite magnetite when titanium containing iron oxides were reduced. In order to get more information about the mechanism and reduction phenomenon higher

resolution for identification would be required. Recommendation for further research is to use transmission electron microscopy (TEM). In this thesis, static reduction experiments were executed, but recommendation for further research is to use a precision-controlled reduction programme to simulate the conditions corresponding to those in the blast furnace shaft. Also a further in-depth research for multi-component system would be needed with static and dynamic reduction experiments.

8 REFERENCES

[1] International standard ISO 4700:2007 (E), Iron ore pellets for blast furnace and direct reduction feedstocks - Determination of the crushing strength.

[2] International standard ISO 3271 1995 (E). Iron ores - Determintation of tumble strength.

[3] International ISO9001 standard ISO4696-1. Iron ores - Static test for low-temperature reduction-disintegration.

[4] International standard ISO 13930:1998 (E), Iron ores - Dynamic test for low-temperature reduction disintegration.

[5] Heinänen, K, 1993. Mineralogy and Metallurgical Properties of iron Ore Sinter Based on Magnetite Fines. Thesis for the Degree of Doctor of Philosophy, University of Helsinki, Finland

[6] Kinnunen K, Heinänen K, 2005. The reduction Degradation Property of Iron Ore Sinter. The 5th European Coke and ironmaking Congress, Proceedings, Vol. 2, 2005, pp Tu12:3 1-13.

[7] Murty C.H., De A., Chatterjee A. and Rao V.-S.: Reduction of alumina in iron ore classifier fines and its influence on sinter. ISSN 0971-5975,) Tata Searh, 1994, pp. 7-13 (Reprinted from International Journal of Minerals, Metals and Materials Engineering, 59(5), 2006, pp 551-568.

[8] Heinänen K. & Kinnunen, K.: Viimeisimpiä tutkimustuloksia raudanvalmistuksen prosesseista, Presentation collected from process data 2001 - 2004. Rautaruukki Oyj (19.8.2004).

[9] Waychunas G A. Crystal chemistry of oxides and oxyhydroxides. In: Lindsley D. H: Reviews in mineralogy Volume 25. Oxide minerals: Petrologic and magnetic significance. Mineralogical Society of America, Washington, 1991, Ch. 2., pp. 11 - 68.

[10] Von Bogdandy L and Engell H.J.: The reduction of iron ores - scientific basis and technology, Springer - Verlag, Berlin 1971. 576 s.

[11] Klein, C. and Hurlbut, C. S. Jr.(after Dana J.D.). Manual of Mineralogy. New York 1993, John Wiley and Sons, Inc. Ch. 12.

[12] Klein C (after Dana J.D.): The 22nd edition of the manual of mineral science. John Wiley & sons, inc., New York, 2002, 641 p.

[13] Deer W. A., Howie R. A. & Zussman J.: An introduction to the Rock-Forming Minerals, 2nd edition, Pearson Education Limited, Harlow 1992, 696 p.

[14] Biswas, A.K.: Principles of Blast Furnace Ironmaking, Cootha Publishing House, Australia, 1981.

[15] Shchepetkin, A. A. & Chufarov, G. I.: Dissociation of solid solutions of oxides in metal-iron-oxygen systems under equilibrium conditions, Zh. Neorg. Khim., 17 [6] 1533 – 1537 (1972). Engl. Transl: Russ. J. Inorg. Chem., 17, [6], 792 – 794, 1972.

[16] Roller P.W: The Theoretical Volume Decrease on Reduction of Hematite to Magnetite. Transaction ISIJ, 26(1986)9, pp. 834-835.

[17] Sasaki Y., Bahgat M.Iguchi M. and Ishii K.: The preferable growth direction of iron nuclei on wüstite surface during reduction, ISIJ, 45(2005)8, pp. 1077 – 1083.

[18] El-Geassy A.A.: Stepwise Reduction of CaO and/or MgO Doped-Fe2O3 Compacts to Magnetite Then Subsequently to Iron at 1173-1473 K. ISIJ International 37(1997)9, pp. 844-853.

[19] de Bruijin W.: The reduction of iron oxides with special reference to the presence of foreign elements, PhD Thesis, Delft University, 1990, p. 183.

[20] R. Piepenbrock: Doctor Thesis, Technical University of Clausthal, 1974, p. 35.

[21] Edström, J.O.: The mechanism of reduction of iron oxides. Journal of the iron and steel institute, 175(1953)11, pp. 289 - 304.

[22] Y. Iguchi, Y. Uyeda and S. Hayashi: ICSTI, ISIJ, Sendai, 1994, p. 92.

[23] T. El Kasabgy and W.-K. Lu: The Influence of calcia and magnesia in wustite on the kinetics of metallization and iron whisker formation. Metall. Trans. B, 11B (1980) No.3, pp. 409-414.

[24] S. Geva, M. Farren, D.H. St. John and P.C. Hayes: The effects of impurity elements on the reduction of wustite and magnetite to iron in CO/CO_2 and H_2/H_2O gas mixtures. Met. Trans. B, 21B (1990), No 4, pp. 743-751.

[25] K. Takahashi, M. Asada and M. Kawakami: ICSTI/Ironmaking Conference Proceedings, ISS, Toronto, 1998, p. 1705.

[25] J. Härkki: Doctor Thesis, Technical University of Helsinki, 1978, p. 32.

[26] J. Molenda, A. Stoklosa and H. Soliman: Transport properties of manganese-doped ferrous oxide at high temperature. Solid State Ionics, 45 (1991), 109-121

[27] Kim, J-R, Je, J-H, Jeong, S-K, 2003. Behavior of reduction degradation of sintered ore by synchrotron X-rays. Iron & Steel Society International Technology Conference and Exposition 2003; Indianapolis, IN; USA; 27-30 Apr. 2003. pp 175-180.

[28] Lecomte P, 1971. Vidal R. Study on the reduction strength of sinter. Metallurgical Reports C. R. M., No. 26 (March 1971), pp 5-14.

[29] Grebe, K, Sticker, K-P, Winzer, G, Engel, K, 1991. Unexpected Phenomena of Burden Behaviour in Blast Furnaces and Their Impact on Control Strategies. Ironmaking Conference Proceedings. Vol. 50; Washington, DC; USA; 14-17 Apr. 1991. pp 379-394.

[30] Panigrahy, S C, Rigaud, M, Dilewijns J, 1984. Effect of MgO on low temperature reduction strength. Iron and Steel Int., Feb. 1984, pp 29 – 33.

[31] Mishra, U N, Thakur, B, Mediratta, S R, 1996. Control of sinter quality for blast furnaces of SAIL through characterisation of high temperature properties. Ironmaking Conference Proceedings. Volume 55; Pittsburgh, Pennsylvania; USA; 24-27 Mar. 1996. pp 407-412.

[32] Hsieh, L-H, Whiteman, J A, 1993. Effect of Raw Material Composition on the Mineral Phases in Lime-Fluxed Iron Ore Sinter. ISIJ International, 33(1993)4, pp 462-473.

[33] Pimenta, H P, Seshadri, V, 2002. Influence of Al sub 2 O sub 3 and TiO sub 2 on reduction degradation behaviour of sinter and hematite at low temperatures. Ironmaking and Steelmaking (UK). Vol. 29, no. 3, pp 175-179. June 2002

[34] Kim, H S, Park, J H, Cho, Y C, 2002. Crystal structure of calcium and aluminium silicoferrite in iron ore sinter. Ironmaking and Steelmaking (UK). Vol. 29, no. 4, pp 266-270. Aug. 2002.

[35] Pimenta, H P, Seshadri, V, Cardoso, M B, Azevedo, A T, 1993. Influence of Al sub 2 O sub 3 and TiO sub 2 on the reduction degradation behaviour of sinter and hematite at low temperatures. Sixth International Symposium on Agglomeration; Nagoya; Japan; 15-17 Nov. 1993. pp 332-337. 1994

[36] Pimenta, H P, Seshadri, V, 2002. Characterisation of structure of iron ore sinter and its behaviour during reduction at low temperatures. Ironmaking and Steelmaking (UK). Vol. 29, no. 3, pp 169-174. June 2002.

[37] Loo, C E, Bristow, N J, 1993. Resistibility of iron ore sinters to low-temperature reduction degradation. Sixth International Symposium on Agglomeration; Nagoya; Japan; 15-17 Nov. 1993. pp 338-343. 1994

[38] Bristow N J, Loo C E, 1992. Sintering Properties of Iron Ore Mixes Containing Titanium. ISIJ International, 32(1992)7, pp 819-828.

[39] Kinnunen K. & Laitinen P.: Investigation of Sinter Plant production Rate and RDI using Neural Networks. In: Revue de Metallurgie, Cahiers d'Informations Techniques. No. 25es Journees Siderurgiques Int. 2004 Suppl, pp 144-145.

[40] Yang L. X. & Matthews E.: Sintering reactions of magnetite concentrates under various atmospheres. ISIJ International, 37(1997)11, pp 1057-1065.

[41] Panigrahy S. C., Verstraeten P. and Dilewijns J.: Influence of MgO Addition on Mineralogy of Iron Ore Sinter. Metallurgical Transactions B, Vol. 15B, (1984), pp 23 – 32.

[42] Karinen, Tuomo: Doctoral thesis. The Koillismaa Intrusion, northeastern Finland – evidence for PGE reef forming processes in the layered series. Geological Survey of Finland, Bulletin 404, 2010, 176 p.

[43] Tanskanen P and Paananen T.: Emäksisen sintterin mineraloginen karakterisointi. Report II in Stara-project, University of Oulu, 2008.

[44] Forsmo, S.: Influence of Green Pellet Properties on Pelletizing of Magnetite Iron Ore, Doctoral Thesis, Luleå University of Technology, 2007.

[45] Analysis data of Ruukki Metals Oy.

[46] LKAB Products 2012, 53 p.

[47] Ryösä, E.: Mineral Reactions and Slag Formation During Reduction of Olivine Blast Furnace Pellets, Doctor thesis, Acta Universitaties Upsaliensis, Uppsala, 2008.

[48] Tanskanen P., Paananen T. Huttunen S. & Talonen A-M.: Panama-project Final report, University of Oulu, Laboratory of Process Metallurgy, 18.4.2005.

[49] Presentation material of Ruukki.

[50] Hooey, P L, 1999. Reduction and High temperature Behaviour of Iron Ore Sinter Made from Magnetite Fines. Thesis for the Degree of Doctor of Technology, May 1999, University of Oulu, Department of Process Engineering.

[51] Paananen T.: Synteetisten materiaalien valmistus ja pelkistys. Report III in STARA-project, University of Oulu, Laboratory of Process Metallurgy, 2008.

[52] Haapanen Satu, Work instruction of Ruukki, 6215023, 2-Arvoisen raudan (Fe2+) määritys. Potentiometrinen titraus. 27.7.2010.

[53] Haapanen Satu: Work instruction of Ruukki, 6215025 A, Kokonaisrautapitoisuuden määritys mikroaaltouuniliuotuksella. Potentiometrinen titraus. 27.7.2010.

[54] Holme B., Skaugset P., Taftö J.: Microstructure of reduced magnetite as a function of aluminum content and reduction temperature, Applied Catalysis A: General 162 (1997) 149-159.

SUPPLEMENT I

PAANANEN T, HEINÄNEN K & HÄRKKI J: DEGRADATION OF IRON OXIDE CAUSED BY ALUMINA DURING REDUCTION FROM MAGNETITE, ISIJ INTERNATIONAL, 2003, PP. 597-605.

SUPPLEMENT I

Paananen T, Heinänen K & Härkki J: Degradation of Iron Oxide Caused by Alumina during Reduction from Magnetite, ISIJ International, 2003, pp. 597 - 605.

SUPPLEMENT I

PAANANEN T, HEINÄNEN K & HÄRKKI J: DEGRADATION OF IRON OXIDE CAUSED BY ALUMINA DURING REDUCTION FROM MAGNETITE, ISIJ INTERNATIONAL, 2003, PP. 597-605.

ISIJ International, Vol. 43 (2003), No. 5, pp. 597–605

Degradation of Iron Oxide Caused by Alumina during Reduction from Magnetite

Timo PAANANEN, Kyösti HEINÄNEN[1)] and Jouko HÄRKKI

Laboratory of Process Metallurgy Department of Environmental and Process Engineering, P.O. BOX 4300, 90014 OULUN YLIOPISTO, Finland. E-mail: Timo.Paananen@oulu.fi 1) RAUTARUUKKI OYJ Corporate R&D, P.O. Box 93, FIN-92101 RAAHE Finland.

(*Received on June 28, 2002; accepted in final form on December 13, 2002*)

The degradation mechanism of iron oxides caused by alumina during reduction from magnetite has been studied. The experiments were carried out by reducing briquettes containing various mixtures of commercial magnetite fines and Al_2O_3 in a CO/CO_2 atmosphere at 950°C in thermo-gravimetric equipment. Following reduction, samples were examined using optical microscopy, SEM-EDS and XRD.

The diffusion of Al cations into the magnetite during reduction induces swelling and cracking of the briquettes. The composition of the magnetite phase approaches the composition of hercynite during reduction. Assuming the spinel structure is that of hercynite, reduction to non-stoichiometric wüstite ($Fe_{0.88}O$) causes an expansion of over 16%. This transformation causes high tension forces in the magnetite/hercynite phase in the vicinity of the interface with the wüstite which presumably account for the breakdown of the structure during the reduction.

KEY WORDS: degradation; degradation mechanism; reduction; hercynite; magnetite; wüstite; alumina.

1. Introduction

The effects of alumina on the degradation of iron oxides during reduction have been investigated much recently by evaluating reduction degradation index (RDI). A correlation between the concentration of dissolved alumina and the degree of degradation of iron oxides during reduction has been shown in many papers.[1–3)] The fundamental mechanism behind the degradation has not however been revealed. The deleterious effect of alumina on RDI is associated with the hematite–magnetite reduction step or the effect of aluminium on calcium ferrite.[1)]

The effect of alumina on pore radius in the reduction of wüstite, has been examined by Suzuki *et al.*[4)] using H_2/H_2O-reduction and Iguchi *et al.*[5)] using CO/CO_2-reduction. Both of them noticed that alumina reduces the pore size in iron formed by the reduction. De Bruijn examined the effects of additives on the reduction of hematite under dynamic conditions (gas, temperature) and concluded that Al dissolved in iron oxide retarded the reduction by forming a hercynite cover between the iron oxide and iron.[6)] On the other hand according to Piepenbrock[7)] reduction is promoted by the formation of hercynite, because the reduction proceeds along the grain boundaries intersected by the hercynite. The effect of additives in hematite pellets on reduction swelling and the crushing strength has been studied by Sharma *et al.*[8)] Alumina clearly decreased the crushing strength. The swelling of the alumina bearing pellets was less than that of the pure pellets, but not as low as that in pellets containing other additives like CaO, SiO_2 and MgO. All the above phenomena are related to the reduction mechanism. The cation size of the additive and its solubility in iron oxides has a very significant effect on the mechanisms in the all the hematite→magnetite→wüstite→iron reduction steps.

Crystallography is an important tool when researching reduction and reduction mechanisms of iron oxides. Reduction from magnetite to wüstite means forming of wüstite phase in magnetite. Crystal structure of both mineral phases is based on cubic crystal system. Magnetite has an inverse spinel structure and wüstite has a halite structure.[9,10)] In the reduction process, crystallographic orientation of the host magnetite and wüstite replacing it are detected to be epitaxial.[11)] With hydrogen reduction orientation relations of both (100) magnetite // (100) wüstite and (011) magnetite // (011) wüstite has been found.[12)] In the case of oxidation from steel orientation relations as (100) steel // (100) wüstite // (100) magnetite has been identified.[13)]

In the present work, the degradation mechanism of iron oxides caused by alumina during reduction from magnetite has been studied.

2. Experimental

2.1. Materials

The test material comprised commercial magnetite fines from a Swedish mine mixed with various amounts of Al_2O_3. The magnetite content of the fines was 96.1 wt% and the total iron oxide content, including hematite, was about 97.8

SUPPLEMENT I

PAANANEN T, HEINÄNEN K & HÄRKKI J: DEGRADATION OF IRON OXIDE CAUSED BY ALUMINA DURING REDUCTION FROM MAGNETITE, ISIJ INTERNATIONAL, 2003, PP. 597-605.

wt%. The most significant quantities of other oxides are shown in **Table 1**.

The aluminium additive was α-Al_2O_3 powder with a grain size of less than 44 μm and a purity of 99.99%.

2.2. Preparation of Samples

The magnetite concentrate was ground and sieved into a grain size less than 74 μm. Then α-Al_2O_3 was mixed into the fines in amounts corresponding to 0.95, 1.89 or 3.78 wt%. The powder mix to which about 15 wt% of purified ethyl alcohol had been added was pressed into the briquettes with compressive stress of 50 MPa. The wet briquettes were dried at 110°C for a few hours.

2.2.1. Preparation of Porous Samples for Reduction (Program A)

The briquettes (23ϕ×5 mm) were first heated in a 34 mm diameter tube furnace at 900°C for 2 h in a CO/ CO_2 atmosphere (CO/CO_2=5/95 and flow rate 2 *l*/min). The hot briquettes were quenched into water and afterward dried at 110°C for a few hours. The dry briquettes were ground and pressed again into briquettes. The heating program described above was performed three times but on the last time, the briquettes were prepared smaller (12ϕ×5 mm). In order to achieve porous structure for more extensive surface area of reaction between iron oxide and reduction gas the samples were not heated after the last pressing process.

2.2.2. Preparation of Dense Samples for Reduction (Program B)

The ground and sieved powder mix was pressed to the briquettes (12ϕ×5 mm) as described above and sintered in a 76 mm diameter tube furnace at 1395°C for 2 h in a CO/ CO_2 atmosphere (CO/CO_2=5/95 and flow rate 8 *l*/min). The briquettes were quickly quenched into water after sintering. After drying the briquettes were ready for the reduction experiments. The aim was to make compact and dense briquettes for topochemical reaction during the reduction.

2.3. Reduction of Samples

Briquettes prepared using programs A and B were reduced in the 34 mm diameter tube furnace, in a reducing gas mixture of CO and CO_2 with a flow rate of 2 *l*/min. The CO/CO_2 ratio was kept constant at 90/10 during the experiments. The reduction temperature was maintained constant at 950°C during the reduction. Before the reduction, the sample was first heated in an argon atmosphere, to about 400°C for 10 min and the heated to 950°C. In order to achieve over 90% reduction, the reduction time was 180–200 min using program A for the porous samples and 450 min using program B for the dense samples. The dense briquettes were also performed the experiments using reduction was interrupted after 30 min.

During the reduction test the sample was held in a platinum basket hanging on a gravimeter connected to a computer for data collecting. After the reduction, briquettes were quenched into water and dried at 110°C.

2.4. Mineralogical and Microprobe Chemical Analyses

Microprobe analyses were performed with a JEOL JSM-6400 scanning electron microscope using energy dispersive spectrometry. The equipment included a digital camera and an Oxford Instruments Inca 3.03 software for evaluation of the analyses. An accelerating voltage of 15 kV and a beam current of 120 nA were used.

Crystallographic analyses were made using a Siemens D5000 X-ray powder diffractometer with Mo Kα radiation. Phase identifications from the diffraction patterns were done with the aid of EVA application software 5.0.1.8.

The samples were also examined with an Olympus BX51 optical microscope.

Table 1. The oxide contents of the magnetite fines, wt%.

Fe_3O_4	Fe_2O_3	SiO_2	TiO_2	MgO	Al_2O_3	V_2O_5	CaO	others
96.10	1.70	0.60	0.40	0.40	0.25	0.24	0.18	0.07

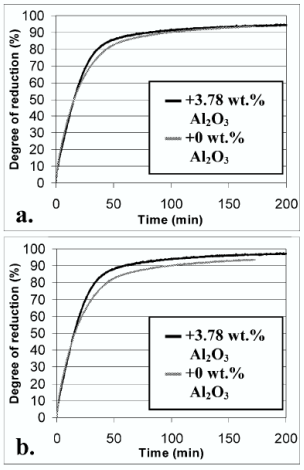

Fig. 1. Reduction curve of doped and un-doped samples, where aluminium is assumed to be (a) Al_2O_3 and (b) bound with FeO as hercynite.

3. Results

3.1. The Reduction Process

3.1.1. Porous Samples (Program A)

Figure 1 shows reduction results. The percentage reduction was calculated from the specimen mass by assuming the decrease was caused by loss of oxygen from iron oxide. The porous briquettes were reduced rapidly and more than 90% reduction was achieved after 80 min. Aluminium did not retard the rate of reduction but, rather, caused it to accelerate after 60% degree of reduction. Aluminium oxide is not reduced under the prevailing conditions; however, it can exist either as Al_2O_3 or hercynite ($FeO \cdot Al_2O_3$). The calculated degree of reduction depends whether aluminium is assumed to be present as pure Al_2O_3 or as $FeO \cdot Al_2O_3$. In the latter case the oxygen of FeO component is excluded from the calculation base.

The briquettes made from magnetite concentrate with no Al_2O_3 addition withstood reduction and cooling very well but Al-doped samples did not, being prone to swelling and cracking as shown in **Fig. 2**.

ISIJ International, Vol. 43 (2003), No. 5

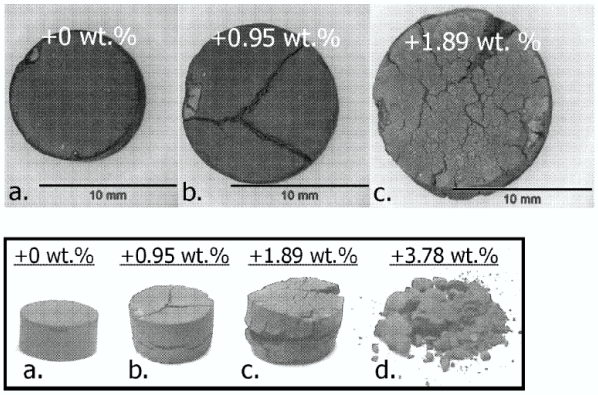

Fig. 2. Appearance of the heated (program A) briquettes, where were increased 0 wt%, 0.95 wt%, 1.89 wt% and 3.78 wt% Al_2O_3, after the reduction (950°C, CO/CO_2=90/10). The upper photographs are showed the briquettes with scale bar interrelated and the lower ones are shown distant shots from same briquettes.

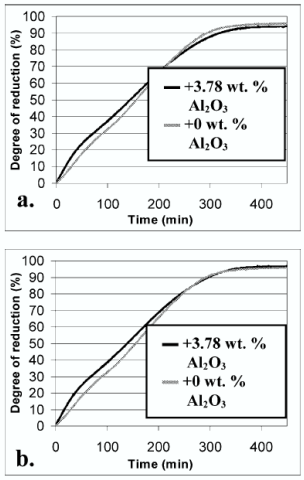

Fig. 3. Reduction curve of doped and un-doped samples, where aluminium is assumed to be (a) Al_2O_3 and (b) bound with FeO as hercynite.

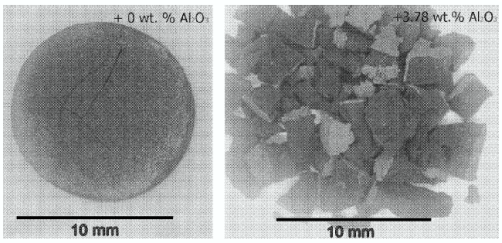

Fig. 4. Appearance of the sintered (program B) briquettes, where were increased 0 wt% and 3.78 wt% Al_2O_3, after the reduction (950°C, CO/CO_2=90/10).

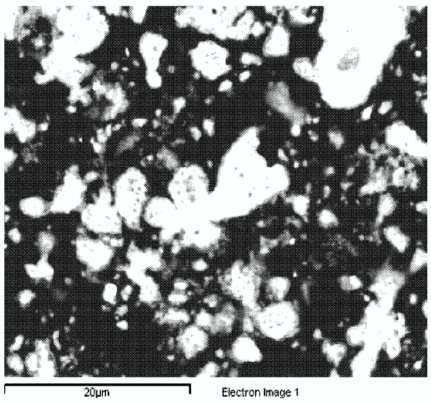

Fig. 5. SEM BSE compo image (3 000×) of a reduced sample, where was increased 3.78 wt% Al_2O_3. The white colour is iron and the darker spots are probably mainly magnetite–hercynite solid solutions.

3.1.2. Dense Briquettes (Program B)

The densely sintered briquettes with no Al_2O_3 (program B) did not break down during or after reduction though a small amounts of very small cracks could be observed (**Fig. 4**). On the other hand Al-doped samples were broken down as shown in Fig. 4. The reduction process took more time because of the denser structure (**Fig. 3**). At the beginning of the reduction process, the Al-doped briquettes were clearly reduced faster than the un-doped briquettes, as shown in Fig. 3. The difference in the degree of reduction at the end of the experiments depends on the assumptions made in the calculation.

3.2. SEM-EDS Analysis

3.2.1. Porous Samples (Program A)

The presence of aluminium in the magnetite phase was observed using SEM-EDS analysis. SEM images showed that there were very small relic phase, which was thought to be magnetite–hercynite solid solution, in the iron phase as shown in **Fig. 5**. The contents of aluminium in those small particles could not be quantified using SEM-EDS analysis because of their very small size. This was the main reason

SUPPLEMENT I

PAANANEN T, HEINÄNEN K & HÄRKKI J: DEGRADATION OF IRON OXIDE CAUSED BY ALUMINA DURING REDUCTION FROM MAGNETITE, ISIJ INTERNATIONAL, 2003, PP. 597-605.

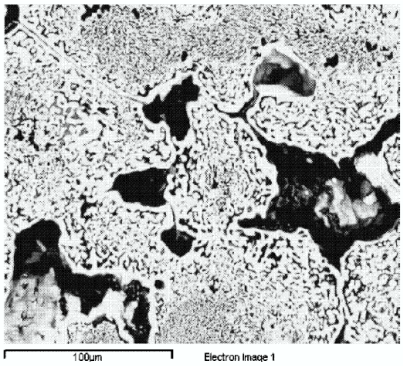

Fig. 6. SEM BSE compo image (500×) of an un-doped sample after reduction.

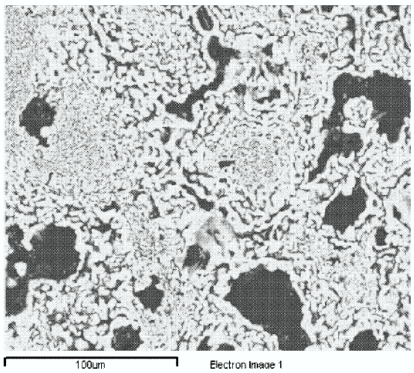

Fig. 7. SEM BSE compo image (500×) of a doped sample (+3.78 wt% Al_2O_3) after reduction.

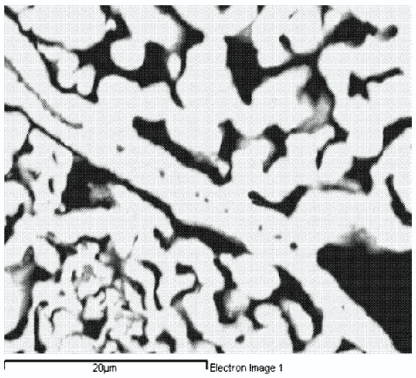

Fig. 8. SEM BSE compo image (3 000×) of an un-doped sample after reduction.

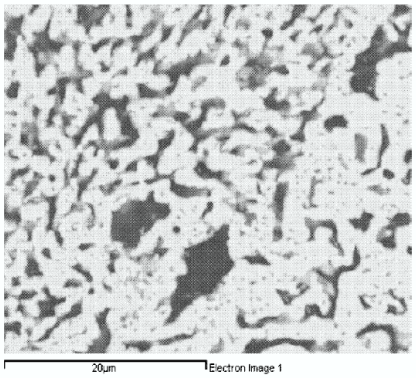

Fig. 9. SEM BSE compo image (3 000×) of a doped sample (+3.78 wt% Al_2O_3) after reduction.

for including sintered samples in the experiments as it was supposed this would increase the scale of the reactions.

3.2.2. Dense Samples (Program B)

At low magnification, the morphology of the doped samples after reduction appears the same as that of the un-doped ones (**Figs. 6** and **7**). However, differences can be identified at higher magnifications. Iron, reduced from un-doped magnetite, was formed mainly as a homogeneous pure iron phase (**Figs. 8** and **10**), although there were grey areas (points 1–3 in Fig. 10) including small content of Al, Si, Ti and V. The reduction product from doped magnetite is heterogeneous, *i.e.* iron containing tiny dark particles or relic phases (**Figs. 9** and **11**). The results of the analysis from the relic phases (points 1, 2 and 3 in Fig. 11) are shown in **Fig. 12**. The point 4 shows that the white phase in the SEM-image is iron. The right column shows the composition of stoichiometric hercynite ($FeAl_2O_4$) and it is not result of any point. There can be seen that the composition of the relic phase is almost same with that of stoichiometric hercynite.

It is generally accepted that reduction of magnetite to wüstite is a topochemical phenomena. However, as can be seen in the **Fig. 13**, the reduction process clearly seems to

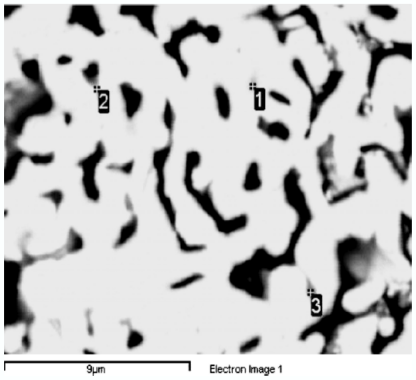

Fig. 10. SEM BSE compo image (6 000×) of an un-doped sample after reduction. The grey areas (points 1–3) include small contents (0.3–0.8 wt% analysed) of Al, Si, Ti and V.

favour certain internal lattice planes of the magnetite host. The lamellae or network like replacement of magnetite with wüstite most likely seems to advance along (100), or per-

SUPPLEMENT I

PAANANEN T, HEINÄNEN K & HÄRKKI J: DEGRADATION OF IRON OXIDE CAUSED BY ALUMINA DURING REDUCTION FROM MAGNETITE, ISIJ INTERNATIONAL, 2003, PP. 597-605.

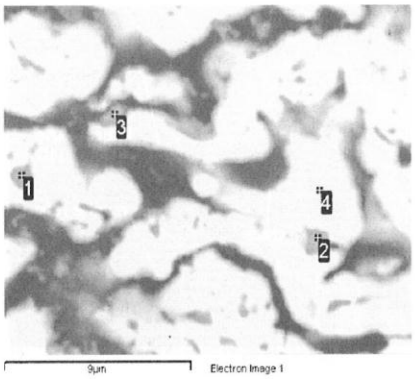

Fig. 11. SEM-image (6 000×) of a doped sample after reduction (+3.78 wt% Al_2O_3). (The results of analysis points is showed in Fig. 12.)

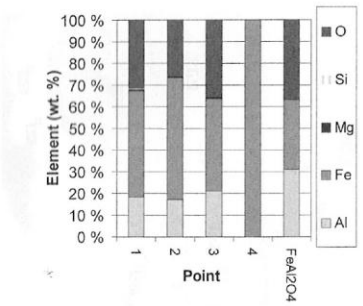

Fig. 12. Normalised results of analysis points in Fig. 11.

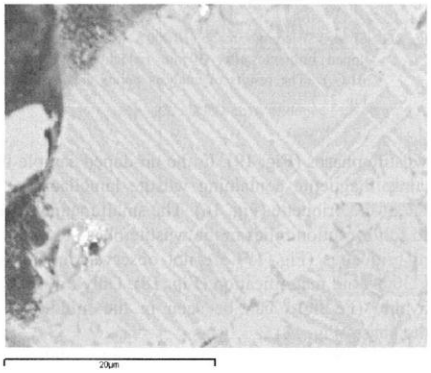

Fig. 13. SEM BSE compo image (3 000×) of a doped sample (+3.78 wt% Al_2O_3) after 30 min reduction. The lighter grey phase is wüstite and the darker one magnetite.

ps also along (011), lattice planes of the host. The adja-nt allotriomorphic magnetite grains are randomly orient-, which can be seen from the different orientation of the istite lamellae in each grain (**Fig. 14**).

In the reduction tests interrupted after 30 min the un-ped sample has reduced about 4 percentage units less in the doped sample as shown in **Fig. 15**. The un-doped

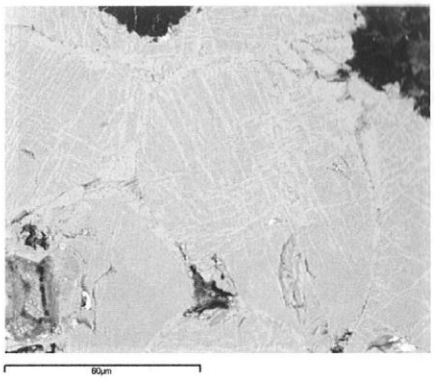

Fig. 14. SEM BSE compo image (1 000×) of a doped sample (+3.78 wt% Al_2O_3) after 30 min reduction. The lighter grey phase is wüstite and the darker one magnetite.

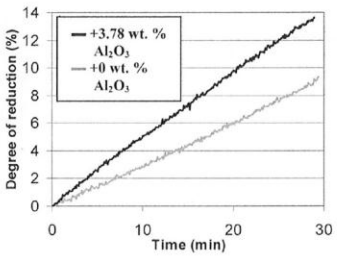

Fig. 15. The degree of reduction up to 30 min.

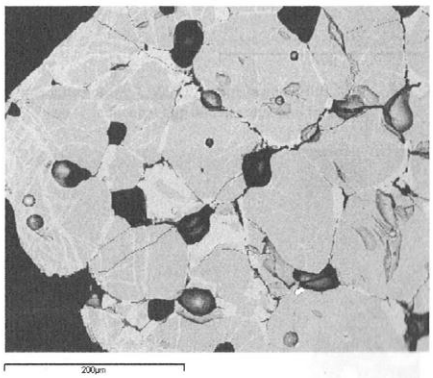

Fig. 16. SEM BSE compo image (250×) of the surface of an un-doped briquette after 30 min reduction. The light grey phase is wüstite, the darker one is magnetite. The black areas are pores.

sample has reduced to wüstite on the surface of the bri-quette and the structure of the briquette is still unbroken (**Fig. 16**). Wüstite lamellae are also apparent in the mag-netite, where reduction has proceeded along the lattice planes. Also the surface of the doped briquettes has reduced more than the centre of briquettes and a small amount of metallic iron is also present at the surface (**Fig. 17**). The doped sample is split, where iron has formed and the reduc-

SUPPLEMENT I

PAANANEN T, HEINÄNEN K & HÄRKKI J: DEGRADATION OF IRON OXIDE CAUSED BY ALUMINA DURING REDUCTION FROM MAGNETITE, ISIJ INTERNATIONAL, 2003, PP. 597-605.

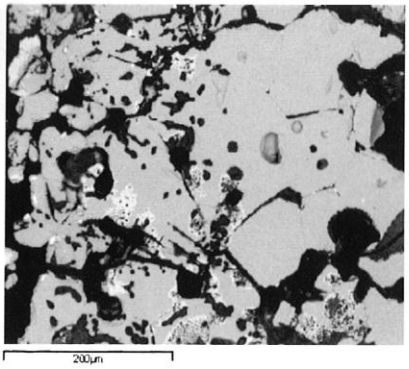

Fig. 17. SEM-image (250×) of the surface of a doped briquette after 30 min reduction (+3.78 wt% Al_2O_3). The white phase is iron and the grey one the wüstite/magnetite matrix.

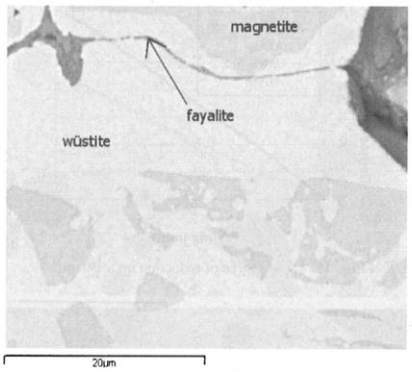

Fig. 18. SEM BSE compo image (3 000×) of the surface of an un-doped briquette after 30 min reduction.

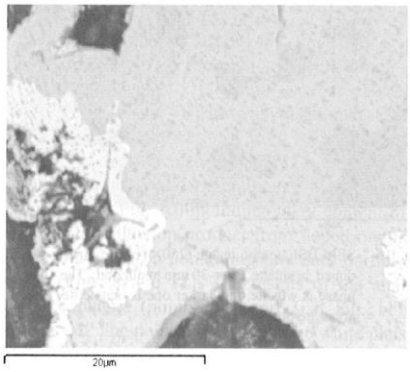

Fig. 19. SEM BSE compo image (3 000×) of the surface of a doped briquette after 30 min reduction (+3.78 wt% Al_2O_3).

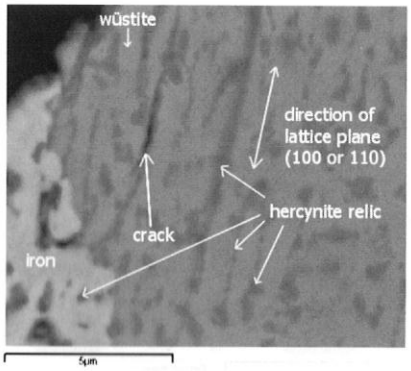

Fig. 20. SEM BSE compo image (10 000×) of the surface of a doped briquette after 30 min reduction (+3.78 wt% Al_2O_3).

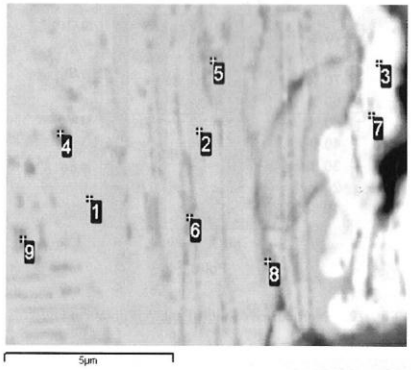

Fig. 21. SEM BSE compo image (10 000×) of the surface of a doped briquette after 30 min reduction (+3.78 wt% Al_2O_3). (The results of analysis points are showed in Fig. 22.)

tion can be seen to have progressed further. The main oxide around the iron phase is wüstite. Apparent darker magnetite–hercynite solid solution grains appear in both iron and wüstite phases (**Fig. 19**). In the un-doped sample there is mainly magnetite containing wüstite lamellae near the surface of the briquette (Fig. 16). The small magnetite–hercynite solid solution relics in the wüstite phase found in the doped briquettes (Fig. 19) are not observed in un-doped using 3000-fold magnification (**Fig. 18**). Only a few stripes of fayalite (Fe_2SiO_4) can be seen in the middle of the wüstite phase (Fig. 18).

The dark particles of magnetite–hercynite solid solution in wüstite would look like continuing as cracks near the reduced iron phase (**Fig. 20**). The structure of wüstite grains containing the particles, seem to be split mainly along lattice planes (Fig. 20 and **Fig. 21**). Some hercynite relics can be also observed as inclusions in iron. Analysis results for the most important elements from the points shown in Fig. 21 are shown in **Fig. 22**. Because the particles are smaller than the analysis spot the results are only semi-quantitative. However content of aluminium is clearly increased in the points 4, 5, 6, 8 and 9 with respect to wüstite (analysis points 1 and 2). The same trend can be observed with iron

SUPPLEMENT I

PAANANEN T, HEINÄNEN K & HÄRKKI J: DEGRADATION OF IRON OXIDE CAUSED BY ALUMINA DURING REDUCTION FROM MAGNETITE, ISIJ INTERNATIONAL, 2003, PP. 597-605.

analysis (points 7 and 3).

3.3. XRD Analysis

According to the X-ray diffraction results, the minerals in sintered briquettes doped with 3.78 wt% Al_2O_3 are magnetite (Fe_3O_4) and maghemite (γ-Fe_2O_3). The reduced samples contained α-iron and hercynite (**Fig. 23**).

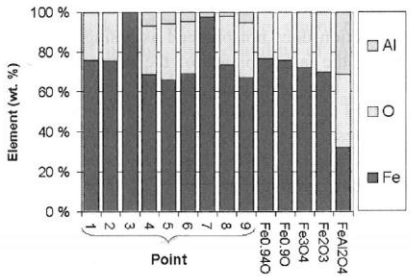

Fig. 22. Normalised compositions of the points in Fig. 21.

4. Discussion

The experiments clearly show that there is a correlation between the amount of alumina and degradation of magnetite during reduction at 950°C (Fig. 2). This degradation phenomenon above is not, however, the same as break down during the hematite-magnetite reduction step.

Above 858°C, the solubility of Al^{3+} in magnetite is about 30 wt%[14] and in the case of that, the phase of the spinel group is hercynite. For temperatures above 900°C solid solution between magnetite and hercynite is complete.[15] On the other hand the solubility of Al^{3+} in wüstite is only about 0.5 wt% at 900°C.[16] Consequently during the reduction of magnetite to wüstite Al cations must diffuse away from the wüstite accumulating in the surrounding magnetite. The more the reduction advances the higher the average content of Al in magnetite and the composition of the phase approaches that of hercynite. This is also energetically favourable, because a new phase need not form. The process is shown schematically in **Fig. 24**. Step 1: Magnetite reduces to wüstite (light grey) and only part of

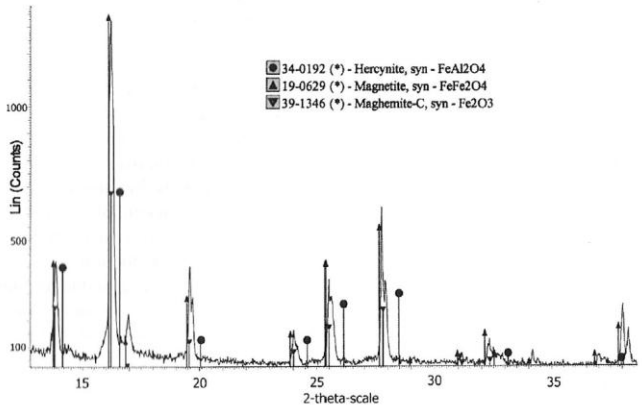

Fig. 23. XRD-chart of doped (+3.78 wt% Al_2O_3) and sintered (1 400°C) magnetite briquette before reduction.

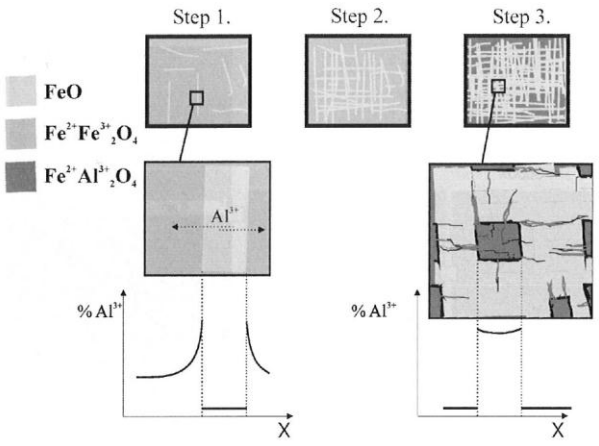

Fig. 24. A schematic diagram of the cracking mechanism during the reduction of Al-containing magnetite to wüstite.

ISIJ International, Vol. 43 (2003), No. 5

dissolved aluminium in magnetite (darker grey) can remain in wüstite so that it has to diffuse into magnetite. Content of aluminium is highest on the interface of wüstite and magnetite. Step 2: The amount of wüstite increases. Step 3: The content of aluminium in magnetite phase increases and the composition of the phase approaches that of hercynite. The volumetric difference between hercynite and wüstite causes cracks at the time. These phenomena can also be observed in the SEM micrographs (Figs. 17–20 and **Fig. 26**). The existence of hercynite in the reduction product could also be observed using XRD. The maghemite found in the initial doped unreduced material using XRD may have been magnetite, containing a little dissolved alumina, which would make the lattice constant smaller (Fig. 23 and **Fig. 25**). On the other hand the peaks were a quite sharp and matched well with maghemite.

When magnetite is reduced to wüstite, the crystal structure transforms from spinel to fcc structure. There is a volumetric difference between the two structures, which can easily be calculated from the values of lattice constants. The volumetric change depends on the degree of non-stoichiometry of the wüstite and the Al content of the spinel structure as shown in Fig. 25.[17–19] If wüstite has the formula $Fe_{0.88}O$ and the magnetite is pure, the structure expands about 6% during reduction to wüstite, but if the spinel structure is as hercynite the expansion is over 16%. Wüstite formation should then cause high tension forces in the magnetite/hercynite near the interface which may enough to fracture the structure during the reduction of magnetite to wüstite.

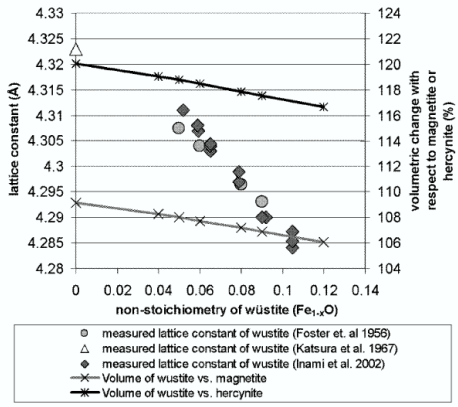

Fig. 25. Volumetric changes in the reduction step from magnetite/hercynite to wüstite calculated from the value of the lattice constants.[17–19]

The reduction does not proceed as a single front, but it rather along the lattice planes of the magnetite forming a kind of grid structure (Figs. 13 and 14). The magnetite phase shrinks to small particles or islands between the expanding plates of wüstite. The presence of Al promotes the reduction by causing cracks (Fig. 26). The three images on left side show development of magnetite reduction to wüstite. The direction of lattice planes is clearly seen especially in two middle images and in the latter one hercynite relics begin to form. Both of the images on right side can be observed cracks on the interface of hercynite relic and wüstite phase and the cracks seem to be in the direction of lattice plane. Those images show also that hercynite relics exist in the phase. This also explains why the densely sintered (B) briquettes were reduced faster in the beginning of the reduction and the porous briquettes at the "end" of the reduction. The grain size was small in the porous samples and the smallest particles were reduced first without any substantial accumulation of Al cations, thus the surface area between iron/iron oxides and gas became the limiting factor when there were only the largest particles unreduced. At that stage cracking of the structure by Al became significant as it was in the case of the sintered samples even at the beginning of the reduction.

The final degree of reduction indicates that Al_2O_3 binds with FeO creating hercynite, which was not reduced in the prevailing conditions used in the experiments (Fig. 3). This is also supported by Bruijn, because there has been represented that hercynite is stability up to $CO/CO_2=97/3$ gas composition in 950°C.[6] The swelling could be a consequence of the formation of micro-pores between iron and the hercynite phase.

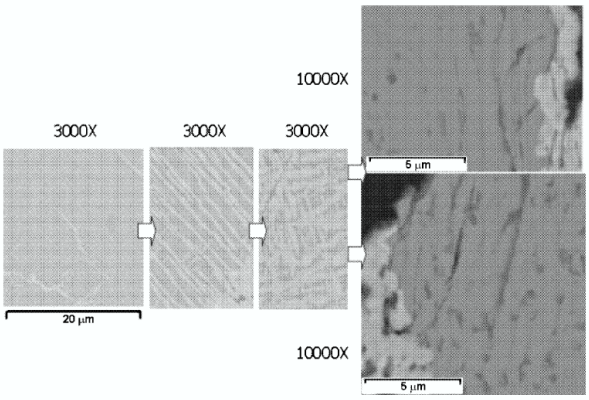

Fig. 26. SEM images showing the development of doped magnetite reduction (+3.78 wt% Al_2O_3).

SUPPLEMENT I

PAANANEN T, HEINÄNEN K & HÄRKKI J: DEGRADATION OF IRON OXIDE CAUSED BY ALUMINA DURING REDUCTION FROM MAGNETITE, ISIJ INTERNATIONAL, 2003, PP. 597-605.

ISIJ International, Vol. 43 (2003), No. 5

5. Conclusions

The degradation mechanism of iron oxides caused by alumina during reduction from magnetite to wüstite has been studied. The experiments were carried out by reducing briquettes containing various mixtures of commercial magnetite fines and Al_2O_3 in a CO/CO_2 atmosphere at 950°C in thermo-gravimetric equipment.

(1) The presence of Al cations in magnetite induced swelling and cracking of the briquettes during reduction.

(2) Because of the low solubility of Al cations in wüstite during the reduction of Al_2O_3 doped magnetite to wüstite Al cations have to diffuse in the magnetite away from the growing wüstite. As the reduction process proceeds the average content of Al in magnetite increases approaching that of hercynite.

(3) If the stoichiometry of wüstite is $Fe_{0.88}O$ and magnetite is pure, the structure expands about 6% during the reduction from magnetite to wüstite, but if the spinel structure is hercynite the expansion is over 16%. In the latter case high tensile forces are generated in the hercynite/magnetite solid solution at the interface with the wüstite which presumably cause the fracturing of the structure during the reduction from hercynite/magnetite to wüstite.

(4) Aluminium in magnetite promoted the reduction of porous briquettes after 60% reduction. On the other hand, in the case of densely sintered briquettes, the Al-doped material was reduced faster than the un-doped material at the beginning of the reduction. The explanation for this difference is that Al cracked the structure of iron/iron oxide when the surface area became the limiting factor controlling the rate of reduction.

Acknowledgements

The authors are grateful to the Academy of Finland for financial support of this research, and also wish to express their gratitude to Dr. D. Porter for his valuable advice and help in preparing this manuscript.

REFERENCES

1) I. Shigaki, M. Sawada, K. Yoshioka and T. Takahashi: Iron and Steel Soc. Inc., (1986), 537.
2) A. De, S. S. Gupta and A. Chatterjee: *SEAISI Q.*, **21** (1992), 35.
3) M. Kvak, C. Lee and M. Dzo: *J. Korean Inst. Met. Mater.*, **35** (1997), 996.
4) Y. Suzuki, M. Yamamoto, T. Kotanigawa and K. Nishida: *Metall. Trans. B*, **12B** (1981), 691.
5) Y. Iguchi and M. Inouye: *Trans. Iron Steel Inst. Jpn.*, **22** (1982), 678.
6) W. de Bruijn: PhD Thesis, Delft University, (1990), 183.
7) R. Piepenbrock: Doctor Thesis, Technical University of Clausthal, (1974), 35.
8) T. Sharma, R. Gupta and B. Prakash: *ISIJ Int.*, **33** (1993), 446.
9) C. Klein and C. S. Hurlbut, Jr. (after J. D. Dana): Manual of Mineralogy, 21st ed., John Wiley & Sons, Inc, New York, (1993), 378.
10) G. A. Waychunas: Reviews in Mineralogy, Vol. 25, Oxide Minerals, ed. by D. H. Lindsley, Mineralogical Society of America, Washington D. C., (1991), 11.
11) R. M. Hazen and R. Jeanloz: *Rev. Geophys. Space Phys.*, **22** (1984), 37.
12) Y. Sasaki, Y. Kashiwaya, K. Ishii and Y. Watabe: *CAMP-ISIJ*, **10** (1997), 712.
13) B.-K. Kim and J. A. Szpunar: *Scr. Mater.*, **44** (2001), 2605.
14) A. C. Turnock and H. P. Eugster: *J. Petrol.*, **3** (1962), 533.
15) A. C. Turnock and D. H. Lindsley: Fe–Al and Fe–Ti Spinels and Related Oxides, Year Book—Carnegie Inst. Washington, No. 1363, (1961), 152.
16) L. M. Atlas and W. K. Sumida: *J. Am. Ceram. Soc.*, **41** (1958), 150.
17) D. H. Lindsley: Reviews in Mineralogy, Vol. 3, Oxide Minerals, ed. by D. Rumble III, Mineralogical Society of America, Washington D. C., (1976), 1.
18) W. A. Deer, R. A. Howie and J. Zussman: Rock-Forming Minerals, Vol. 5, Longmans, London, (1961), 371.
19) T. Inami and K. Suzuki: *ISIJ Int.*, **42** (2002), 150.

SUPPLEMENT II

Paananen, T: Effect of Impurity Element on Reduction Behaviour of Magnetite,

Steel research international, 78(2007)2, pp. 91 - 95.

SUPPLEMENT II

PAANANEN, T: EFFECT OF IMPURITY ELEMENT ON REDUCTION BEHAVIOUR OF MAGNETITE, STEEL RESEARCH INTERNATIONAL, 78(2007)2, PP. 91-95.

Effect of Impurity Element on Reduction Behaviour of Magnetite

Timo Paananen

Laboratory of Metallurgy, Department of Process and Environmental Engineering, PO BOX 4300, FIN-90014 University of Oulu

The present paper investigates the effect of impurity elements on sintering and reduction behaviour of magnetite solid solution. The main impurity elements of magnetite are Mg, Al, Ca, Mn and small amount of Si. The effects on reduction kinetics and phenomena are studied separately and for each element as well as combinations of them. The content of elements doped in magnetite are at the same levels as in industrially produced sinter. It is found that CaO and MgO significantly accelerate the reduction of magnetite to iron, MnO, however, slightly retards reduction.

Keywords: Reduction, iron oxide, impurity, magnetite

Introduction

The blast furnace burden material has to be agglomerated because the permeability of the burden bed must be sufficient for reduction gases to flow up from the low part of the furnace. The agglomeration is generally carried out by pelletizing or sintering the iron concentrate. Quality of sinter includes two main factors, i.e. strength and reducibility that are partly opposite to each other. The cold strength and the reduction strength must be good and, however, reducibility should hold on a high level. Since the sampling from the BF-process is difficult, the quality of the agglomerates is measured using standard tests like the reducibility, the cold strength and the reduction strength for ensuring good BF operation. Similarly, sinter is often tested according to these tests.

Most of the minerals in BF agglomerates consist of iron oxides (hematite and magnetite), but also calcium ferrites, vitreous slag and crystallized slag exist. Hematite and magnetite are not pure iron oxides, but contain impurity elements in solid solution. Some impurities have a radical effect on reduction kinetics and reduction strength via various mechanisms. The impurity elements can generate disintegration of oxide phases [1], accelerate reduction, enhancing diffusion, increasing gas-solid reaction surface area and have an influence on thermodynamic stability of oxides [2]. The retardation or acceleration of reduction can occur, if impurity components cause the formation of new phases at the reaction front. The direction of the effect depends on the stoichiometry and the stability of the existing phases [3,4]. The reduction step from wüstite to iron demands the thermodynamically most reducing gas and it is mostly the restrictive factor of the total reduction rate. However, previous reduction steps have a significant effect on the following step via morphology and surface area at the interface between the reduction gas and wüstite. The dissolution of impurity elements or their insolubility in iron oxides has an important effect on the reducibility of iron oxides.

Even a small amount of Ca (0.05 – 0.2 mol-%) was observed to have a strong enhancing effect on the reducibility of wüstite [5]. The presence of MgO and CaO (2 and 5 wt %) were found to promote the metallization of wüstite [6] and cause the formation of porous iron when reduced from wüstite in CO/CO_2-atmosphere [7]. The formation of pores can be caused by the precipitation of micro oxide particles at the interface of wüstite and iron [8]. According to J. Molenda et al., the electrical conductivity of mangano-wüstite was decreased when the content of manganese was increased [9].

The purpose of this paper is to investigate the effect of impurity elements on magnetite solid solution. The composition of magnetite crystals in industrially produced sinter was analysed in order to prepare synthetic magnetite with corresponding contents of the impurity elements. That was only possible using a heating process in a controlled gas atmosphere. Reduction tests for these pre-sintered samples were executed to find out the effect on reduction kinetics and mechanisms.

Experimental

Materials. The test material comprised commercial magnetite fines from a Swedish mine mixed with various amounts of MgO, CaO, MnO. The magnetite content of the fines was 96.1 wt% and the total iron oxide content, including Fe_2O_3, was about 97.8 wt%. The most significant quantities of other oxides are shown in **Table 1**.The impurity additives MgO, MnO and burnt CaO were powders with a purity of 95%, 99% and 99.9%, respectively.

Preparation of samples. The magnetite concentrate was ground and sieved into a grain size less than 74 μm. Then impurity oxide powders were mixed into fines in amounts presented in **Table 2**. The powder mix to which about 15 wt. % of purified ethyl alcohol had been added was pressed into briquettes with a compressive stress of 50 MPa. The wet briquettes were dried at 110°C for a few hours.

Sintering of samples for reduction. The aim was to make compact and dense briquettes to ensure topochemical reaction during the reduction. The ground and sieved powder mix was pressed to briquettes (ϕ12 x 5 mm) as described above and sintered in a tube furnace of 34 mm diameter at 1300°C for five hours in a CO/CO_2 atmosphere (CO/CO_2 = 5/95 and flow rate 1 l/min). The briquettes were

Table 1. Chemical composition of the magnetite fines, wt%.

Fe_3O_4	Fe_2O_3	SiO_2	TiO_2	MgO	Al_2O_3	V_2O_5	CaO	Others
96.10	1.70	0.60	0.40	0.40	0.25	0.24	0.18	0.07

SUPPLEMENT II
PAANANEN, T: EFFECT OF IMPURITY ELEMENT ON REDUCTION BEHAVIOUR OF MAGNETITE, STEEL RESEARCH INTERNATIONAL, 78(2007)2, PP. 91-95.

Table 2. Typical SEM-EDS analysis of magnetite doped with 2 wt% of MgO. (Fe content is presented as FeO and oxygen has been calculated)

Component	Content (wt%)
Na_2O	0.05
MgO	1.88
Al_2O_3	0.29
SiO_2	0.26
P_2O_5	0.01
S	0.02
K_2O	0.03
CaO	0.02
TiO_2	0.27
V_2O_5	0.21
MnO	0.02
FeO	89.08
ZnO	0.06
Total	92.21

Table 3. Typical SEM-EDS analysis of magnetite doped with 1 wt% of MnO. (Fe content is presented as FeO and oxygen has been calculated)

Component	Content wt%)
Na_2O	0.07
MgO	0.32
Al_2O_3	0.31
SiO_2	0.35
P_2O_5	0.00
S	0.02
K_2O	0.00
CaO	0.04
TiO_2	0.28
V_2O_5	0.37
MnO	1.06
FeO	91.16
ZnO	0.01
Total	93.99

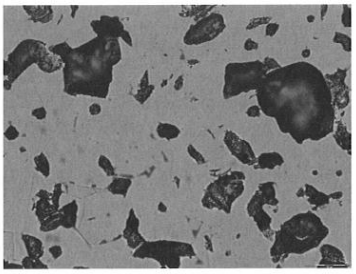

Figure 1. Magnetite sample sintered after adding 2 wt% MgO (Magnification of 500x).

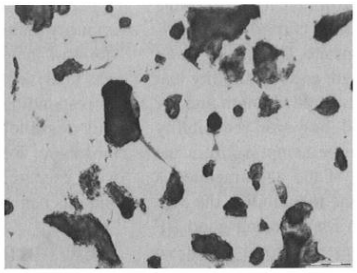

Figure 2. Magnetite sample sintered after adding 1 wt% MnO (Magnification of 500x).

quenched after sintering under argon atmosphere in a water cooled copper chamber. After the cooling the briquettes were ready for the reduction experiments.

Reduction of Samples. The sintered briquettes were reduced in the tube furnace, in a reducing gas mixture of CO and CO_2 with a flow rate of 2 l/min. The CO/CO_2 ratio was kept constant at 90/10 during the experiments. The reduction temperature was 950°C. Before the reduction stage the sample was preheated in an argon atmosphere at 950°C for 5 minutes. In order to achieve nearly 90 % reduction, the reduction time was 360 minutes. Other samples were reduced according to the same program, but with an interruption after 60 minutes. During the reduction test the sample was held in a platinum basket hanging on a gravimeter connected to a computer for data collecting. After the reduction, the briquettes were cooled in argon atmosphere in the water cooled copper chamber.

Mineralogical and microprobe analyses. Microprobe analyses were performed with a scanning electron microscope using energy dispersive spectrometry. An accelerating voltage of 15 kV and a beam current of 120 nA were used. The content of oxygen has not been analysed but calculated according to stoichiometry. The samples were also examined with an Olympus BX51 optical microscope.

Results

Sintered samples. The solution of added impurity components into magnetite was first checked using optical microscopy and searching different phases formed after exceeding the component solubility limit in magnetite. The composition of the phases were analysed using X-ray energy dispersive analysis (SEM-EDS).

Solubility of 2 wt% MgO into magnetite was not a problem. A nearly constant content of MgO was achieved throughout the magnetite phase (**Figure 1 and Table 2**). An analogous behaviour occurred with 1 wt% MnO content (**Figure 2 and Table 3**).

When the MgO content was increased to 8 wt%, part of MgO was dissolved into magnetite (~6 wt%) and the rest was in a newly formed magnesio-wüstite phase as can be seen in **Figure 3 and Table 4**. The same kind of phenomena occurred in magnetite doped with 2 wt% and 4 wt% CaO (**Figure 4 and Table 5**). The solubility of CaO into magnetite in prevailing conditions was about 1 wt% and the rest of CaO formed calcium ferrites (Table 5). The sum of the analysis in Tables 2 – 5 deviates from 100%, because the iron content is presented as FeO (oxygen calculated). When the sum is near 93%, the analysed iron oxide can be assumed to be magnetite (and wüstite at 98-100%).

Reduction examinations. The content of 1 wt% MnO and 2 wt% MgO in magnetite have an almost identical retardation effect on the reduction of magnetite in the beginning of the experiment (**Figure 5**). However, the effect was slightly stronger with MnO. The duration of the effect was about 30 minutes. After the 30 minutes the pure magnetite sample was reduced about 20 %. The sample doped with 1 wt% MnO was reduced 5%-units less and that with 2wt% MgO was reduced 2%-units less than the non-doped sample.

The reduction rate was considerably increased with every addition level of CaO as well as 8 wt.% of MgO. The degree of reduction for a pure magnetite sample was 33.5 % after an hour. For the sample with 4 wt% CaO addition it was 84 % (33.5% + 50.5%) as can be seen in Figure 5. A double degree of reduction compared to without doping was achieved with as low as 2 wt% addition of CaO.

The same effect of the impurities on the reduction of magnetite can be seen with optical microscopy of the pol-

Table 4. Typical SEM-EDS analysis of two different phases in the sample doped with 2 wt% of MgO, contents in wt%. (Fe content is presented as FeO and oxygen has been calculated.)

Component	Magnetite	Magnesio-wüstite
Na_2O	0.23	0.17
MgO	5.91	15.16
Al_2O_3	0.28	0.08
SiO_2	0.23	0.35
P_2O_5	0.02	0.06
S	0.01	0.03
K_2O	0.01	0.02
CaO	0.04	0.03
TiO_2	0.27	0.01
V_2O_5	0.27	0.15
MnO	0.01	0.08
FeO	85.91	81.96
ZnO	0.01	0.33
Total	93.22	98.44

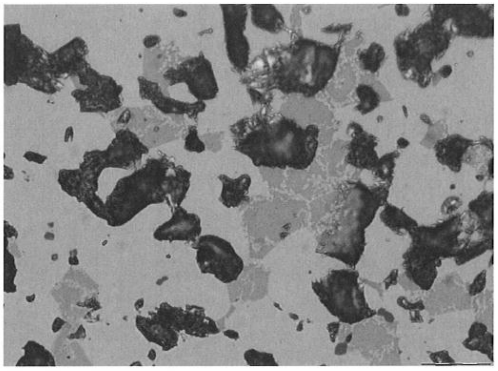

Figure 3. Magnetite sample sintered after adding 8 wt% MgO (Magnification of 500x).

ished samples (**Figure 6 – Figure 11**). The white phase is iron and the grey one is wüstite. The amount of iron phase is much higher in the samples doped with 4 wt% CaO and 8 wt% MgO compared with the sample doped 1 wt% MnO.

Discussion

Problems of the preparation. The effect of the sample preparation on the reduction rate was strong. Even a small variety of gas composition or temperature during sintering caused a radical change to the reduction rate (**Figure 12**). It was tried to prepare every sample with similar grain size, compression pressure and sintering procedure for achieving sufficient repeatability.

Solution of components. MgO causes a shift of the stability line between wüstite and magnetite extending the stability area of wüstite in certain CO/CO_2-atmospheres. This phenomenon appears during sintering in an atmosphere corresponding to the thermodynamic stability field of magnetite. High MgO content (8 wt%) causes the formation of wüstite in "magnetite"-atmosphere. Magnetite having 8 wt% MgO and 4 wt% CaO in solid solution was found in industrially produced sinter. The difference between the real sintering process and experimental sintering is caused by different oxygen pressures. The conditions are a lot of more oxidative in the end of real sintering processes than in the experimental procedure having a CO/CO_2 ratio of 5/95.

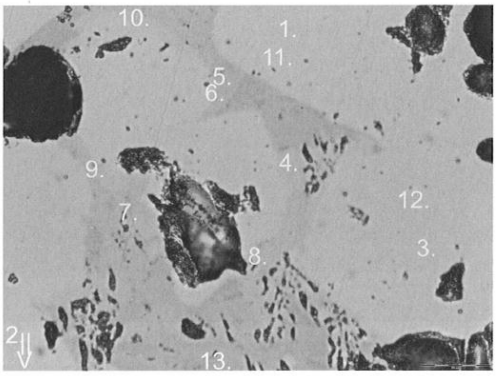

Figure 4. Magnetite sample sintered after adding 4 wt% CaO (Magnification of 500x). The marked numbers are points of SEM-EDS analysis seen in Table 5.

Table 5. SEM-EDS analysis of the phases existing in the magnetite sample sintered after doping 4 wt% CaO. (Fe content is presented as FeO and oxygen has been calculated.)

Point	Na_2O	MgO	Al_2O_3	SiO_2	P_2O_5	S	K_2O	**CaO**	TiO_2	V_2O_5	MnO	FeO	ZnO	Total
1	0.00	0.39	0.34	0.13	0.06	0.01	0.01	**1.06**	0.32	0.17	0.08	**91.52**	0.63	94.72
2	0.13	0.40	0.22	0.11	0.05	0.01	0.01	**1.22**	0.23	0.19	0.02	**91.96**	0.14	94.69
3	0.00	0.41	0.29	0.17	0.00	0.00	0.00	**1.05**	0.19	0.24	0.00	**91.63**	0.00	93.98
4	0.08	0.13	0.15	0.10	0.03	0.00	0.01	**17.33**	0.61	0.23	0.00	**77.39**	0.00	96.05
5	0.12	0.11	0.30	0.28	0.00	0.00	0.01	**17.04**	0.78	0.16	0.03	**78.02**	0.44	97.30
6	0.00	0.01	0.22	0.16	0.07	0.02	0.00	**17.34**	0.61	0.30	0.08	**77.97**	0.19	96.97
7	0.00	0.17	0.32	0.11	0.00	0.02	0.01	**1.00**	0.13	0.18	0.00	**92.44**	0.30	94.69
8	0.00	0.42	0.07	0.00	0.00	0.04	0.00	**4.19**	0.00	0.15	0.04	**94.92**	0.00	99.83
9	0.35	0.51	0.19	0.10	0.00	0.00	0.00	**0.75**	0.02	0.07	0.04	**96.20**	0.00	98.22
10	0.00	0.11	0.12	0.08	0.13	0.03	0.07	**16.99**	0.61	0.48	0.00	**78.15**	0.00	96.75
11	0.00	0.27	0.15	0.00	0.00	0.00	0.00	**1.03**	0.36	0.20	0.16	**90.47**	0.23	92.86
12	0.17	0.30	0.34	0.07	0.07	0.01	0.02	**1.01**	0.22	0.21	0.21	**91.07**	0.38	94.07
13	0.15	0.10	0.18	0.54	0.01	0.08	0.00	**18.31**	0.74	0.43	0.07	**75.15**	0.00	95.76

SUPPLEMENT II
PAANANEN, T: EFFECT OF IMPURITY ELEMENT ON REDUCTION BEHAVIOUR OF MAGNETITE, STEEL RESEARCH INTERNATIONAL, 78(2007)2, PP. 91-95.

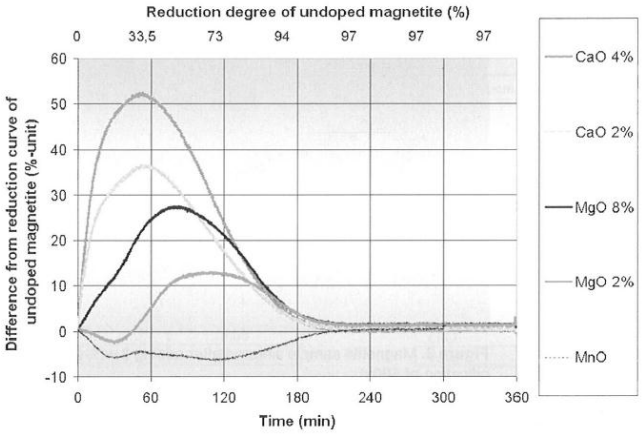

Figure 5. Effect of impurity components on reduction of magnetite.

Reduction of samples. The effect of 1 wt% MnO and 2 wt% MgO slowing down the reduction rate in the beginning of the reduction indicates the retardation effect existing in the magnetite-wüstite stage. After that stage MnO has no significant effect but MgO has a strong accelerating effect on the reduction. Addition of 8 wt% MgO increases the rate of reduction from the beginning of the experiment. The same effect occurs with CaO contents of 2 and 4 wt%.

The reasons are not yet clear but addition of CaO has been seen to form a lot of pores in the iron oxide, thus enlarging the surface area at the interface of gas and oxide phases. Ca-cations are clearly bigger than Fe-cations causing defects in the lattice of wüstite and furthermore accelerating the diffusion of cations and

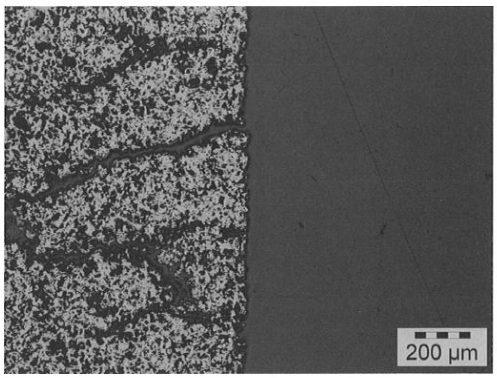

Figure 6. Edge of magnetite briquette doped with 1% MnO, after 60 min reduction.

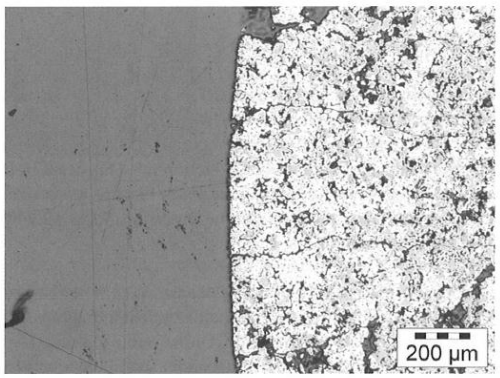

Figure 8. Edge of magnetite briquette doped with 8% MgO, after 60 min reduction.

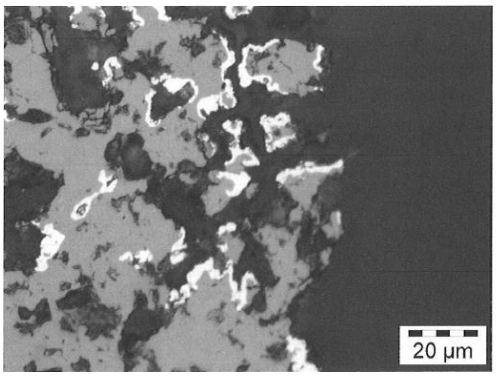

Figure 7. Edge of magnetite briquette doped with 1% MnO, magnified section of Figure 6.

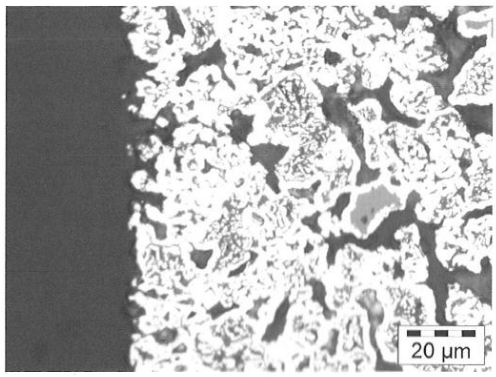

Figure 9. Edge of magnetite briquette doped with 8% MgO, magnified section of Figure 8.

SUPPLEMENT II
PAANANEN, T: EFFECT OF IMPURITY ELEMENT ON REDUCTION BEHAVIOUR OF MAGNETITE, STEEL RESEARCH INTERNATIONAL, 78(2007)2, PP. 91-95.

gas molecules to the reaction zone. Mg-cations are slightly smaller than Fe-cations. Previous results have shown that a large amount of MgO in wüstite reduced by hydrogen gas did not accelerate reduction [10]. In this study, however, CO/CO_2 atmosphere was used and the result was that the higher the MgO content, the faster is the reduction.

Summary

The purpose of this paper was to bring out some results concerning the effect of impurity elements on sintering and reduction behaviour of magnetite solid solution. The content of the elements doped in magnetite were at the same levels as analysed from magnetite in industrial sinter. The test material comprised commercial magnetite fines sintered after mixing with various amounts of MgO, CaO and MnO. In the dissolution procedure it was found that the solubility of MgO and CaO into magnetite is a function of oxygen pressure. The amounts which completely dissolved into magnetite at a gas atmosphere of CO/CO_2=5/95 were not as high as analysed from magnetite of real sinter.

CaO and MgO clearly accelerated the reduction of magnetite to iron regardless of the impurity content. However, a slight retardation effect could be observed with 2 wt% MgO at the beginning of the reduction. MnO (1 wt%) has a quite small slowing effect on the reduction of magnetite to iron.

Acknowledgements

The author is grateful to the Academy of Finland for financial support in the beginning of the research and wishes to express gratitude to Kyösti Heinänen (Rautaruukki) for his valuable advice and help during the study.

(A2006141; accepted on 4 July 2006; presented at the 2nd Nordic Symposium for Young Scientists in Metallurgy)

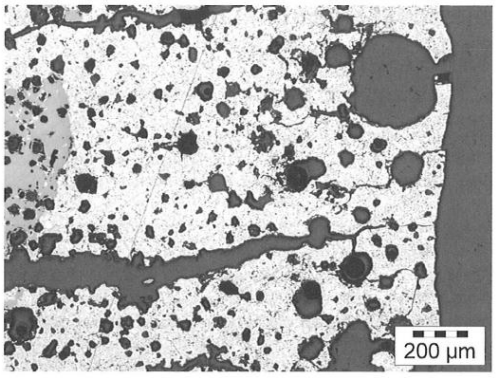

Figure 10. Edge of magnetite briquette doped with 4% CaO, after 60 min reduction.

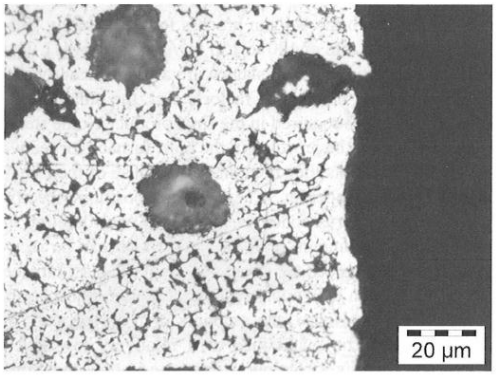

Figure 11. Edge of magnetite briquette doped with 4% CaO, magnified section of Figure 10.

References

[1] T. T. Paananen, K. J. Heinänen and J. J. Härkki: ISIJ, 43 (2003), No. 5, 597.
[2] A.A. El-Geassy: ISIJ 37 (1997), No. 9, 844.
[3] W. de Bruijin: PhD Thesis, Delft University, 1990, p. 183.
[4] R. Piepenbrock: Doctor Thesis, Technical University of Clausthal, 1974, p. 35.
[5] Y. Iguchi, Y. Uyeda and S. Hayashi: ICSTI, ISIJ, Sendai, 1994, p. 92.
[6] T. El Kasabgy and W.-K. Lu: Metall. Trans. B, 11B (1980) No.3, 409.
[7] S. Geva, M. Farren, D.H. St. John and P.C. Hayes: Met. Trans. B, 21B (1990), No 4, 743.
[8] K. Takahashi, M. Asada and M. Kawakami: ICSTI/Ironmaking Conference Proceedings, ISS, Toronto, 1998, p. 1705.
[9] J. Molenda, A. Stoklosa and H. Soliman: Solid State Ionics, 45 (1991), 109
[10] J. Härkki: Doctor Thesis, Technical University of Helsinki, 1978, p. 32.

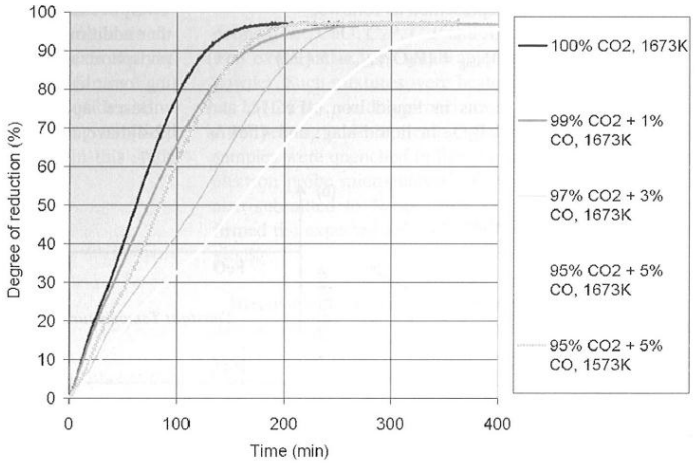

Figure 12. Effect of sintering temperature and gas composition on reduction of pure (non-doped) magnetite.

SUPPLEMENT III

Paananen, T & Kinnunen K: The Effect of Titanium on Reduction Degradation of Iron Ore Agglomerates, In proceedings: Iron ore conference, Australia Perth, 2007, pp. 361 - 367.

SUPPLEMENT III

PAANANEN, T & KINNUNEN K: THE EFFECT OF TITANIUM ON REDUCTION DEGRADATION OF IRON ORE AGGLOMERATES, IN PROCEEDINGS: IRON ORE CONFERENCE, AUSTRALIA PERTH, 2007, PP.361 - 367.

The Effect of Titanium on Reduction Degradation of Iron Ore Agglomerates

T Paananen[1] and K Kinnunen[2]

ABSTRACT

A strong correlation between the reduction degradation index (RDI) of production sinter and the titanium content of the sinter mix was identified at the Ruukki sintering plant between 2000 and 2004. The titanium distribution in different mineral phases was studied using samples from pot sintering tests. Titanium additions were made using two different materials: rutile and crushed titanium-bearing haematite pellets. While both titanium additions clearly increased the RDI, titanium seemed to favour secondary haematite. The study focused on the effect of titanium in haematite, because haematite is reduced to magnetite in the RDI test. During the haematite-magnetite reduction, reduction degradation was observed. To increase accuracy, the phenomenon was investigated first by sintering and then reducing synthetic minerals under controlled laboratory conditions at the University of Oulu. The effect of titanium oxide in solid solution in magnetite on the magnetite to haematite transformation rate was studied first in order to simulate the final stage of the sintering process. In other experiments, haematite samples doped with 0.5, 2.0 and 5.0 wt per cent titanium oxide were studied using thermogravimetry under a controlled gas atmosphere ($CO/CO_2/H_2/N_2$). Sintered samples were reduced using the same gas composition as in the RDI test. Polished sections for optical microscopy and SEM-EDS analysis were prepared from both reduced and oxidised samples and unreduced sintered samples. The titanium oxide content of haematite had a clear effect on reduction degradation of the samples. Furthermore, increasing titanium oxide content in solid solution in magnetite radically accelerated the oxidation rate. Similar observations regarding the effects of titanium have been reported earlier, but this was the first time the effect of very small additions of titanium were shown to deteriorate blast furnace burden quality and a reason suggested behind the process.

INTRODUCTION

The Rautaruukki sintering plant at Raahe Works consists of three identical *Dwight-Lloyd*-type sintering machines. The suction area of the sintering machines totals 225 m^2 with an annual blast furnace sinter production of 2.9 million tonnes. The main raw material is magnetite fines. Sinter basicity (CaO/SiO_2) has been typically 2.2 and the MgO content 2.3 per cent. The Fe content is 61 per cent and the FeO content has been high (ten to 12 per cent) because of the high amount of relic magnetite. The reduction degradation index $RDI_{-3.15\,mm}$ (ISO4696-1) was 22.2 per cent on average with variations from 13 to 33 per cent during 2006. The large variation of RDI was found to correlate strongly with the titanium content of the sinter. The sinter produced is used in two small blast furnaces (about 1200 m^3) with a relatively smaller amount of pellets (390 kilograms per tonne of hot metal (kg/tHM)). About 117 kg/tHM of heavy oil was used as an auxiliary reductant. The oil replaces coke and relieves volumetric space inside the furnaces for iron burden reduction, resulting in increased production capacity of hot metal. Practical experiments show that an improvement in the reduction degradation property of sinter enables a higher oil injection rate.

1. Assistant and Researcher, Laboratory of Metallurgy, Department of Process and Environmental Engineering, University of Oulu, PO Box 4300, Oulun Yliopisto FI-90014, Finland. Email: timo.paananen@oulu.fi

2. Development Engineer, Rautaruukki Oyj, Ruukki Production, Rautaruukintie 155, PO Box 93, Raahe FI-92101, Finland. Email: kimmo.kinnunen@ruukki.com

Mury *et al* (1984) reported that an improvement of sinter RDI by six per cent would lower the blast furnace coke rate by approximately 14 kg/tHM and increase blast furnace productivity by three per cent. Kim, Je and Jeong (2003) reported that the degradation of self-fluxed sintered ore during low temperature reduction of iron-bearing material increases the permeability resistance in the upper shaft of the blast furnace. Lecomte and Vidal (1976) reported on a test in which eight types of iron-rich sinters were charged into a blast furnace. They found a clear correlation between burden permeability and blast furnace operation using different sinters with measured reduction strengths. Grebe *et al* (1991) reported on a large number of laboratory-based quality tests versus production scale and basket sample experiments. They discovered that a real production scale atmosphere can smooth the effect of a large change in quality observed under laboratory conditions. For example, sulfur, alkalis and chlorine compounds in the gas have some unexpected effects on burden behaviour. Nevertheless, Grebe *et al* (1991) observed a notable influence of fines rate on deterioration of permeability in the blast furnace.

The factors affecting sinter RDI have been discussed in a great number of papers. The parameters affecting the RDI can be categorised as sintering parameters, properties of raw materials and chemical composition of the sintering mix. For example, increasing the MgO content (Panigrahy *et al*, 1984a; Mishra, Thakur and Mediratta, 1996; Heinänen, 1993; Hsieh and Whiteman, 1993), basicity CaO/SiO_2 (Panigrahy *et al*, 1984b; Mishra, Thakur and Mediratta, 1996), and fuel rate improves the reduction degradation property of the sinter. On the other hand, increasing the content of Al_2O_3 (Hsieh and Whiteman, 1993; Mishra, Thakur and Mediratta, 1996; Pimenta and Seshadri, 2002a; Kim, Park and Cho, 2002; Pimenta *et al*, 1993; Pimenta and Seshadri, 2002b) and TiO_2 (Loo and Bristow, 1993; Pimenta *et al*, 1993; Pimenta and Seshadri, 2002a; Bristow and Loo, 1992) has a negative effect on RDI. Moreover, the mineralogy of sinter is a significant factor in reduction strength. One controlling factor of mineralogy is the chemical composition, especially the CaO/SiO_2 ratio, and even small changes in the content of minor components, such as MgO, Al_2O_3 and TiO_2, have a clear effect on the sinter mineralogy (Hsieh and Whiteman, 1993; Yang and Matthews, 1997). An increase in the alumina content has been shown to cause more calcium ferrites or SFCA-phase in sinter (Heinänen, 1993). Similarly, MgO has been shown to stabilise magnetite in sinter (Panigrahy *et al*, 1984).

The amount of haematite and secondary haematite in particular is widely regarded as the main cause of disintegration of sinter in low temperature reduction. However, the amount of haematite in sinter does not alone explain the RDI variation observed (Heinänen, 1993).

As mentioned earlier, the negative effect of titanium oxide on RDI has been demonstrated previously in several papers. However, neither the degradative mechanism of TiO_2 nor the phase in which the phenomenon has an effect is unambiguous. This study focuses on the distribution of titanium oxide in sinter, and in particular on the effect of the titanium content on reduction degradation of haematite.

A deeper understanding of high basicity magnetite-based sinter is convenient for the operation of blast furnaces at Raahe Works, especially for burden permeability. A high oil injection

rate increases the significance of reduction strength due to a decrease in the coke rate. In this study, the test sinters with varying TiO_2 contents were prepared and the properties of sinters evaluated. The aim of the thorough analysis of the test sinters and laboratory scale tests was to deepen the understanding of the reduction disintegration phenomenon.

EXPERIMENTS

Pilot experiments

Materials

Raw materials and test equipment were designed to resemble the production scale characteristics and materials as closely as possible. Oversized particles were carefully screened off (>10 mm) to stabilise the chemical analysis. The materials included magnetite fines, pellet fines (12 per cent), burnt lime (1.7 per cent), limestone (6.4 per cent), coke breeze, LD-slag (2.1 per cent), quartzite (0.7 per cent), olivine (2.2 per cent), return fines (30 per cent), TiO_2-bearing haematite pellets and rutile. All of these materials, with the exception of rutile, have been in production-scale use at Raahe Works. The coke breeze rate was adjusted to achieve equilibrium with the return fines rate similar to that for a production scale *Dwight-Lloyd*-type sintering process. The haematite pellets were a by-product of another plant and used at Raahe Works because of their high iron-content and titanium that is believed to protect the blast furnace hearth. Titanium as a protective material of the hearth is a quite widely accepted theory, but at present information on the subject in the literature is somewhat limited.

In order to avoid unwanted changes in sintering conditions, the tests were prepared using two totally different TiO_2-bearing materials: TiO_2-bearing haematite pellets and fine rutilite. Rutilite is a material containing rutile, magnesium titanium oxide ($(Mg_{0.75}Ti_{2.25})O_5$), quartz and hedenbergite ($CaFeSi_2O_6$). Haematite pellets were crushed to a grain size distribution corresponding to that of the pellet fines. The amount of pellet fines was decreased in relation to the amount of crushed haematite pellets used in order to minimise the effect in permeability. Test materials containing TiO_2 had different thermal properties affecting the solubility of titanium during the sintering process. The chemical composition of the materials is presented in Table 1.

TABLE 1

Chemical composition of TiO_2-bearing additives in test sintering.

Material	Fe	MgO	Al_2O_3	SiO_2	CaO	TiO_2
WO	58.7	0.43	2.3	3.0	1.51	7.0
Rutilite	3.9	2.94	5.2	25.2	3.21	54.5

Test equipment

The sintering mix was prepared using a separate granulation drum to achieve the optimal permeability and properties corresponding to those of the production scale process. The final moisture content of approximately 4.2 per cent was adjusted in order to maximise the average permeability during sintering. The permeability was adjusted to the optimum level using separate test equipment that measures the gas flow with a constant pressure drop. The test sinter mix (110 kg) was then charged into the cylindrical pot sintering equipment. The pot diameter was 400 mm and the bed height 400 mm, which is fairly low due to the relatively low permeability of the mix. The bed was ignited for at least 1.5 minutes with a direct flame burner until a certain ignition temperature was achieved. Low suction during ignition was applied. For the ignition gas, propane was used instead of coke oven gas that would be used at production scale. The under-pressure below the bed was controlled to remain constant at about 13 kPa after ignition until the end of sintering. The sintering was completed one minute after the maximum exhaust gas temperature was reached. Temperature was monitored continuously at three sinter bed depths beginning from the top (ignition temperature). The completed sinter was cooled and processed in a specially designed apparatus that simulates the stress and abrasion during handling to obtain the correct return fine generation rate. The ratio of return fines was accepted only if it was between 0.95 and 1.05. The sinter was analysed very thoroughly, including for example sieve analysis, reduction degradation test and mineralogical and chemical analysis. The reduction degradation index (RDI, reduction degradation index <3.15 mm) equipment was constructed in total compliance with the relevant international standard (ISO 4696-1).

Laboratory experiments

Materials

The test material comprised commercial magnetite fines from a Swedish mine mixed with varying amounts of TiO_2. The magnetite content of the fines was 96.1 wt per cent and the total iron oxide content, including haematite, was approximately 97.8 wt per cent. The most significant quantities of inpurities are SiO_2, TiO_2, MgO (0.6, 0.4, 0.4 wt per cent correspondingly) and other >0.45 wt per cent. The other test material was an analytical grade haematite chemical (99.5 wt per cent) also mixed with varying amounts of TiO_2.

Rutile powder with a grain size below 44 µm and a purity of 99 per cent or above was used as the titanium oxide additive.

Preparation of samples

Preparation of mixture

The magnetite grain size was less than 74 µm and the haematite 44 µm. TiO_2 was mixed into the fines in amounts corresponding to 0.5, 2 and 5 wt per cent. The powder mix to which approximately 15 wt per cent of purified ethyl alcohol had been added was forced into the briquettes with a pressure of 50 MPa. The wet briquettes were dried at 110°C for a minimum of two hours.

Preparation of dense samples for reduction and oxidation

Pressed magnetite briquettes (12ϕ × 5 mm), as described earlier, were sintered in a 34 mm diameter tube furnace at 1300°C for five hours in a CO/CO_2 atmosphere (CO/CO_2 = 5/95 and flow rate 1 L/min) for magnetite. The briquettes were quickly quenched in a copper chamber cooled by water in an argon atmosphere after sintering. After cooling, the briquettes were ready for the reduction experiment. The aim was to produce compact and dense briquettes for topochemical reaction during the reduction. Haematite briquettes were sintered in air at the same temperature and for the same duration as the magnetite samples.

Reduction of samples

Once prepared and sintered, the briquettes were reduced in the 34 mm diameter tube furnace in a reducing gas mixture of N_2, H_2, CO and CO_2 at a flow rate of 2 L/min. The gas composition was the same as that for the RDI test and was kept constant during the experiments. The reduction temperature was maintained constant at 500°C during the reduction. Before the reduction, the sample was first heated in an argon atmosphere to 500°C for five minutes. Processing the briquettes took 60 minutes.

During the reduction test, the sample was located in a platinum basket hanging on a gravimeter connected to a computer for data collection. After the reduction, the briquettes were rapidly cooled in a copper chamber in an argon atmosphere described earlier.

Oxidation of samples

Four magnetite briquettes (0, 0.5, 2 and 5 wt per cent doped), sintered as described earlier, were set on a platinum crucible at the same time. The briquettes were oxidised in a chamber furnace in air for 15 minutes and cooled at room temperature. The oxidation temperature of 950°C was measured using a thermoelement placed at the centre point of the furnace at the same depth level as the samples.

Mineralogical and microprobe chemical analyses

The polished sections from the sintered, reduced and oxidised samples were examined optically and by a scanning electron microscope. An Olympus BX51 optical microscope was used for the optical examination and texture analysis. The analysis was capable of separating plastic, vitreous slag/silicate phases, calcium ferrites, magnetite and haematite. The reflectivity of some of the calcium ferrite types and magnetite/magnesioferrite were partly overlapping, which compromised the validity of some of the results. Microprobe analyses were performed with a JEOL JSM-6400 scanning electron microscope using energy dispersive spectrometry. The equipment included a digital camera and Oxford Instruments Inca 3.03 software for evaluation of the analyses. An accelerating voltage of 15 kV and a beam current of 120 nA were used.

Crystallographic analyses were made using a Philips X'Pert PW3040/00 X-ray powder diffractometer with a PW3376/00 Co LFF ceramic X-ray tube and Philips Data Collector 2.0c (2003). Phase identifications from the diffraction patterns were performed with the aid of PANanalytical X'Pert HighScore 1.0d software (2003). All of the chemical components were analysed using XRF, with the exception of FeO content that was analysed chemically.

RESULTS

Sintering tests

The chemical compositions and the most significant quality indexes of the test sinters produced are presented in Table 2. The marking *WO* refers to the test sinter in which crushed haematite pellet was used as TiO_2-bearing material and *RU* refers to the same procedure using rutilite additions to increase the total TiO_2 content. B_2 is short for the basicity index (CaO/SiO_2). The target values for chemical composition were Fe 61.5 per cent, MgO 2.1 per cent and B_2 2.1. The realised values differ from the goals, but most of the variation is considered to be the result of disturbances in chemical analysis or sample preparation. The raw materials were weighted very carefully and therefore there cannot be big differences in preparing the mixtures. The test sintering was performed only once, which explains the variation in results. However, the sintering test always requires repetition if the amount of generated return fines differs from the charged amount. Disturbances obviously occurred also in the RDI values, but the differences were so small that no more tests were necessary.

The TiO_2 distribution of the test sinters was not investigated, because it was well known and already had been analysed previously (Kinnunen, 2005; Heinänen, 1993). It is known that titanium favours haematite, dicalciumferrite ($(CaO)_2{\cdot}Fe_2O_3$), monocalciumferrite ($CaO{\cdot}Fe_2O_3$), the hemicalciumferrite ($CaO{\cdot}(Fe_2O_3)_2$)/SFCA-phase and some presently unknown phase that resembles dicalciumferrite but contains more SiO_2. The unknown phase seems to be formed of residue melt or it may be a phase that has a most favourable structure for titanium and therefore a high amount of titanium has dissolved into its structure. Unlike dicalciumferrite, hemicalciumferrite and monocalciumferrite are not very favourable structures. The amount of vitreous slag phases was typically very low in the tests sinters, similar to typical high basicity sinter. Figure 1 demonstrates the correlation between the TiO_2 content and the RDI for two different TiO_2-bearing materials. An increase in the titanium content deteriorated the RDI when using both additives containing TiO_2.

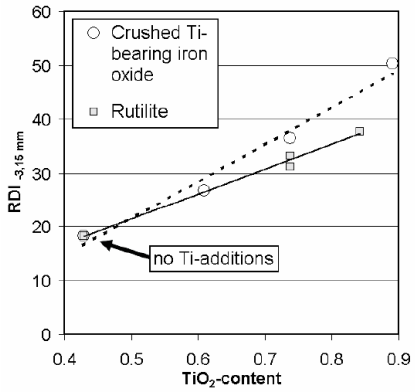

FIG 1 - Correlation between TiO_2 content and reduction degradation index for two different additives containing TiO_2.

Figure 2 illustrates the optically analysed mineralogical composition of the test sinters. The results are reported in area-contents. The higher titanium content increased the haematite content systematically while simultaneously decreasing the magnetite content. The main part of the slag phase is relict olivine crystals.

The chemical composition of various fractions of the partly disintegrated test sinters was analysed after the RDI test. The test

TABLE 2

Chemical composition and quality analysis of test sinters.

Test	Fe	CaO	SiO_2	MgO	Al_2O_3	TiO_2	B_2	FeO	RDI
Ref	61.63	6.49	3.15	2.04	0.49	0.43	2.06	5.2	18.3
WO 0.44	61.21	6.66	3.16	2.02	0.59	0.73	2.11	5.2	36.5
RU 0.44	61.41	6.44	3.08	2.12	0.52	0.73	2.09	5.1	31.2
WO 0.35	61.30	6.65	3.20	2.06	0.53	0.62	2.08	5.1	26.8
RU 0.50	61.50	6.57	2.98	1.87	0.54	0.83	2.20	4.9	37.7
WO 0.52	61.14	6.55	3.11	2.10	0.60	0.88	2.11	4.9	50.8

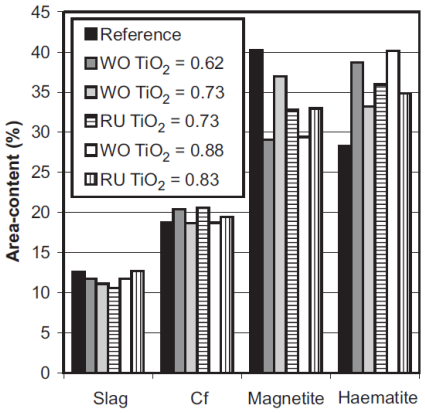

FIG 2 - Mineralogical composition of test sinters for different TiO_2-additions.

sinter in which TiO_2 content was increased to 0.73 wt per cent using rutile addition was compared to the reference case. In addition to an increase in the MgO content in the -0.5 mm fraction, the TiO_2 content was also higher than the average content in tested sinter. The TiO_2 content of the reference sinter (10.0 mm to 12.7 mm) was 0.43 wt per cent and in the -0.5 mm fraction the content was higher at 0.54 wt per cent, which was 25 per cent higher that the average content. The change was more pronounced when fractions were analysed for the doped sinter. TiO_2 content was 1.11 wt per cent in the -0.5 mm fraction, which was 52 per cent higher than the original average of 0.73 wt per cent. Titanium clearly was enriched in the smallest fraction after the RDI test, which indicated that the TiO_2-rich parts of the sinter were the weakest in the low temperature reduction stage.

Dissolution of TiO_2 into iron oxides

TiO_2, up to the maximum amount used in the experiment with 5 wt per cent TiO_2, completely dissolved into haematite and magnetite. Moreover, TiO_2 was uniformly distributed and the content was practically constant according to the SEM-EDS analysis. The XRD analysis from haematite synthesis showed only the alpha haematite phase in all the contained TiO_2. However, a slight shift from haematite peaks towards peaks of ilmenite with haematite doped with 5 wt per cent TiO_2 could be observed. In the case of haematite, the dissolution of the Ti^{4+}-cation was caused by reduction of the Fe^{3+}-cation to the Fe^{2+}-cation as described in Equation 1. Increasing the TiO_2 content from 0 to 5 wt per cent increased the content of the Fe^{2+}-cation from <0.1 to 3.0 wt per cent (Table 3). Considered on an atomic level, this means that each Ti^{4+}-cation caused reduction of one Fe^{3+}-cation to a Fe^{2+}-cation. The lattice

TABLE 3

Effect of titanium oxide on Fe^{2+}-cation content in haematite (-ilmenite solid solution) represented as FeO.

Addition of TiO_2 wt %	FeO content wt %	Fe total wt %
0.0	<0.1	70.2
0.5	0.4	69.9
2.0	1.3	69.3
5.0	3.0	67. 5

structure remained unchanged despite of reduction of the Fe^{3+}-cation, which was proved by XRD analyses:

$$Fe_2O_3 + a\,TiO_2 \rightarrow (a\,Fe^{2+},[1-\tfrac{1}{2}a]Fe^{3+})(a\,Ti^{4+},[1-\tfrac{1}{2}a]Fe^{3+})O_{3+1,5a} + a/4\,O_2(g) \quad (1)$$

where:

$0 \le a \le 2$ and the composition of solid solution changes from pure haematite to ilmenite respectively

Reduction

TiO_2 has an irrelevant retarding effect on the reduction of haematite to magnetite in the beginning of the reduction. However, the slope of the reduction graph continuously rises in the experiments using the samples doped with 2 and 5 wt per cent TiO_2, unlike the samples undoped and doped with 0.5 wt per cent. One hour after initiating the test, the reduction process was interrupted in compliance with the standard RDI test. The results revealed that the degree of reduction exceeded 50 per cent with the samples doped with 2 and 5 wt per cent TiO_2 and was approximately 20 per cent with samples undoped and doped with 0.5 wt per cent.

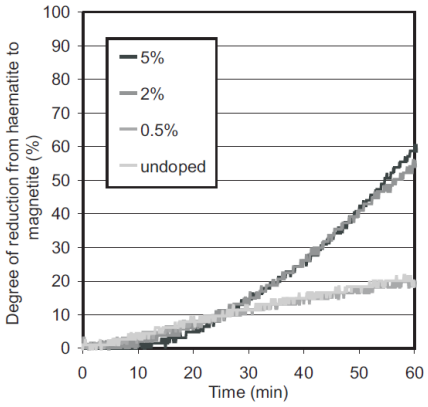

FIG 3 - Curves for undoped and TiO_2 doped haematite samples during reduction in a reduction degradation index atmosphere.

Visual and optical observations

TiO_2 has a clear visual effect on degradation of samples during the RDI test (Figure 4). The undoped and 0.5 per cent doped samples appear unchanged, but the sample doped with two per cent TiO_2 is thoroughly cracked and the sample doped with five per cent TiO_2 totally disintegrated.

According to images examined using the optical microscope, TiO_2 dissolving into haematite fractured the sample during RDI reduction. The higher the content of TiO_2, the clearer is the disintegration. The major disintegration seemed to be in the magnetite phase in which macro-cracks and a considerable amount of micro-cracks could be observed in the sample doped with 5 wt per cent TiO_2 (Figure 5).

Oxidation

Titanium oxide had an accelerative effect on oxidation of magnetite. Differences in oxidation between undoped and 0.5 per

SUPPLEMENT III

PAANANEN, T & KINNUNEN K: THE EFFECT OF TITANIUM ON REDUCTION DEGRADATION OF IRON ORE AGGLOMERATES, IN PROCEEDINGS: IRON ORE CONFERENCE, AUSTRALIA PERTH, 2007, PP.361 - 367.

cent TiO_2 doped samples were insignificant. However, apparent differences could be observed in the sample doped with two per cent TiO_2 (Figure 3). The quantity of haematite lamellae clearly increased. Furthermore, the oxidation of the sample doped with five per cent TiO_2 was considerably faster than that of the others.

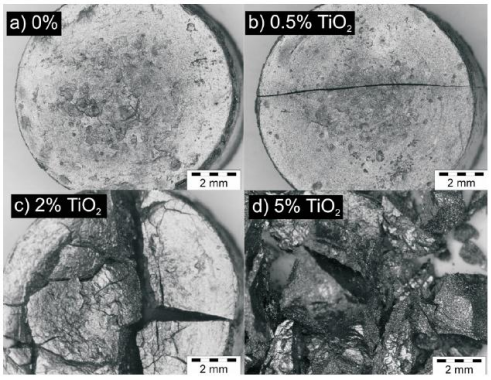

FIG 4 - Samples after the reduction program corresponding to the reduction degradation index test.

The zone oxidised to haematite was clearly less than 10 µm in the samples undoped and doped with 0.5 per cent TiO_2, with the exception of a few haematite lamellae. The corresponding zone was 100 - 300 µm and an even wider area full of haematite lamellae could be detected in the sample doped with five per cent TiO_2.

SEM-EDS analysis

The polished sections of a haematite sample reduced in the laboratory tests using similar conditions to the RDI test were analysed using SEM-EDS after optical microscopy. The polished section illustrated in Figure 5, from the sample doped with 5 wt per cent TiO_2, was analysed using point and line analysis. The titanium content of magnetite and haematite was roughly constant after the reduction tests performed under conditions resembling those for the RDI test. The analysed content of TiO_2 in magnetite was 4.5 - 5.1 wt per cent (average 4.9 wt per cent) and in haematite 4.7 - 5.1 wt per cent (average 4.9 wt per cent) respectively. According to the line analysis, no change in the Ti content occurred across phase boundaries between magnetite and haematite, but instead Ti was roughly constant throughout both of the phases (Figure 7).

The polished sections of a partly oxidised magnetite sample were also analysed using SEM-EDS after optical microscopy. The polished section illustrated in Figure 6, from the sample doped with 5 wt per cent TiO_2, was analysed using point and line analysis. SEM-EDS line analysis across the haematite and

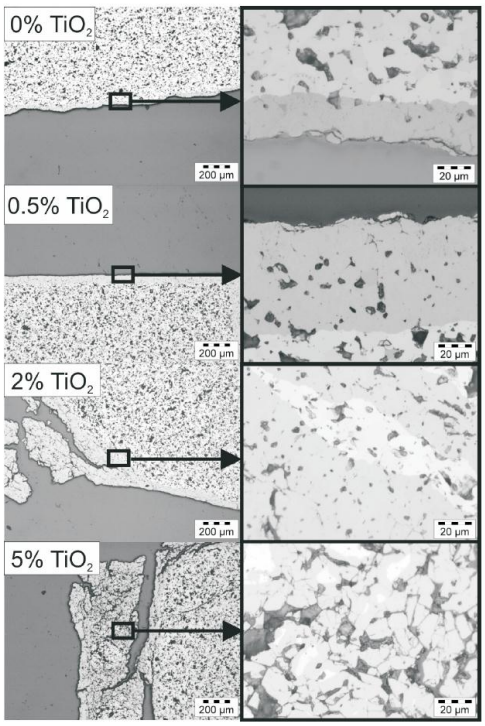

FIG 5 - Optical images from polished sections of samples doped with varying TiO_2 content after the reduction program corresponding to the reduction degradation index test. The white phase is haematite and the darker one magnetite. Magnifications were 40× (left column) and 500× (right column).

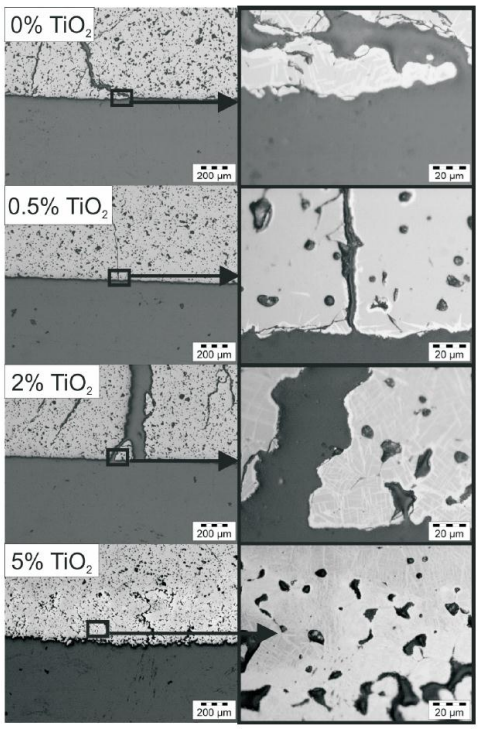

FIG 6 - Optical images from the polished section of the samples doped with varying TiO_2 content after the 15 minute oxidation program. The white phase is haematite and the darker one magnetite. Magnifications were 40× (left column) and 500× (right column).

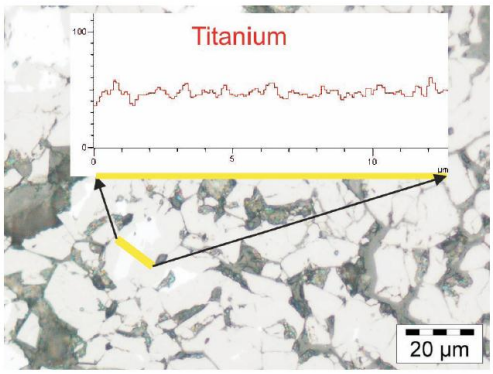

FIG 7 - SEM-EDS line analysis illustrated in the optical microscope image for the reduced haematite sample. The grey phase is magnetite and the white one haematite. The black areas are pores and cracks. The yellow line represents the scanned line.

magnetite phases indicated clearly that Ti^{4+}-cation favoured the haematite phase and diffused there from magnetite during oxidation (Figure 8). The TiO_2 content in haematite was higher (up to 15 wt per cent) than in magnetite (about 2.5 wt per cent), as was the TiO_2 content in the magnetite in the central area between the haematite lamellas. The Ti^{4+}-cation substituted for the Fe^{3+}-cation in haematite, decreasing the iron content. A slight decrease in the oxygen content of haematite could also be observed, but the reason for that is yet unknown. Similar line analyses were also performed for the undoped sample, but then the oxygen content was higher in the haematite than in the magnetite as expected.

XRD analysis

The results of the XRD analysis of doped haematite samples indicated that dissolution of TiO_2 into haematite was complete; the other phases did not occur in the XRD analysis. The peaks of the XRD-spectrum analysed for the sample doped with 5 wt per cent TiO_2 shifted slightly from those of haematite towards those of ilmenite, which complies with complete solid-solution of haematite and ilmenite at sintering temperature.

DISCUSSION

An increase in the TiO_2 content clearly deteriorated the RDI of the test sinter using both rutile and crushed haematite pellets containing TiO_2, although the change in chemical composition was quite small. When the TiO_2 content increased from the original 0.43 per cent to 0.88 per cent, $RDI_{-3.15\,mm}$ increased from 18.3 to 50.8 per cent respectively. Such a marked change in the RDI could be expected to affect blast furnace operation and productivity. The changes in the TiO_2 content of the production sinter at Raahe Works are considered the most prominent factors causing variation in the sinter RDI.

A higher TiO_2 content caused an increase of approximately 30 per cent in the optically analysed amount of haematite phase from 27 area per cent to 35 area per cent. It is generally known (Pimenta and Seshadri, 2002a) that increasing the TiO_2 content stabilises haematite both in sinter and pellets. The purpose of the laboratory experiments, in which magnetite was partly oxidised was to simulate the oxidation phenomenon during the final stage of sintering. Therefore the effect of TiO_2 on formation of secondary haematite was assumed to be a significant phenomenon in contrast to the general literature (Pimenta and Seshadri, 2002a). The result of the present study is that the main part of secondary haematite in magnetite-based sinter is considered to be formed from magnetite via oxidation. A small portion of the haematite is crystallised from the melt, but the amount of haematite (so-called tertiary haematite) is low in Raahe sinter. Relict haematite has a different effect from that of secondary euhedral haematite in which the titanium content is typically higher depending on other phases that are in the same structure. The formation of secondary haematite was simulated in laboratory tests, which showed clearly the accelerative effect of titanium on oxidation of doped magnetite. The difference in oxidation rate between undoped and doped samples with five per cent TiO_2 was tremendous (20 to 100 times). The TiO_2 content of sinter is low, typically 0.5 per cent. However, it isn't distributed uniformly into all phases, but favours haematite. The TiO_2 content in haematite can be locally up to 7 wt per cent in both production and test sinter. Therefore the TiO_2 content in magnetite briquettes was very high in the laboratory tests. The accelerative effect of TiO_2 on oxidation of magnetite can be explained by the structure of the haematite-ilmenite solid solution. Fe^{2+} is not forced to oxidise to Fe^{3+} when the Ti^{4+}-cation is present and the O^{2-}-anion does not necessarily diffuse on the oxidation front (Equation 1). Transformation of the crystal structure occurs at a specific content of TiO_2. However,

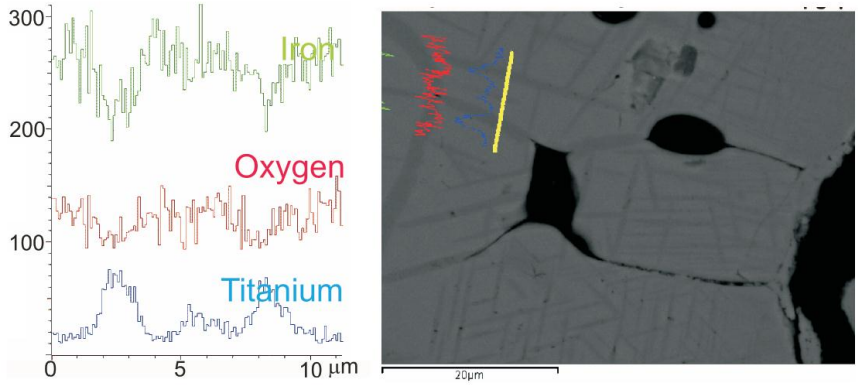

FIG 8 - SEM-EDS line analysis and SEM backscattered image for the partly oxidised magnetite sample. The darker grey lamellas are haematite and the lighter one is magnetite. The black areas are pores and cracks. The yellow line represents the scanned line.

SUPPLEMENT III

PAANANEN, T & KINNUNEN K: THE EFFECT OF TITANIUM ON REDUCTION DEGRADATION OF IRON ORE AGGLOMERATES, IN PROCEEDINGS: IRON ORE CONFERENCE, AUSTRALIA PERTH, 2007, PP.361 - 367.

an increase in the haematite content was not supposed to be the only factor affecting degradation. Titanium dissolves into haematite in a partly oxidised structure even if titanium is able to dissolve also into magnetite. Figure 8 shows a line analysis for partly oxidised magnetite. Titanium obviously has a tendency to favour the haematite structure over magnetite. The TiO_2 content of magnetite is higher in the central area between the haematite lamellas. Thus Ti^{4+}-cations seem to diffuse into haematite and the diffusion rate in magnetite is likely to be a limiting factor in cationic diffusion from magnetite to haematite.

TiO_2 was uniformly distributed in the magnetite and haematite in the sample reduced partly from haematite to magnetite in an atmosphere corresponding to the RDI test. This observation contrasts with partly oxidised samples in which diffusion of Ti^{4+}-cation from magnetite to haematite occurred as illustrated in Figure 8. The phenomenon is still partly unknown, but it is believed to be caused by the temperature difference between the tests. Thus, the diffusion rate is much slower in the RDI test (500°C) than in the oxidation tests (1200°C) due to the exponential dependency of the diffusivity coefficient according to Fick's law:

$$D = D_0 e^{-\frac{E_A}{RT}} \quad (2)$$

On the other hand, a high Ti content in the catalytic phase is believed to be present in the reaction front during the oxidation tests but not in the reduction tests. While the phase could not occur in reductive conditions, it was possible in oxidising ones. Further examination of the unclear phenomenon should be continued along with the degradation mechanism occurring in the magnetite phase during the RDI test on TiO_2 doped samples.

CONCLUSIONS

The reduction degradation strength seems to have quite a clear but sometimes ambiguous impact on the blast furnace process at Raahe Works. The opportunity to reduce coke consumption by injecting heavy oil in tuyeres appeared to be possible only if the sinter $RDI_{-3.15\ mm}$ was improved to a sufficiently low level below 25 per cent. The RDI is affected by several factors, but variation in TiO_2 content was observed to be the most significant factor at Raahe Works at the present, while other variables were quite stable. The main conclusions based on the data analysis, test sintering results, and finally, reduction and oxidation experiments with laboratory-scale doped synthetic materials reported in this paper are:

- An increase in TiO_2-content clearly deteriorates the RDI index of test sinter using both rutile and crushed haematite pellets containing TiO_2 as additives, although the change in the TiO_2 content was quite small. When the TiO_2 content increased from the original 0.43 per cent to 0.88 per cent, $RDI_{-3.15\ mm}$ increased from 18.3 per cent to 50.8 per cent respectively.
- TiO_2 additions to test sinter mixes increased the amount of haematite phase in the sinter.
- The higher the TiO_2 content of doped haematite briquettes, the more significant their disintegration, which was detected visually and also by microscope.
- Oxidation of TiO_2 doped magnetite briquettes showed that an increase in the TiO_2 content of magnetite accelerated the oxidation of magnetite to haematite.

Degradation mechanisms demand further study, but the phenomenon seems to occur in the magnetite phase during low temperature reduction. However, other phases in some mineralogical structures may also react under the RDI test conditions and are capable of dissolving TiO_2. They, too, require further study.

ACKNOWLEDGEMENTS

The authors are grateful to the TEKES Finnish Funding Agency for Technology and Innovation, and Rautaruukki for financial support for the research, and wish to express their gratitude to PhD Kyösti Heinänen for his valuable advice and help with the research.

REFERENCES

Bristow, N J and Loo, C E, 1992. Sintering properties of iron ore mixes containing titanium, *ISIJ International*, 32(7):819-828.

Grebe, K, Sticker, K-P, Winzer, G and Engel, K, 1991. Unexpected phenomena of burden behaviour in blast furnaces and their impact on control strategies, in *Proceedings Ironmaking Conference,* vol 50, pp 379-394, Washington, 14 - 17 April.

Heinänen, K, 1993. Mineralogy and metallurgical properties of iron ore sinter based on magnetite fines, PhD thesis, University of Helsinki.

Hooey, P L, 1999. Reduction and high temperature behaviour of iron ore sinter made from magnetite fines, PhD thesis, Department of Process Engineering, University of Oulu.

Hsieh, L-H and Whiteman, J A, 1993. Effect of raw material composition on the mineral phases in lime-fluxed iron ore sinter, *ISIJ International,* 33(4):462-473.

International ISO9001 Standard ISO4696-1. Iron ores – Static test for low-temperature reduction-disintegration.

International Standard ISO 3271 1975 (E). Tumbler strength of iron ores, pellets and sinter.

Kim, H S, Park, J H and Cho, Y C, 2002. Crystal structure of calcium and aluminium silicoferrite in iron ore sinter, *Ironmaking and Steelmaking,* 29(4):266-270.

Kim, J-R, Je, J-H and Jeong, S-K, 2003. Behavior of reduction degradation of sintered ore by synchrotron X-rays, in *Proceedings Iron and Steel Society International Technology Conference and Exposition 2003,* pp 175-180, Indianapolis, 27 - 30 April.

Kinnunen, K and Heinänen, K, 2005. The reduction degradation property of iron ore sinter, in *Proceedings Fifth European Coke and Ironmaking Congress*, Vol 2, pp 1-13.

Kinnunen, K and Laitinen, P, 2004. Investigation of sinter plant production rate and RDI using neural networks, in *Revue de Metallurgie, Cahiers d'Informations Techniques*, No 25es Journees Siderurgiques Int 2004 Suppl, pp 144-145.

Lecomte P, 1971. Vidal R Study on the reduction strength of sinter. *Metallurgical Reports C R M,* 26(March):5-14.

Loo, C E and Bristow, N J, 1993. Resistibility of iron ore sinters to low-temperature reduction degradation, in *Proceedings Sixth International Symposium on Agglomeration,* pp 338-343, Nagoya, 15 - 17 November.

Mishra, U N, Thakur, B and Mediratta, S R, 1996. Control of sinter quality for blast furnaces of SAIL through characterisation of high temperature properties, in *Proceedings Ironmaking Conference,* vol 55, pp 407-412, Pittsburgh, 24 - 27 March.

Murty, C H V G K, De, A, Chatterjee, A and Rao, V S, 1994. Reduction of alumina in iron ore classifier fines and its influence on sinter, *Tata Search*, pp 7-13.

Panigrahy, S C, Rigaud, M and Dilewijns J, 1984a. Effect of MgO on low temperature reduction strength, *Iron and Steel Int*, February, pp 29-33.

Panigrahy, S C, Verstraeten, P and Dilewijns, J, 1984b. Influence of MgO addition on mineralogy of iron ore sinter, *Metallurgical Transactions B,* 15B(March):23-32.

Pimenta, H P and Seshadri, V, 2002a. Characterisation of structure of iron ore sinter and its behaviour during reduction at low temperatures, *Ironmaking and Steelmaking,* 29(3):169-174.

Pimenta, H P and Seshadri, V, 2002b. Influence of Al_2O_3 and TiO_2 on reduction degradation behaviour of sinter and hematite at low temperatures, *Ironmaking and Steelmaking,* 29(3):175-179.

Pimenta, H P, Seshadri, V, Cardoso, M B and Azevedo, A T, 1993. Influence of Al_2O_3 and TiO_2 on the reduction degradation behaviour of sinter and hematite at low temperatures, in *Proceedings Sixth International Symposium on Agglomeration,* pp 32-337, Nagoya, 15 - 17 November.

Yang, L X and Matthews, E, 1997. Sintering reactions of magnetite concentrates under various atmospheres, *ISIJ International,* 37(11): 1057-1065.

SUPPLEMENT IV

Paananen T, Heikkinen E-P, Kokkonen, T & Kinnunen K: PREPARATION OF MONO-, DI- AND HEMICALCIUM FERRITE PHASES VIA MELT FOR THE REDUCTION KINETICS INVESTIGATIONS, Steel research international, 80(2009)6, pp. 402 - 407. (Presented also in Scanmet III conference, 2008).

SUPPLEMENT IV

PAANANEN T, HEIKKINEN E-P, KOKKONEN, T & KINNUNEN K: PREPARATION OF MONO-, DI- AND HEMICALCIUM FERRITE PHASES VIA MELT FOR THE REDUCTION KINETICS INVESTIGATIONS, STEEL RESEARCH INTERNATIONAL, 80(2009)6, PP. 402-407.

Process Metallurgy

Preparation of Mono-, Di- and Hemicalcium Ferrite Phases via Melt for Reduction Kinetics Investigations

Timo Paananen[1], Eetu-Pekka Heikkinen[2], Tommi Kokkonen[2], Kimmo Kinnunen[1]

[1] Rautaruukki Oyj, Ruukki Production, Rautaruukintie 155, P.O. Box 93, FI-92101 Raahe, Finland, timo.paananen@ruukki.com
[2] Department of Process and Environmental Engineering, Laboratory of Metallurgy, PO Box 4300, FI-90014 University of Oulu, Finland

Iron ore concentrates that are used in the iron production are usually agglomerated into sinter or pellets in order to improve their properties in the blast furnace. The main minerals in the magnetite base sinters are hematite, magnetite and Si and Al containing calcium ferrites of which the latter can exist as either monocalcium ferrite, dicalcium ferrite or hemicalcium ferrite depending on the conditions and on the material's iron/calcium-ratio. In order to study the reduction behaviour of the sinter in the iron production, samples of monocalcium ferrite, dicalcium ferrite and hemicalcium ferrite were prepared by melting different proportions of pure calcium and iron oxides. After melting the samples were cast and cooled. Samples of hemicalcium ferrite were also heated at a certain temperature before the actual reduction experiments in order to ensure the wanted phase composition of the samples. The mineral compositions of the samples were verified using scanning electron microscopy (SEM-EDS) as well as X-ray diffraction (XRD). The verification showed that it was possible to produce the samples of calcium ferrites via melting. The conditions needed to reduce the calcium ferrites were estimated with thermodynamic calculations.

Keywords: calcium ferrites, sample preparation, reduction, SFCA, hemi-calcium ferrite, monocalcium ferrite, dicalcium ferrite

DOI: 10.2374/SRI09SP016; submitted on 4 December 2008, accepted on 3 February 2009

Introduction

In order to improve the properties of blast furnace burden materials, iron ore concentrates are usually agglomerated into sinter or pellets. The mineralogical as well as the macroscopic structure of the material is changed due to melting and crystallization phenomena that take place in the sintering due to high temperatures (close to 1400°C). The main minerals in the magnetite based sinters are hematite, magnetite and Si and Al containing calcium ferrites (SFCA; Silico Ferrite of Calcium and Alumina). Although the content of calcium ferrites is low compared with the amount of hematite and magnetite, it is a determining factor in melt formation and crystallization of high bacisity, magnetite based sinters ($CaO/SiO_2 > 2$).

Calcium ferrites have a significant effect on the cold strength and reduction strength of the sintered material since it causes particles to stick to each other. In oxidizing conditions the calcium ferrites can exist as either mono-calcium ferrite ($CaFe_2O_4$), dicalcium ferrite ($Ca_2Fe_2O_5$) or hemicalcium ferrite ($CaFe_4O_7$) depending on the conditions and on the material's and especially melt's iron/calcium ratio. It should be noted that in real processes the sinters - as well as the iron concentrates they are made from - always include some impurities (e.g. aluminium and silicon) and therefore it is very unusual for calcium ferrites to exist as pure phases.

A lot of examinations concerning the preparation of synthetic calcium ferrite and SFCA samples for the reduction tests have been published. The methods presented in the literature can be divided in three categories (i.e. solid state sintering, sintering in a partly molten state and via melt) of which the first two were reported to be functional in practice. In most cases the calcium ferrites were prepared using a solid state sintering method [1,2], in which the formation of calcium ferrites takes place in solid state via diffusion between CaO and Fe_2O_3 at low temperatures (below 1200°C). In another method (sintering in a partly molten state) the temperature is slightly higher (approximately 1300 - 1400°C) than in the solid state sintering method, which causes calcium ferrite formation to take place via solid-melt reaction [3-6]. In order to achieve crystallisation from completely molten material, the temperature has to be even higher depending on the ratio of CaO and Fe_2O_3. However, there are problems such as high reactivity of calcium ferrite melt that has been reported in the literature concerning the preparation of calcium ferrites via melt [7,8]. In this study the purpose was to prepare all main calcium ferrite types (hemi-, mono- and di-) via melt.

This study consists of two main topics. In the first part thermodynamic calculations were used to estimate the equilibrium conditions to be used in the preparation of calcium ferrite samples as well as in the reduction tests of these materials in which the reaction kinetics and mechanisms of the calcium ferrites were defined. The second part of this study consists of actual preparation of the calcium ferrite samples via melt. The purpose of the study was to investigate the stability of calcium ferrites in various gas atmospheres and temperatures. Thermo-dynamic calculations were used to estimate the partial pressures of oxygen in equilibrium with different oxide phases with various iron/calcium ratios.

Methods

Thermodynamic calculations. In order to estimate the partial pressures of oxygen ($p(CO)/p(CO_2)$ ratio to be

SUPPLEMENT IV

PAANANEN T, HEIKKINEN E-P, KOKKONEN, T & KINNUNEN K: PREPARATION OF MONO-, DI- AND HEMICALCIUM FERRITE PHASES VIA MELT FOR THE REDUCTION KINETICS INVESTIGATIONS, STEEL RESEARCH INTERNATIONAL, 80(2009)6, PP. 402-407.

exact) in equilibrium with different oxide phases with various iron/calcium ratios, equilibrium compositions of the Ca-Fe-O-C-systems were determined computationally using a FactSage software and its databases [9]. The software, its database and its possibilities and restrictions have been presented thoroughly elsewhere by the authors of the software [10], thus making it unnecessary to present the software here.

The purpose of the computations was to determine predominance area diagrams describing the stability regions of different phases as a function of partial pressures of CO and CO_2 at different temperatures. The stabilities of different calcium ferrites and iron compounds (oxides, carbide and metallic iron) were considered using three different Ca/Fe ratios. The systems that were considered computationally are presented in **Table 1**. In all the calculations, all the solid compounds were assumed to be pure phases with a single composition.

Table 1. Descriptions of the systems considered for thermodynamical calculations.

Elements	Variables	Temp. [°C]	Fe/(Ca+Fe) -ratios		
Ca-Fe-O-C	p_{CO}: p_{CO2}	950	0.50 …0.67	0.67 …0.80	0.80 …1.00
Ca-Fe-O-C	p_{CO}: p_{CO2}	1000	0.50 ... 0.67	0.67 ... 0.80	0.80 ... 1.00
Ca-Fe-O-C	p_{CO}: p_{CO2}	1050	0.50 ... 0.67	0.67 ... 0.80	0.80 ... 1.00
Ca-Fe-O-C	p_{CO}: p_{CO2}	1100	0.50 ... 0.67	0.67 ... 0.80	0.80 ... 1.00
Ca-Fe-O-C	p_{CO}: p_{CO2}	1150	0.50 ... 0.67	0.67 ... 0.80	0.80 ... 1.00
Ca-Fe-O-C	p_{CO}: p_{CO2}	1200	0.50 ... 0.67	0.67 ... 0.80	0.80 ... 1.00

Table 2. CaO/Fe_2O_3 ratios and chemical compositions of calcium ferrites.

	CaO (wt.%)	Fe_2O_3 (wt.%)	Ca (wt.%)	Fe (wt.%)	O (wt.%)	Fe/(Ca+Fe)
$2CaO{\cdot}Fe_2O_3$	41.3	58.7	29.5	41.1	29.4	0.58
$CaO{\cdot}Fe_2O_3$	26.0	74.0	18.6	51.8	29.7	0.74
$CaO{\cdot}2Fe_2O_3$	14.9	85.1	10.7	59.5	29.8	0.85

Preparation of calcium ferrites. Calcium ferrites were prepared from synthetic CaO and Fe_2O_3 powders with the purities of 99.95 wt.% and 99.998 wt.%, respectively. In order to ensure that the CaO powder is free of hydroxides, it was calcinated before the powder mixtures with different CaO/Fe_2O_3 ratios were prepared. CaO/Fe_2O_3 ratios and chemical compositions of calcium ferrites are described in **Table 2**.

The powder mixes with certain CaO/Fe_2O_3 ratios were set in a platinum crucible placed in a spinel ($MgO{\cdot}Al_2O_3$) crucible and melted in a chamber furnace in air. The Temperature was increased slowly to 1500 or 1600°C depending on the type of calcium ferrite (cf. **Figure 1** in which the numbers 1-3 describe conditions and compositions of the initial melts). Calcium ferritic melt was quickly cast into a mould and cooled down as described in **Figure 2**.

Metastable hemicalcium ferrite samples were annealed at 1170°C which is located in the stability area of hemicalcium ferrite in air (cf. number 4 in Figure 1).

Polished sections were prepared from the calcium ferrite samples for optical and scanning electron microscopy and analyses.

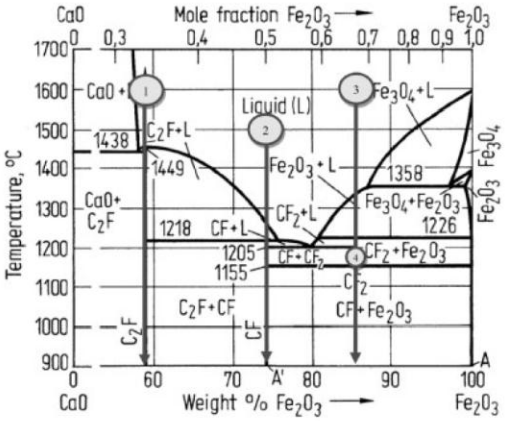

Figure 1. Binary phase diagram of system CaO-Fe2O3 [11].

Figure 2. Casting of calcium ferrite melt into a copper mould placed on a water cooled copper plate.

Results and Discussion

Predominance area diagrams describing the phase stabilities of the Ca-Fe-O-C system at 950°C (with two different Fe/Ca-ratios) and 1200°C (with one Fe/Ca-ratio) are presented in **Figures 3 to 5** as examples of the results from the thermodynamics computations.

The predominance area diagrams were used to define the partial pressures of oxygen ($p(CO)/p(CO_2)$ ratio to be exact) in equilibrium with different phases. As an example a phase boundary between the stability areas of $CaFe_2O_4$ + Fe_3O_4 and $Ca_2Fe_2O_5$ + Fe_3O_4 (i.e. the phase boundary between mono- and dicalcium ferrites in contact with magnetite) in Figure 3 can be examined. It is seen that the ratio between the partial pressures of CO and CO_2 has a constant value of approximately $0.24{\cdot}10^{-3}$, which corresponds to a partial pressure of oxygen of approximately $1.6{\cdot}10^{-8}$ atm. At higher values of p_{O2} monocalcium ferrite is thermodynamically more stable than dicalcium ferrite and at lower values the situation is opposite. A similar approach can be used to define the equilibrium values of p_{O2} (or p_{CO}/p_{CO2}) for other phase boundaries in the system. The plus symbols (+) in Figures 3 to 5 signify the area in which the sum of partial pressures of CO and CO_2 equals 1 atm (i.e. the atmospheric pressure with only these two components in the gas phase).

SUPPLEMENT IV

PAANANEN T, HEIKKINEN E-P, KOKKONEN, T & KINNUNEN K: PREPARATION OF MONO-, DI- AND HEMICALCIUM FERRITE PHASES VIA MELT FOR THE REDUCTION KINETICS INVESTIGATIONS, STEEL RESEARCH INTERNATIONAL, 80(2009)6, PP. 402-407.

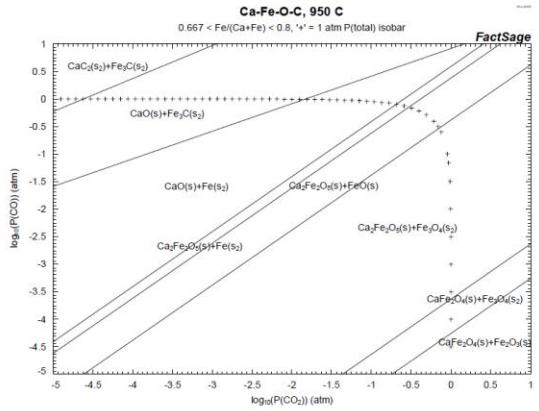

Figure 3. Predominance area diagram describing phase stabilities of a system containing calcium, iron, oxygen and carbon with an Fe/(Fe+Ca) ratio between 0.67 and 0.8 at 950°C .

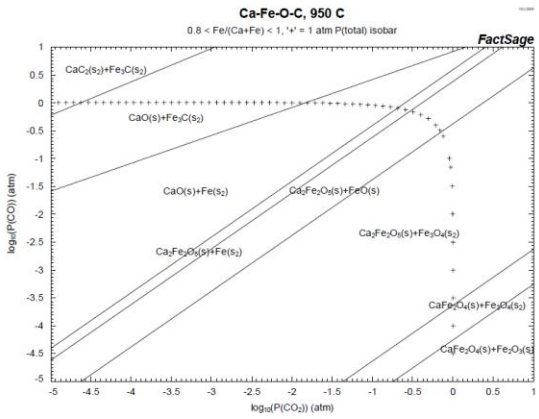

Figure 4. Predominance area diagram describing phase stabilities of a system containing calcium, iron, oxygen and carbon with an Fe/(Fe+Ca) ratio between 0.8 and 1 at 950°C .

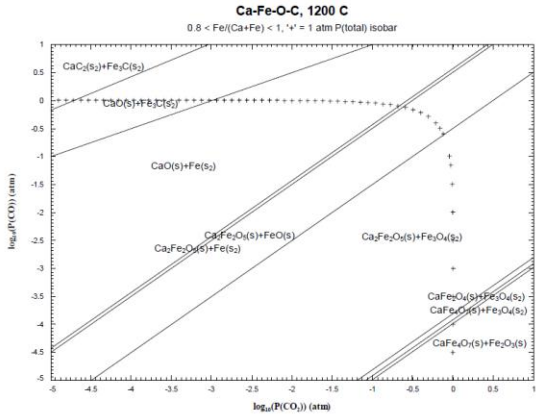

Figure 5. Predominance area diagram describing phase stabilities of a system containing calcium, iron, oxygen and carbon with an Fe/(Fe+Ca) ratio between 0.8 and 1 at 1200°C .

According to the calculations the CO/CO_2 ratio in the gas is approximately 22/78 at the phase boundary between magnetite and wüstite in equilibrium with dicalcium ferrite. This differs from the value of pure magnetite reduction, where the CO/CO_2 ratio is 10/90 [12].

Thermodynamic computations were used to estimate the stability regions of pure calcium ferrites in order to define the conditions in which different phases were prepared experimentally and especially to define the conditions for reduction experiments. However, due to limitations of available databases, it was not possible to computationally estimate the distribution of trace elements (e.g. silicon) in different solid solutions.

Dicalcium ferrite was crystallized straight from the melt, and it formed a homogeneous matrix in which distinct dicalcium ferrite crystals could be observed as is seen in **Figure 6**. The stoichiometric composi-tions of the calcium ferrites (C2F, CF and 2CF) are presented in the same diagram as a bar chart together with the compositions from the sample. This bar chart shows that the composition of the crystals in the sample is close to the stoichiometric composition of the dicalcium ferrite.

In the casting of the melt, corresponding to the composition of monocalcium ferrite, the formation of columnar dicalcium ferrite crystals was observed to take place from the surface to the core of the samples (Figure 2). Between the dicalcium ferrite crystals there was a streaky area where the chemical composition varied between hemicalcium ferrite and monocalcium ferrite as can be seen in **Figure 7**. It is proposed that both phases co-exist due to quick cooling. Quenching caused a situation in which the samples did not have enough time to form the thermodynamically most stable phases. Thus both calcium ferrites are proposed to occur in the area.

Homogenous hemicalcium ferrite was not achieved by only casting the melt to the mould. The sample had to be annealed after the casting in order to achieve the wanted structure. The crystallised sample before annealing was full of CaO-bearing iron oxide and one or two calcium ferrites as seen in **Figure 8**.

The chemical analyses of the present phases did not correspond accurately to the stoichiometric phases. This implies that two separate phases exist that cannot be detected separately by electron microscopy due to the tiny crystal size in proportion to the analysis spot of the electron microscope. Therefore, they did not match the composition of either hemi- or monocalcium ferrite as described in **Figure 9**.

After heating at 1170°C, the sample consisted mainly of hemicalcium ferrite, although a few hematite crystals could also be observed in the sample (cf. **Figure 10**). The chemical composition was close to the composition of stoichiometric hemicalcium ferrite as can be seen in **Figure 11**.

SUPPLEMENT IV

PAANANEN T, HEIKKINEN E-P, KOKKONEN, T & KINNUNEN K: PREPARATION OF MONO-, DI- AND HEMICALCIUM FERRITE PHASES VIA MELT FOR THE REDUCTION KINETICS INVESTIGATIONS, STEEL RESEARCH INTERNATIONAL, 80(2009)6, PP. 402-407.

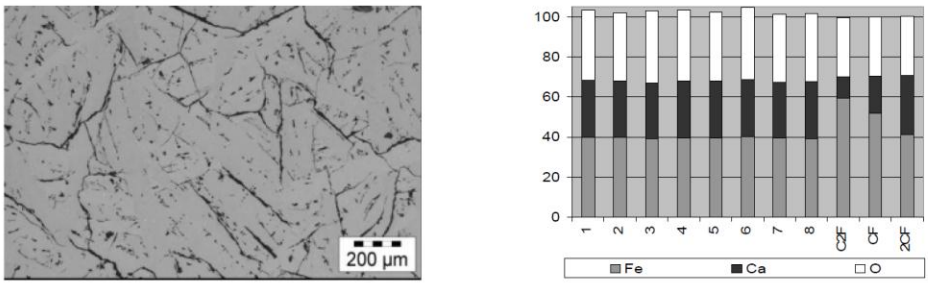

Figure 6. Optical microscope images from a polished section made from the cast sample with the total composition corresponding to dicalcium ferrite.

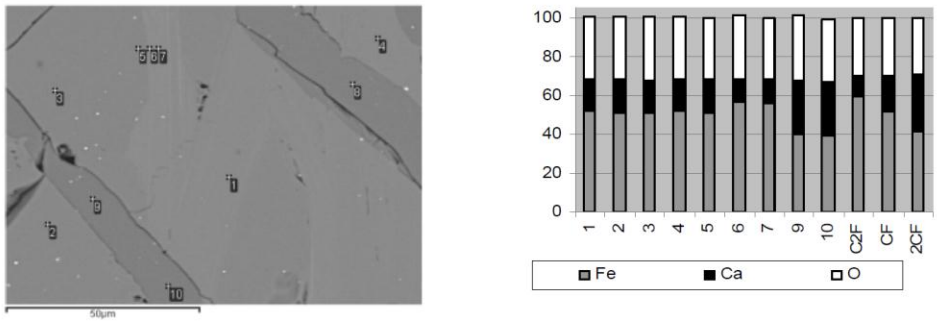

Figure 7. SEM-image and analysis from a polished section made from the cast sample with the total composition corresponding to monocalcium ferrite.

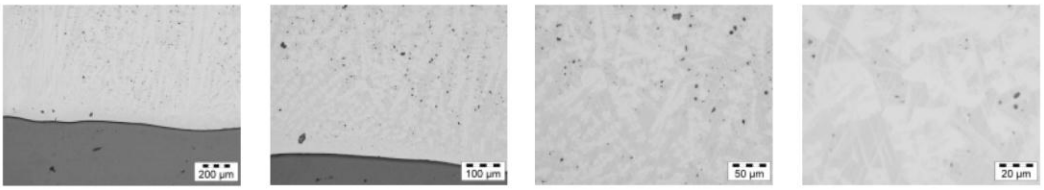

Figure 8. Microscope images from polished sections made from the cast sample with the total composition corresponding to hemicalcium ferrite.

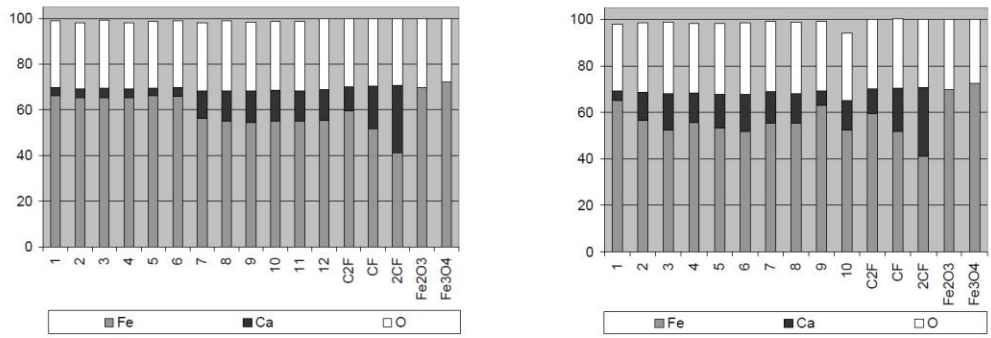

Figure 9. Results of analysis from cast melt corresponding to the composition of hemicalcium ferrite. The last five patterns on the right show chemical compositions of calcium ferrites, hematite and magnetite.

SUPPLEMENT IV

PAANANEN T, HEIKKINEN E-P, KOKKONEN, T & KINNUNEN K: PREPARATION OF MONO-, DI- AND HEMICALCIUM FERRITE PHASES VIA MELT FOR THE REDUCTION KINETICS INVESTIGATIONS, STEEL RESEARCH INTERNATIONAL, 80(2009)6, PP. 402-407.

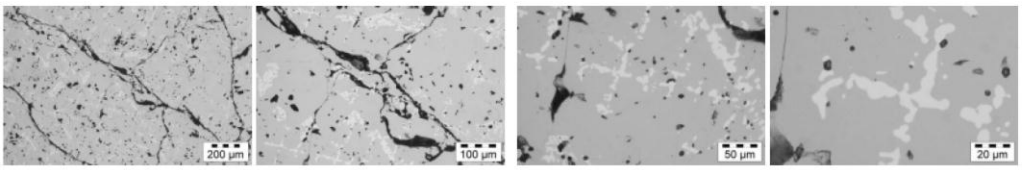

Figure 10. Microscope images from polished sections made from the cast and annealed sample with the total composition corresponding to hemicalcium ferrite.

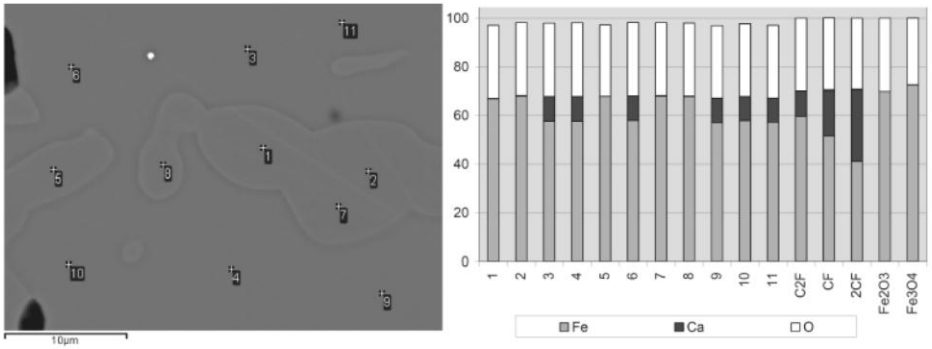

Figure 11. Scanning electron microscope image and analysis from the cast and heated sample. The total chemical composition of the sample corresponds to that of hemicalcium ferrite. The result of the analysis is described in the bar chart.

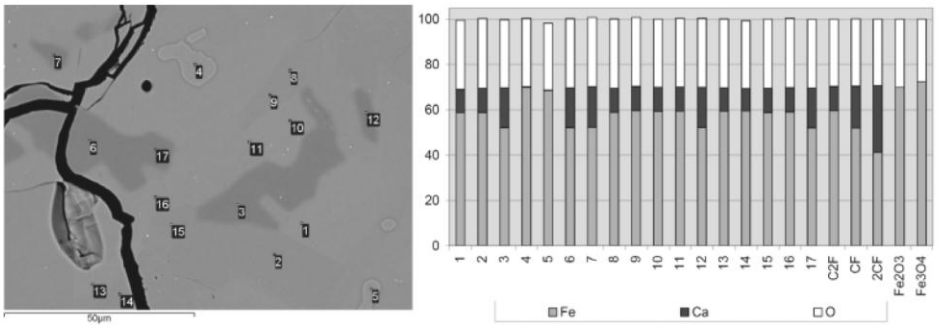

Figure 12. Scanning electron microscope image and analysis from the cast and heated sample. The total chemical composition of the sample corresponds to that of hemicalcium ferrite. The result of the analysis is described in the bar chart.

Small areas of monocalcium ferrites could also be observed in the core of the sample as seen in **Figure 12**. This means that the annealing time should have been longer in order to have enough time for the formation of hemicalcium ferrite from the CaO-rich monocalcium ferrite and CaO-pore hematite.

In addition to the predominance area diagrams presented in Figures 3 to 5 computational thermodynamics were used to define the reduction route for the calcium ferrites as well as the $p(CO)/p(CO_2)$ ratios at which the different phases are in equilibrium with each other. The results of these computations are presented in **Figure 13**.

Conclusions

Thermodynamic computations were used to support the experimental procedures for the reduction of hemi-, mono- and dicalcium ferrites, and the main results are described in Figure 13. However, due to the limited resources of available databases, it was not possible to computationally estimate the behaviour of trace elements in solid solutions.

Preparations of hemi-, mono- and dicalcium ferrites were executed and confirmed. Dicalcium ferrite demanded the highest casting temperature but was the easiest to prepare as nearly homogeneous phase. The other calcium

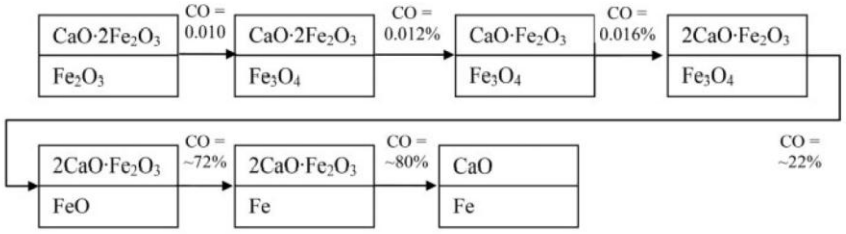

Figure 13. Stepwise reduction of hemicalcium ferrite in equilibrium with iron oxide at 1200°C in CO/CO_2-atmosphere according to thermodynamic calculations.

ferrites demanded either very slow cooling (for the preparation of the monocalcium ferrite samples) or heating after casting (for the preparation of the hemicalcium ferrite samples).

Acknowledgement

Research has been financially supported by the Finnish Funding Agency for Technology and Innovation (Tekes) which is kindly acknowledged by the authors.

References

[1] D. Sichen, N.S. Srinivasan, L-I. Staffansson: Scandinavian Journal of Metallurgy, 17 (1988), No. 5, 232.
[2] H.S. Kim, J.H. Park, Y.C. Cho: Ironmaking and Steelmaking, 29 (2002), No. 4, 266.
[3] S.C. Panigrahy, M. Rigaud: Steel Research, 59 (1988), No. 4, 153.
[4] R. Chaigneau, R.H. Heerema: Calcium Ferrites and the diversity in their reduction behaviour, Ironmaking conference proceedings, 1992, p. 111.
[5] L-H. Hsieh, J.A. Whiteman: ISIJ Int., 33 (1993), No. 4, 462.
[6] H.P. Pimenta, V. Seshadri: Ironmaking and Steelmaking, 29 (2002), No. 3, 169.
[7] R. Chaigneau: Complex Calcium Ferrites in the Blast Furnace Process. Doctoral thesis, Delft University Press, 1994, p. 192.
[8] Y. Takeda, S. Nakazawa, A. Yazawa: Can. Metall. Quaterly, 19 (1980), No. 3, 297.
[9] C.W. Bale, A.D. Pelton, W.T. Thompson, G. Eriksson, K. Hack, P. Chartrand, S. Degterov, J. Melancon, S. Petersen: FactSage Version 5.4 Software and its databases. ThermFact. 2006.
[10] C.W. Bale, P. Chartrand, S.A. Degterov, G. Eriksson, K. Hack, R. Ben Mahfoud, J. Melancon, A.D. Pelton, S. Petersen: Calphad, 26 (2002), No. 2, 189.
[11] B. Phillips, A. Muan: J. Am. Ceram. Soc., 42 (1959), No. 9, 413.
[12] L. von Bogdandy, H-J. Engel: The Reduction of Iron Ores, Scientific Basis and Technology, Springer-Verlag, Düsseldorf, 1971, p. 448.

SUPPLEMENT V

Paananen, T & Kinnunen, K: Effect of TiO2-content on Reduction of Iron Ore Agglomerates, Steel research international, 80(2009)6, pp. 408 - 414. (Presented also in Scanmet III conference, 2008).

SUPPLEMENT V

PAANANEN, T & KINNUNEN, K: EFFECT OF TIO2-CONTENT ON REDUCTION OF IRON ORE AGGLOMERATES, STEEL RESEARCH INTERNATIONAL, 80(2009)6, PP. 408-414.

Process Metallurgy

Effect of TiO_2-content on Reduction of Iron Ore Agglomerates

Timo Paananen and Kimmo Kinnunen

Rautaruukki Oyj, Ruukki Production, Rautaruukintie 155, P.O. Box 93, FI-92101 Raahe, Finland, timo.paananen@ruukki.com

The effect of titanium oxide on iron ore agglomerates is studied by the use of test sinter, test pellets and synthetic briquettes under laboratory conditions. Titanium favours secondary hematite rather than magnetite, which is the main phase in the sinter of Rautaruukki's Raahe plant. Additionally, the effects of sinter RDI and pellet LTD on the blast furnace process are evaluated using the test results of basket trials in LKAB's Experimental Blast Furnace. The effect of titanium in synthetic hematite is studied as hematite is reduced to magnetite in the RDI test. This occurrence causes deterioration in burden permeability.

Synthetic titanium-bearing iron oxides under controlled conditions are investigated at the University of Oulu. The effect of TiO_2, in solid solution in magnetite, on the magnetite to hematite oxidation is studied separately in order to simulate the final stage of the sintering process. In other experiments, hematite samples doped with various contents of TiO_2 are studied using thermogravimetry under a controlled gas atmosphere ($CO/CO_2/H_2/N_2$). The TiO2 content of hematite has a clear effect on reduction degradation. Also increasing content of TiO_2 in solid solution in magnetite radically accelerates the oxidation rate. In the pilot tests, TiO_2 content has a similar negative effect on the reduction strength of both sinter and pellets

Keywords: pellet, reduction degradation, iron ore, titanium oxide, hematite, RDI, LTD

DOI: 10.2374/SRI09SP023; submitted on 4 December 2008, accepted on 3 February 2009

Introduction

Approximately 3 million tonnes of magnetite based iron ore sinter is produced at Raahe sinter plant annually, which accounts for more than 70% of the blast furnace iron burden. The magnetite iron ore and some titanium bearing secondary raw materials contain some TiO_2. Sinter basicity (CaO/SiO_2) is been typically approximately 2 and the MgO content 2.3 mass-%. The Fe content is close to 61 mass-% and the FeO content is high (10 - 12 mass-%) because of the high amount of relic magnetite. During the year 2006 the average of the reduction degradation index $RDI_{-3.15mm}$ (ISO4696-1) was 22.2 %, with variation being from 13 to 33 %. The RDI was found to correlate strongly with the titanium content of the sinter. The sinter produced is used in two small blast furnaces (about 1200 m^3) along with a relatively small amount of pellets (390 kg per ton of hot metal (kg/tHM)). About 117 kg/tHM of heavy oil was used as an auxiliary reductant. The oil replaces coke and relieves volumetric space inside the furnaces for iron burden reduction, resulting in increased hot metal production capacity. Practical experiments have shown that an improvement in the sinter RDI enables a higher oil injection rate.

A number of papers have been published regarding the factors affecting sinter RDI. The parameters affecting the RDI can be categorized as sintering parameters, properties of the raw materials, and chemical composition of the sintering mix. For example, increasing the MgO content [1-3], basicity CaO/SiO_2 [4,1,2] and fuel rate improves the reduction degradation properties of the sinter. On the other hand, increasing the content of Al_2O_3 [3,2,5,6] and TiO_2 [4,6-10] has a negative effect on RDI. Moreover, the mineralogy of sinter is a significant factor in reduction strength. One controlling factor of mineralogy is the chemical composition, especially the CaO/SiO_2 ratio, and even small changes in the content of minor components, such as MgO, Al_2O_3 and TiO_2, have a clear effect on the sinter mineralogy [1,11]. An increase in the alumina content has been shown to cause more calcium ferrites or SFCA-phase in sinter [10]. Similarly, MgO has been shown to stabilize magnetite in sinter [1].

An adequate range of pellet $LTD_{-6.3mm}$ (ISO 13930: 1998(E)) suitable for the blast furnace process has not been widely published, probably because the reduction strength of pellets is generally assumed to be significantly better than that of sinter [12]. Both RDI- and LDT-tests are used in analysing pellet quality, these test values are not easily comparable, however, The effect of pellet chemical composition on reduction degradation properties has been discussed in several papers [13,14]. Also, the effect on pellet microstructure of the chemical composition, the physical properties of the raw materials and the sintering temperature has been studied [15]. A high content of skeletal rhombohedral hematite has been found to be detrimental to pellet reduction strength [15]. Additionally, reduction strength is affected by mineral hardness/density surrounding characteristically hematite (secondary hematite) shaped crystals [6].

The negative effect of titanium oxide on RDI has been studied previously in several papers but there are no published studies of the effect of titanium on LTD for pellets. Laboratory made test pellets having different TiO_2-contents are investigated in this paper. The pilot scale tests of this study additionally focus on the relevance of LTD results in the BF process under pilot scale experimental blast furnace (EBF) conditions. The correspondence between analysed LTD-values and behaviour under EBF-conditions is compared. The mechanism affecting both sinter and pellet reduction strength is investigated by preparing synthetic briquettes and subjecting these to reduction. This laboratory study focuses on the effect of

dissolved TiO_2 in iron oxides on the reduction reactions of hematite and magnetite and on the oxidizing of magnetite to hematite. The latter indicates that the phenomenon occurs after the sintering process when sinter or pellets are cooling down under oxidizing conditions.

Methods

Pilot scale experiments

The test pellets were prepared under laboratory conditions. The pelletizing mix was prepared by weighing the amount of raw materials, mixing and feeding manually to the pelletizing drum. The green pellet size after pelletizing was screened to 10 – 12.7 mm and the moisture content was very close to 7.2 %, thus, a little extra moisture was required in the case of the hematite concentrate compared with magnetite concentrate.

After pelletizing the green pellets were dried at a temperature of 105ºC for one day. The dried pellets were then sintered in a small electric furnace. The furnace was preheated to 600ºC and the sintering atmosphere was adjusted to enable oxidizing of magnetite to hematite. The target FeO-content of the sintered pellets was set to 0.5 %. Therefore, a constant amount of air was blown into the furnace during the sintering stage. Sintering time in these tests was 1-2 hours. The chemical compositions of the iron ore concentrates used are presented in **Table 1**. The grain size distribution of materials was similar to that of typical production scale materials.

The chemical compositions of the additives used are presented in **Table 2**. Bentonite was used to improve the pelletizing process. Rutilite is a rutile-containing material used to increase the TiO_2-content in the test pellets. Lime stone was also used as an additive to adjust the pellet quality and mineralogy.

Two separate test sets were carried out. The aim of the first test was to study the effect of TiO_2-content on test pellet LTD using different sintering parameters. The second test set was carried out to study the test pellet behaviour under experimental blast furnace (EBF) conditions.

Test pellets: Set 1. The first set of test pellets were sintered under the conditions presented in **Table 3**. The aim of this test program was to study the effect of increased TiO_2-content on iron ore pellets. The bentonite addition to each pellet type was identical. Rutilite additions were realized at two levels. Sintering temperature was kept constant. Sintering time is always an

Table 1. Chemical composition of iron ore concentrates, in mass-%.

Concentrate	Fe	CaO	SiO_2	MgO	Al_2O_3	TiO_2	V_2O_5	Sum
Magnetite A	71.1	0.12	0.39	0.25	0.24	0.46	0.32	72.88
Hematite	68.2	0.14	1.04	0.15	0.35	0.30	0.14	70.32
Magnetite B	71.4	0.16	0.57	0.18	0.12	0.11	0.22	72.76

Table 2. Chemical composition of additive materials for test pellets, in mass-%.

Raw material	Fe	CaO	SiO_2	MgO	Al_2O_3	TiO_2	V_2O_5	FeO	Weight loss in % at 900ºC
Bentonite	3.18	9.95	48.40	2.95	16.50	0.74	0.03	0.30	14.70
Rutilite	3.86	3.21	25.20	2.94	5.20	55.05	0.50	0.00	0.43
Lime stone	0.24	52.90	0.85	0.94	0.45	0.03	0.00	-	42.90

Table 3. Sintering conditions and composition of test pellet set 1.

Test Set 1	Concentrate	Bentonite [mass-%]	Rutilite [mass-%]	Temperature [ºC]	Sintering time [min]
MaA 1h	Magnetite A	1.0	0.00	1250	60
MaA 2h	Magnetite A	1.0	0.00	1250	120
MaA 1h TiO_2	Magnetite A	1.0	0.31	1250	60
MaA 2h TiO_2	Magnetite A	1.0	0.31	1250	120
He 1h	Hematite	1.0	0.00	1250	60
He 2h	Hematite	1.0	0.00	1250	120
He 1h ++TiO_2	Hematite	1.0	0.80	1250	60
He 2h ++TiO_2	Hematite	1.0	0.80	1250	120
MaB 1h	Magnetite B	1.0	0.00	1250	60
MaB 2h	Magnetite B	1.0	0.00	1250	120
MaB 1h +TiO_2	Magnetite B	1.0	0.31	1250	60
MaB 2h +TiO_2	Magnetite B	1.0	0.31	1250	120
MaB 1h ++TiO_2	Magnetite B	1.0	0.70	1250	60
MaB 2h ++TiO_2	Magnetite B	1.0	0.70	1250	120

Table 4. Sintering conditions and composition of test pellet set 2.

Test Set 2	Concentrate	Bentonite [mass-%]	Calcite [mass-%]	Rutilite [mass-%]	Temperature [ºC]	Sintering time [min]
MaB 1.5h	Magnetite B	1.0	0.0	0.00	1250	90
MaB 1.5h + TiO_2	Magnetite B	1.0	0.0	1.39	1250	90
MaB 1.5h + TiO_2 + CaO	Magnetite B	1.0	3.0	1.39	1250	90
MaB 1.5h + CaO	Magnetite B	1.0	3.0	0.00	1250	90

important parameter and therefore all of the tests were carried out using two sintering times (1 h and 2 h).

Test pellets: Set 2. The second set of test pellets was sintered under slightly different conditions (**Table 4**). Bentonite addition, sintering time and temperature were constant for each of these tests. Lime stone and rutilite rates were the variables adjusted, affecting pellet mineralogy and quality. The aim of CaO-addition was to affect pellets mineralogy and produce pellets of very poor quality, and then study the mechanism affecting reduction strength.

Laboratory experiments

Materials. The test material used in the oxidizing experiments was magnetite fines mixed with varying amounts of TiO_2. The magnetite content of the fines was 96.1 mass-% and the total iron oxide content, including hematite, was approximately 97.8 mass-%. The most significant quantities of other oxides are shown in **Table 1** (Magnetite A). The test materials, used in the reduction experiments, were Puratronic grade hematite (99.998 mass-%) and magnetite chemicals (99.997 mass-%) also mixed with varying amounts of TiO_2. Rutile powder (TiO_2) with a grain size below 44 µm and a purity of 99 % or above was used as the titanium oxide additive.

Preparation of samples. The Magnetite A fines were ground and sieved to a grain size of less than 74 µm. The Puratronic oxide powders (magnetite and hematite) were used without any additional treatment. TiO_2 was mixed into the fines in amounts corresponding to 0.5, 2 and 5 mass-%. The powder mix to which approximately 15 mass-% of purified ethyl alcohol had been added was pressed into briquettes under a pressure of 50 MPa. The wet briquettes were dried at 110°C for a minimum of 2 h. Pressed briquettes (12 mm ϕ x 5 mm), as described earlier, were sintered in a 34 mm diameter tube furnace at 1300°C for 5 h, the magnetite briquettes in a CO/CO_2 atmosphere (CO/CO_2 = 5/95 and flow rate 1 l/min) and hematite in air. Upon completion of sintering the briquettes were quickly quenched in a water cooled copper chamber, in an argon atmosphere. After cooling, the briquettes were ready for the reduction/oxidizing experiments. The aim was to produce compact and dense briquettes for topochemical reaction during the reduction.

Reduction of samples. Two different types of reduction experiments were carried out. The hematite-magnetite reduction step was examined under the conditions used in the standard RDI-test where the temperature was 500°C and the gas composition $CO/CO_2/H_2/N_2$ = 20/20/2/58 respectively, whilst the reduction of iron oxides to iron was examined under conditions of temperature of 950°C and gas composition of CO/CO_2 = 90/10. The prepared and sintered briquettes were reduced using the thermo-gravimeter (TGA). The TGA included a 34 mm diameter tube furnace in which a reducing gas mixture of H_2, N_2, CO and CO_2 at a flow rate of 2 l/min was achieved. The gas composition and reduction temperature were kept constant during the experiments. Before the reduction, the sample was first heated to reduction temperature in an argon atmosphere for 5 min. The reduction time was 360 min, for the samples reduced to iron (CO/CO_2 = 90/10) and 60 min for the hematite briquettes reduced to magnetite under RDI-conditions. During the reduction test, the sample was located in a platinum basket hanging on a gravimeter connected to a computer for data collection. After the reduction, the briquettes were rapidly cooled in a copper chamber in an argon atmosphere as described earlier.

Results

Effect of TiO_2-content on the LTD of test pellet Set 1. The final chemical composition of the test pellets can be seen in **Table 5**. The only obvious change is in the TiO_2- and SiO_2-contents. SiO_2-content increases slightly with TiO_2 because rutilite also contains a small amount of silica.

The effect of increased TiO_2-content on test pellet LTD is presented in **Figure 1**. All test pellets were sintered using two different sintering times: 1 h and 2 h. The difference in the level of the lines is caused by the properties of the iron ore concentrates used. The only change being made is that of the rutilite content. For example the sample MaA is coarser in grain size distribution. As can be seen, however, the slope of the lines to the X-axis is almost the same.

Table 5. Final chemical composition of test pellet set 1.

Test Set 1	Fe	FeO	MgO	Al_2O_3	SiO_2	CaO	TiO_2
MaA 1h	68.5	0.5	0.24	0.33	0.87	0.23	0.38
MaA 2h	68.5	0.1	0.24	0.33	0.88	0.22	0.38
MaA 1h TiO_2	68.3	0.5	0.25	0.36	1.01	0.23	0.67
MaA 2h TiO_2	68.3	0.2	0.25	0.36	1.02	0.23	0.67
He 1h	68.3	0.1	0.14	0.44	1.23	0.22	0.26
He 2h	68.4	0.2	0.11	0.40	1.07	0.18	0.26
He 1h ++TiO_2	68.0	0.2	0.17	0.48	1.45	0.23	1.00
He 2h ++TiO_2	68.0	0.2	0.17	0.49	1.50	0.23	1.00
MaB 1h	68.6	1.4	0.14	0.21	1.02	0.22	0.09
MaB 2h	68.4	0.2	0.14	0.21	1.03	0.24	0.09
MaB 1h +TiO_2	68.0	0.1	0.15	0.23	1.15	0.23	0.37
MaB 2h +TiO_2	68.1	< 0.1	0.15	0.23	1.15	0.23	0.36
MaB 1h ++TiO_2	68.2	0.1	0.19	0.27	1.33	0.25	0.72
MaB 2h ++TiO_2	68.1	0.1	0.19	0.28	1.38	0.25	0.73

Quality and mineralogy of test pellets Set 2. The quality and chemical composition for test pellet set 2 are presented in **Table 6**. The codes in the table are as follows:

- REXT: Reduction EXTend at 1000 °C, in %
- TDP20: first melt formation temperature in °C, when 20 mbar pressure drop reached
- TK50: softening index, 50% collapse in voidage, °C
- LTD: Low Temperature Disintegration index in %, for pellet fraction < 6.3 mm

The increase in CaO-content by 1.5 % had a very strong effect on the pellet LTD value. Reducibility is not significantly different between the tests, whereas the softening temperature increased in the case in which CaO-content was increased.

LKAB's experimental blast furnace (EBF) located in Luleå was used to compare the LTD test value and disintegration rate under blast furnace conditions. The test materials were charged to 5 separate levels inside the EBF before quenching. The aim was to study material disintegration as a function of reduction degree. The samples in **Figure 2** were the samples from the highest level in the furnace, where the reduction degree was 60-95 % compared to the state when all of the iron is reduced to pure magnetite. The reduction degree followed logically on reducibility presented in Table 6. The results of the EBF-trial and LTD are presented in Figure 2. The LTD value presented is the standardized test result and EBF $_{+6.3mm}$ means the >6.3 mm fraction in the excavated samples, which were treated using the RDI-test drum in order to induce some disintegration.

Dissolution of TiO_2 into iron oxides. The TiO_2 dissolved completely into the hematite and magnetite up to the 5 mass-% which was the maximum amount of TiO_2 used in the experiment. The XRD analysis from hematite synthesis showed only the alpha hematite phase in all the samples containing TiO_2. However, a slight shift from hematite peaks towards peaks of ilmenite with hematite doped with 5 mass-% TiO_2 could be observed. Moreover, TiO_2 was uniformly distributed and the content was practically constant according to the SEM-EDS analysis. In the case of hematite, the dissolution of Ti^{4+}-cations was caused by reduction of Fe^{3+}-cations to Fe^{2+}-cations as described in an earlier publication [7]. Increasing the TiO_2 content from 0 to 5 mass-% increased the content of the Fe^{2+}-cations from <0.1 to 3.0 mass-% as measured using the titration method. Considering on the atomic level, this means that each Ti^{4+}-cation caused the reduction of one Fe^{3+}-cation to one Fe^{2+}-cation. The lattice structure remained unchanged despite the reduction of the Fe^{3+}-cation, which was proved by XRD analyses [7]. It is proposed that this reversible phenomenon is responsible for enhancing the oxidizing of magnetite to hematite in the final stage of sintering when sinter is cooling down under oxidizing conditions [7].

Table 6. Final chemical composition and quality of test pellet set 2.

Test Set 2	MaB 1.5h	MaB 1.5h +Ti	MaB 1.5h +TiO_2 +CaO	MaB 1.5h +CaO
Fe [%]	68.6	68.4	67.1	67.4
FeO [%]	0.60	0.60	0.40	0.20
SiO_2 [%]	1.01	1.31	1.37	1.05
CaO [%]	0.24	0.26	1.70	1.68
TiO_2 [%]	0.09	0.73	0.75	0.09
REXT [%]	62.7	60.8	64.6	61.9
TDP20 [°C]	1126	1145	1155	1285
TK50 [°C]	1227	1221	1259	1325
LTD [%]	92.2	61.2	1.3	7.5
Compression strength [kp]	276	257	241	180

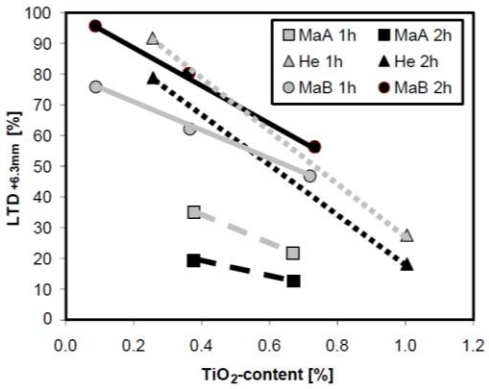

Figure 1. LTD of laboratory made test pellet set 1.

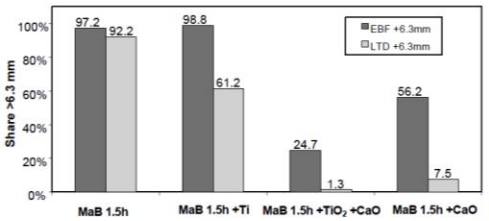

Figure 2. Comparison between LTD value and disintegration rate under EBF-conditions for test pellet set 2.

Reduction of synthesised briquettes. TiO_2 has a clear accelerative effect on reduction of magnetite at contents of 2 and 5 mass-% TiO_2, which can be seen from **Figure 3**, where the reduction curve of the pure sample has been linearized and presented in the graph as the x-axis. The degree of reduction of the pure magnetite sample can be seen at the top of the figure on the secondary x-axis. The three curves presented are the differential degree of reduction for samples with various TiO_2-content compared with the degree of pure sample reduction. For example, the sample doped with 5 wt. % TiO_2 has been reduced 64 %

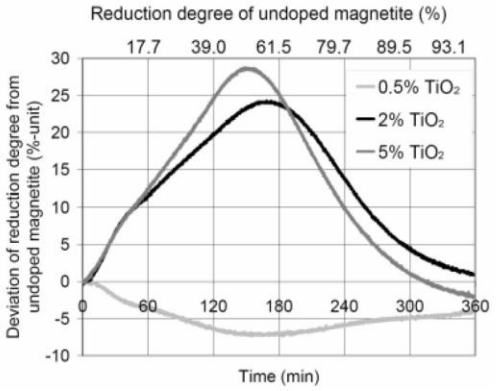

Figure 3. Effect of titanium dioxide on reduction of magnetite. The curves show the difference from the reduction curve of pure magnetite. The degree of reduction for pure magnetite can be read from the secondary x-axis at the top of the figure.

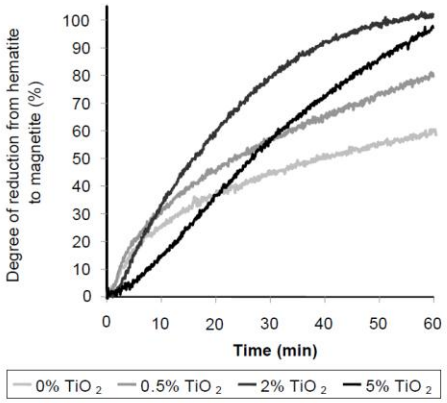

Figure 4. Effect of titanium dioxide on reduction of hematite to magnetite under RDI-conditions.

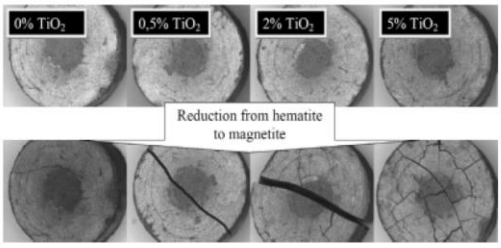

Figure 5. Hematite briquettes before and after RDI-reduction with various TiO_2-contents.

(39% + 25%) as opposed to 39 % for the pure sample, after 120 minutes reduction. Correspondingly the sample doped with 0.5 wt. % TiO_2 has been reduced less than the pure sample, approximately 32 % (39 % - 7 %) after 120 minutes reduction.

TiO_2 had a clear effect on reduction of hematite to magnetite under RDI-conditions (**Figure 4**). At the beginning of the reduction the samples containing 2 and 5 mass-% TiO_2 were reduced more slowly than both the pure sample and that containing 0.5 mass-% TiO_2. However, after a few minutes the rate of reduction increased significantly in the samples containing 2 and 5 mass-% TiO_2. The final degree of reduction was close to 100 % in the samples containing 2 and 5 mass-% TiO_2, but only 60 % in the pure sample.

The largest structural changes during reduction occurred with the samples containing the most TiO_2. The sample containing 5 mass-% TiO_2 showed thorough fracturing and was full of cracks (**Figure 5**). This phenomenon can also be seen with lower TiO_2-content but it is not as strong as with the sample containing 5 mass-% TiO_2.

The hematite to magnetite reduction mechanism was observed to be changed by TiO_2. The reduction front between hematite-magnetite is quite sharp and clear with RDI-reduction of pure hematite. The higher the TiO_2 - content of hematite the more fragmented and disintegrated is the reduction front. The degree of reduction after 15 min reduction was approximately 30 % with pure hematite and correspondingly approximately 25% with the hematite sample containing 5 mass-% TiO_2. Although the degree of reduction was lower with the hematite containing 5 mass-% TiO_2, the reaction penetrated at least three times deeper into the hematite sample, while hematite phases occurred very close to the surface of the sample.

TiO_2 also had an accelerative effect on hematite reduction to iron although during a short period at the beginning of the process retardation of reduction occurred with the samples containing TiO_2 (**Figure 6**). This phenomenon is similar to the RDI-reduction mentioned above in connection with Figure 4. The final degree of reduction is about 99 % for pure hematite but the more TiO_2 the sample contains the lower is the final degree of reduction. Contrary to the RDI-reduction, the samples reduced to iron did not disintegrate.

Discussion

The effect of TiO_2-content on LTD was as dramatic as in the case of sinter [7]. The increasing TiO_2-content caused a systematic deterioration of the reduction strength, which could be observed in both laboratory reduction tests and the standard LTD- and RDI-tests. The results were dependent also on properties of the iron ore concentrates used, chemical composition and grain size distribution. Magnetite A was coarser than the other materials. The results were also dependent on the original TiO_2-content. The added rutile was not fully reacted and relict minerals were found in SEM-EDS-analysis of the sintered pellets. The effect of TiO_2 is even stronger therefore than the results presented according to this study.

$CaCO_3$ addition increased pellet porosity due to being calcinated to CaO. The increased CaO content also caused the formation of large characteristically shaped hematite crystals as can be seen in **Figure 7**. Molten phase formed during the sintering stage increased diffusion. This characteristically shaped hematite crystal structure is very detrimental to the pellets, especially if the surrounding structure is dense or glassy. The glassy phase disintegrated dramatically during the LTD-test due to the expansion of hematite inside the structure. The glassy phase [composition close to Iron-Calcium-Olivine, $2(Fe,Ca)O \cdot SiO_2$)] included a quite high content of TiO_2, but the LTD was still insufficient because of formation of characteristic secondary crystals and a dense structure around them. The pellets with an LTD of 1-8 % are absolutely unsuitable for the blast furnace process.

In this study it was found that the LTD and the disintegration under real blast furnace conditions did not correspond to each other. The LTD-value of 61 % appears to be as good as a value of 92 %. It is widely recognized that pellets have more strength under BF-conditions than sinter and that the LTD-test is harder for the material. Therefore, the LTD value for pellets is not as critical as is RDI for sinter. The reactions are in any case faster under EBF-conditions and obviously the results of this study are not directly comparable with larger, production scale BF conditions. The residence time in the region where hematite is reduced to magnetite is shorter in the EBF and this residence time is very important to the disintegration. Additionally, worse reducibility in the case of samples including higher TiO_2-content enabled surface formation of wüstite and metallic iron before the material was reduced to magnetite in the core. It was also observed in laboratory scale reduction tests that TiO_2 seemed to stabilize and retard the hematite reduction at the beginning of the process, and also at low contents (Figures 4 and 5). In addition, the final degree of reduction to iron was lower with the sample containing 5 mass-% TiO_2 than with pure hematite and magnetite. Contrary to the RDI-reduction, the hematite samples reduced to metallic iron did not disintegrate. This phenomenon was assumed to be the consequence of metallic iron formation on the surface of briquettes and it is proposed that this prevents the degradation of the briquettes. In the laboratory reduction tests under RDI-conditions, TiO_2 caused changes in the reduction mechanism. In the test sample containing 5 mass-% TiO_2 the degree of reduction was interrupted at about 30 %, and the hematite reaction had penetrated at least three times deeper into the hematite sample. However, hematite relict phase occurred very close to the surface of the sample. It is suggested that the cause of this is disintegration of the structure and furthermore, formation of increased surface area contact between reduction gas and hematite. A consequence of this disintegration was the acceleration of the reduction after approximately the 20 minute reduction stage (Figure 4).

Conclusions

The increase in TiO_2-content of iron oxide agglomerates has a clear negative effect on their reduction degradation property. The value of sinter RDI is more significant than pellet LTD under real blast furnace conditions. The residence time for iron burden material in the magnetite facies zone is a critical factor. The magnetite facies is probably shorter in the case of the experimental blast furnace. Wüstite and metallic iron is formed on the surface before the pellet core is fully reduced to magnetite. The metallic iron prevents degradation and repairs the structure.

Two major occurrences can be said to strongly affect the quality of sinter and pellets:

- TiO_2-content of secondary hematite crystals → should be low.
- The amount and crystal size of secondary hematite → should be low/small.
- Structure morphology and porosity surrounding secondary hematite crystals, including structure → should not be dense or glassy.

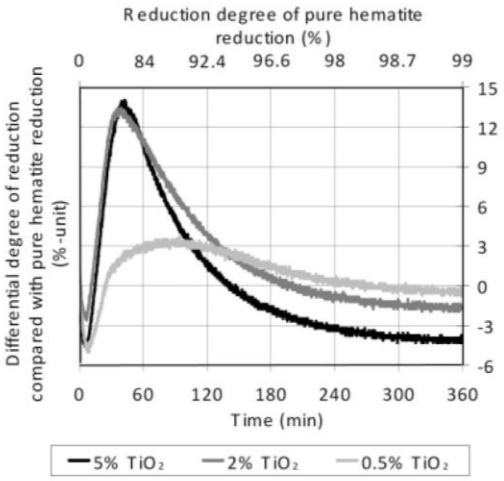

Figure 6. Effect of titaniumodioxide on reduction of hematite. The curves show the difference from the reduction curve of pure hematite. The grade of reduction for pure hematite can be read from the secondary x-axis at the top of the figure.

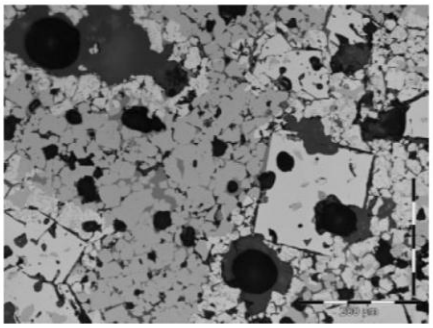

Figure 7. Detrimental structure of characteristically shaped hematite crystals found in the test pellets.

SUPPLEMENT V

PAANANEN, T & KINNUNEN, K: EFFECT OF TIO2-CONTENT ON REDUCTION OF IRON ORE AGGLOMERATES, STEEL RESEARCH INTERNATIONAL, 80(2009)6, PP. 408-414.

The TiO_2-content of sinter and pellets should be minimized in order to maximize the quality. The presence of glassy phase surrounding characteristically shaped hematite crystals is very detrimental to quality. The formation of glassy phase in pellets should be minimized.

Acknowledgement

The authors of this paper are grateful to LKAB for their support in allowing the basket trials to be carried out in the experimental blast furnace located in Luleå. The test pellets prepared are in no way connected with commercial pellets produced by LKAB.

References

[1] Panigrahy, S. C., Rigaud, M., Dilewijns, J.: Effect of MgO on low temperature reduction strength. Iron and Steel Int., 57 (1984), No. 1, 29 – 33.
[2] Mishra, U. N., Thakur, B., Mediratta, S. R.: Control of sinter quality for blast furnaces of SAIL through characterisation of high temperature properties. Ironmaking Conference Proceedings. Vol. 55; Pittsburgh, Pennsylvania; USA; 24-27 Mar. 1996. p. 407-412.
[3] Hsieh L.-H., Whiteman, J. A.: ISIJ Int., 33 (1993), No. 4, p. 462.
[4] Kinnunen, K., Heinänen, K.: The Reduction Degradation Property of Iron Ore Sinter at Raahe Steelworks. The 5th European Coke and Ironmaking Congress 2005, Proceedings, Vol. 2, p. Tu12:3 1-13.
[5] Kim, J.-R., Je, J.-H., Jeong, S.-K.: Behavior of reduction degradation of sintered ore by synchrotron X-rays. Iron & Steel Society International Technology Conference and Exposition 2003; Indianapolis, IN; USA; 27-30 Apr. 2003. p. 175-180.
[6] Pimenta, H. P., Seshadri, V., Cardoso, M. B., Azevedo, A. T.: Influence of Al_2O_3 and TiO_2 on the reduction degradation behaviour of sinter and hematite at low temperatures. 6th Int. Symposium on Agglomeration; Nagoya; Japan; 15-17 Nov. 1993. p. 332-337.
[7] Paananen, T., Kinnunen, K.: The Effect of Titanium on Reduction Degradation of Iron Ore Agglomerates, Iron Ore Conference 2007, Perth, WA, 20 – 22 August, 2007, p. 361 - 368.
[8] Pimenta, H. P., Seshadri, V.: Ironmaking Steelmaking, 29 (2002), No. 3, 175-179.
[9] Loo, C. E., Bristow, N. J.: 1993. Resistibility of iron ore sinters to low-temperature reduction degradation. 6th Int. Symposium on Agglomeration; Nagoya; Japan; 15-17 Nov. 1993. p. 338-343.
[10] Bristow, N. J., Loo, C. E.: ISIJ Int., 32 (1992), No. 7, 819-828.
[11] Yang, L. X., Matthews, E.: ISIJ Int., 37(1997), No. 11, 1057-1065.
[12] Chaigneau, R.; Sportel, H.; Trouw, J.; Vos, R.; Droog, J.: Ironmaking Steelmaking, 24 (1997), No. 6, 461-467.
[13] Srinivas, D; Devi, T. Uma; Prabhu, M.; Gupta, S. S.: Transactions of the Indian Institute of Metals. 57 (2004), No. 5, p. A4.
[14] Dwarapudi, S.; Gupta, P. K.; Gupta, S. S.: Ironmaking Steelmaking, 33 (2006), No. 6, 500-506.
[15] Botelho, M. E. E.; Da Costa, M. L.: Effect of some process parameters on low temperature degradation (RDI) of blast furnace pellets. III Simposio Brasileiro de Minerio de Ferro; Ouro Preto, MG; Brasil; 25-18 Nov. 2001. p, 298 - 306.
[16] Matsuno, F.; Nishikida, S.-I.; Ikeasaki, H: Transactions of the Iron and Steel Institute of Japan, 24 (1984), No. 12, 1040-1048.

SUPPLEMENT VI

Tanskanen P, Kinnunen K & Paananen T: SIGNIFICANT MINERALOGICAL DIFFERENCES BETWEEN BASIC TEST AND PRODUCTION IRON ORE SINTERS WITH EQUAL CHEMICAL COMPOSITION, Molten slags fluxes and salts, Santiago 2009, pp. 947 - 956.

SUPPLEMENT VI

TANSKANEN P, KINNUNEN K & PAANANEN T: SIGNIFICANT MINERALOGICAL DIFFERENCES BETWEEN BASIC TEST AND PRODUCTION IRON ORE SINTERS WITH EQUAL CHEMICAL COMPOSITION, MOLTEN SLAGS FLUXES AND SALTS, SANTIAGO 2009, PP. 947 - 956.

SIGNIFICANT MINERALOGICAL DIFFERENCES BETWEEN BASIC TEST AND PRODUCTION IRON ORE SINTERS WITH EQUAL CHEMICAL COMPOSITION

Pekka Tanskanen
University of Oulu, Finland

Kimmo Kinnunen & Timo Paananen
Ruukki Production, Finland

ABSTRACT

Mineralogical characterization for two ultra basic production sinter-test sinter pairs was made using optical microscopy and scanning electron microscopy. Basicities (CaO/SiO_2) of the sinter pairs were 2.1 and 2.3 respectively. Despite of the equal composition, the mineralogy and microstructure of the corresponding test and production sinters were significantly different.

The production sinters were composed mainly of fine-grained equigranular matrix rich in newly formed magnetite. Sporadically, some coarse magnetite or olivine relicts created a porphyritic-like structure. The matrix magnetite was clearly the primarily crystallized phase with interstitial vitreous slag, SFCA phase, dicalcium silicate, siliceous dicalcium titanoferrite, tertiary hematite and/or hematite-dicalcium silicate intergrowths.

The test sinters were characterized by a porphyritic-like structure with a great amount of relatively coarse magnetite and olivine relicts in a newly formed fine-grained matrix having hemicalcium ferrite as the primary phase. The interstices between the columnar hemicalcium ferrite grains were typically filled with calcium ferrite-dicalcium silicate micro-intergrowths and slightly coarse-grained droplet-like siliceous dicalcium titanoferrite grains. In places the micro-intergrowths were missing and the matrix was composed of randomly oriented acicular hemicalcium ferrite, siliceous dicalcium titanoferrite, and dicalcium silicate. Magnetite and vitreous slag did not typically exist in the test sinter matrix.

Both sinter types contained some secondary hematite existing mainly in the zone around the partially hematitized magnetite relicts.

It is proposed that the main reason for the mineralogical difference is the different melting or reaction degree originating from the difference in the sintering temperatures between the pot and production sintering processes.

SUPPLEMENT VI

TANSKANEN P, KINNUNEN K & PAANANEN T: SIGNIFICANT MINERALOGICAL DIFFERENCES BETWEEN BASIC TEST AND PRODUCTION IRON ORE SINTERS WITH EQUAL CHEMICAL COMPOSITION, MOLTEN SLAGS FLUXES AND SALTS, SANTIAGO 2009, PP. 947 - 956.

INTRODUCTION

Pot sintering is not a standardized test, but it is widely used worldwide to investigate the fundamental phenomena and to test the sintering characteristics of different iron ore blends prior to full scale plant trials and plant production. As studied elsewhere in detail, the test sintering is a very sensitive method for changes in the process conditions and properties of the sinter blend materials [4, 5, 6].

At the Ruukki Production, the produced test sinter is put into different mineralogical and metallurgical tests. Estimations are made about the behaviour of the sinter mix in real sintering process and quality of the sinter and its behaviour in the blast furnace [3].

The quality of sinter is mainly governed by the structure and phase composition of the agglomerate [1, 7]. In principle, most, if not all of the properties of sinter are straightly related to the structure and mineralogy of the agglomerate. However, the sinters are typically very heterogeneous materials in macro- and micro-scale and this connection is very difficult to find out and even more difficult to prove.

Ruukki Production has developed a constant pot sintering procedure, which produces test sinters having quite well the same RDI (Reduction degradation index) values as the production sinters made from the same blend. This is basically quite astonishing, because of the known differences between the condition of the test and production sintering.

The following results were made during a co-operation project between Ruukki Production and Laboratory of Process Metallurgy, University of Oulu. The project aimed to stabilize the blast furnace operation by decreasing the quality variations of the sinter.

METHODOLOGY

Sample materials and Research Methods

The test sinters were produced according to constant pot sintering route of the Ruukki Production [3]. The sinter was screened and the fines were returned into repeated sintering until the ratio between the produced and returned sinter fines was from 0.95 and 1.05. Coke breeze was used to adjust the ratio.

The production sinter samples from Dwight-Lloyd type sinter plant of the Ruukki Production were collected using automatic sampling equipment. The same ratio between the produced and returned sinter fines was used for the sinter optimization.

The reduction degradation tests were done according to international standard (ISO 4696-1)

Polished samples from the test and production sinters were made in the mineralogical laboratory of Ruukki Production. The polished sections from the sinter samples were examined optically with Olympus BX51 polarized microscope. Compositions of the different phases were assayed with a JEOL JSM-6400 scanning electron microscope using energy dispersive spectrometry. An accelerating voltage of 15 kV and a beam current of 120 nA were used. Oxford Instruments Inca 3.03 software was used for the evaluation of the analyses.

SUPPLEMENT VI

TANSKANEN P, KINNUNEN K & PAANANEN T: SIGNIFICANT MINERALOGICAL DIFFERENCES BETWEEN BASIC TEST AND PRODUCTION IRON ORE SINTERS WITH EQUAL CHEMICAL COMPOSITION, MOLTEN SLAGS FLUXES AND SALTS, SANTIAGO 2009, PP. 947 - 956.

RESULTS AND DISCUSSION

Sample Composition and Test Results

Chemical compositions and some test data for the test sinters and production sinters are seen in Table 1. The compositions are quite close to the targeted basicity values (B2) of 2.1 and 2.3, and the Fe content and MgO-contents of 61.5% and 2.1%, respectively.

The image analysis revealed that the phase composition of the production and test sinters were very different. The production sinters were higher in magnetite (MA) and lower in hematite (HE) than the test sinters (See Table 1). The difference in FeO content (titrated analysis) is also an indication of this. The actual content of calcium ferrites (CF) is somewhat uncertain, due to the difficulties to distinguish different calcium ferrites from magnetite. Both the glass phase and the crystals of silicate phases (olivine relicts) are classified as part of the vitreous slag (VS).

Table 1: Composition and test data for test sinters (TS1 and TS2) and production sinters (PS1 and PS2)

Sample	Fe	CaO	SiO_2	MgO	Al_2O_3	Ti	FeO	B_2	RDI	CF	HE	MA	VS
TS1	60,28	7,55	3,57	2,08	0,58	0,23	5,20	2,11	21,7	18,8	31,1	38,8	11,3
TS2	60,43	7,62	3,24	2,15	0,54	0,23	6,00	2,35	18,6	21,2	30,0	37,2	11,7
PS1	60,44	7,45	3,40	1,99	0,59	0,25	10,87	2,09	20,7	15,9	18,7	53,6	11,9
PS2	61,04	7,16	2,97	1,72	0,57	0,27	10,95	2,30	21,6	19,2	16,9	49,9	14,0

The measured RDI values of the test and production sinters were quite low and indicated good behaviour in the blast furnace.

Mineralogy and Structure

Production Sinters

The production sinters were highly magnetite dominated. The total magnetite content was at least 50-60%. Most of the sinter fragments (Figure 1) consisted of newly formed, fine grain granular magnetite (Ma, light grey) matrix with interstitial minor phases (darker areas). Some coarse grain magnetite relicts (Figure 2), partially oxidized to hematite (He, white), occurred sporadically making the structure look porphyritic-like. Proportion of the relicts in the production sinter was about 20%. At the reaction zone between the magnetite relicts and magnetite rich matrix, hybidiomorphic secondary hematite grains were identified.

SUPPLEMENT VI

TANSKANEN P, KINNUNEN K & PAANANEN T: SIGNIFICANT MINERALOGICAL DIFFERENCES BETWEEN BASIC TEST AND PRODUCTION IRON ORE SINTERS WITH EQUAL CHEMICAL COMPOSITION, MOLTEN SLAGS FLUXES AND SALTS, SANTIAGO 2009, PP. 947 - 956.

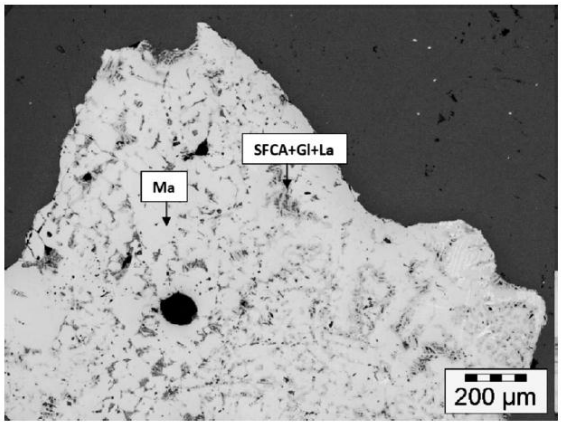

Figure 1: Typical equigranular-like structure of production sinter

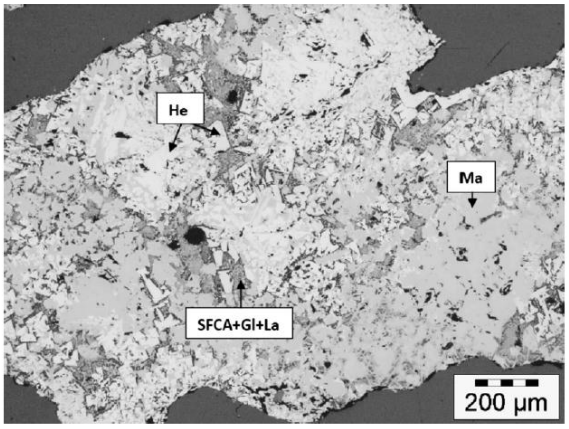

Figure 2: Typical porphyritic-like structure of production sinter

Closer look into the matrix interstices revealed the existence of two kinds of main phase associations. In the first one (Figure 3), matrix magnetite (Ma, light grey) was surrounded by SFCA phase (SFCA,medium grey, columnar) with intervening glass phase (Gl, dark grey, smooth) and dicalcium silicate (La, dark grey, granular). In some cases a few grains of siliceous dicalcium titanoferrite (not seen in Figure 3) was also detected.

The second association (Figure 4) consisted of magnetite with interstitial ternary hematite (He, white), existing mainly as dendritic crystals and as micro-intergrowths with dicalcium silicate. Some glass phase and a few grains of the siliceous dicalcium titanoferrite (DCTif, medium gray, a few grains around the glass phase in the central part of the photo) were typically present.

Variations in phase proportions and mixing and gradation of the types into each other were not rare.

SUPPLEMENT VI

TANSKANEN P, KINNUNEN K & PAANANEN T: SIGNIFICANT MINERALOGICAL DIFFERENCES BETWEEN BASIC TEST AND PRODUCTION IRON ORE SINTERS WITH EQUAL CHEMICAL COMPOSITION, MOLTEN SLAGS FLUXES AND SALTS, SANTIAGO 2009, PP. 947 - 956.

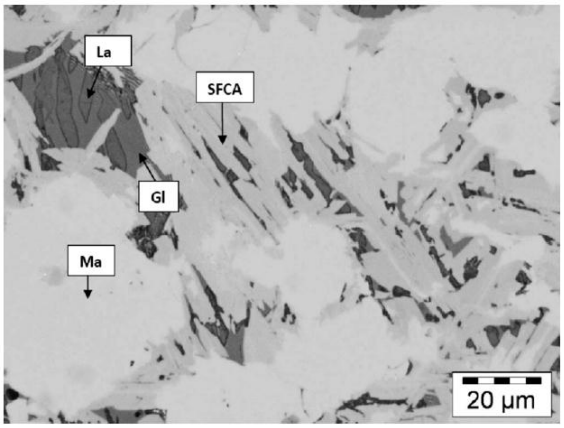

Figure 3: Typical phase association of the production sinter

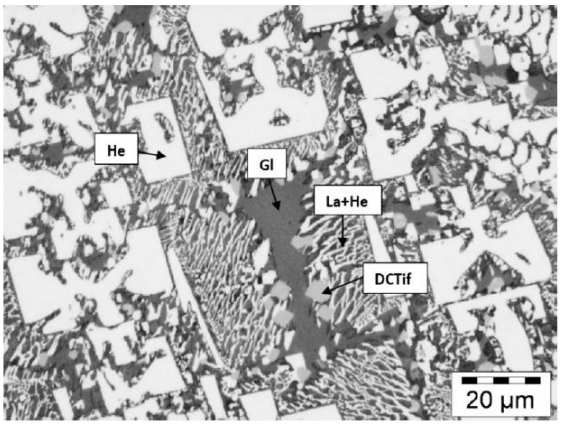

Figure 4: Typical interstitial phase association of the production sinter

Test Sinters

The test sinters were totally different from the production sinters. Most of the test sinter fragments were very distinctively characterized by a porphyritic-like structure (Figures 5 and 6). The relatively coarse grain magnetite and occasional olivine relicts, making up about 50% of the sinter, were surrounded by newly formed fine grain hemicalcium ferrite rich matrix. Oxidation of the magnetite relicts to hematite was generally more pronounced than in the production sinters.

At the contact zone between the magnetite relicts and matrix, idiomorphic secondary hematite was observed.

With very few exceptions, magnetite and vitreous slag were absent from the test sinter matrix.

SUPPLEMENT VI

TANSKANEN P, KINNUNEN K & PAANANEN T: SIGNIFICANT MINERALOGICAL DIFFERENCES BETWEEN BASIC TEST AND PRODUCTION IRON ORE SINTERS WITH EQUAL CHEMICAL COMPOSITION, MOLTEN SLAGS FLUXES AND SALTS, SANTIAGO 2009, PP. 947 - 956.

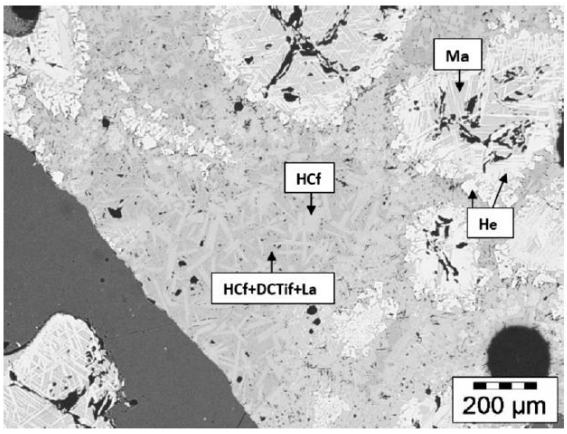

Figure 5: Typical structure of the test sinters

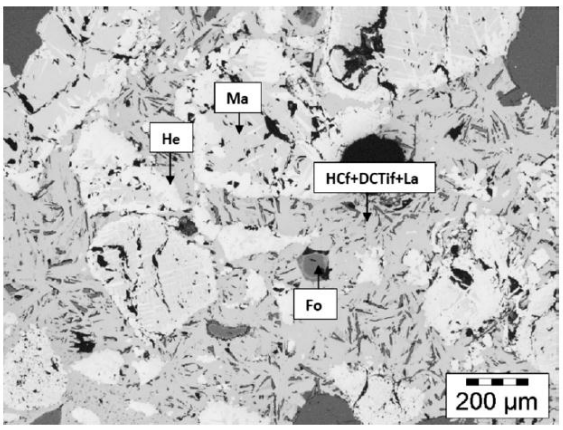

Figure 6: Typical structure of the test sinters

The test sinter matrix had two main phase associations characterized by specific microstructures. In most sinter fragments, the matrix was characterized by randomly oriented columnar hemi-calcium ferrite (Figure 7). Between the hemicalcium ferrite columns (HCf, light grey) existed allotriomorphic droplet-like grains of siliceous dicalcium titanoferrite (DCTif, medium grey) and very fine grain intergrowth of dicalcium silicate and some form of calcium ferrites (almost white with darker spots), probably the hemicalcium ferrite.

The second type of the matrix (Figure 8) was characterized and dominated by randomly oriented acicular to columnar hemicalcium ferrite (HCf, ligh grey), long-shaped dicalcium silicate grains (La, dark grey) and allotriomorphic siliceous dicalcium titanoferrite (medium grey). Grain size of the phases was quite alike. Amount of the dicalcium silicate and dicalcium ferrite phase was low in places.

Variations in phase proportions of the main types and mixing and gradation of the types into each other were not rare.

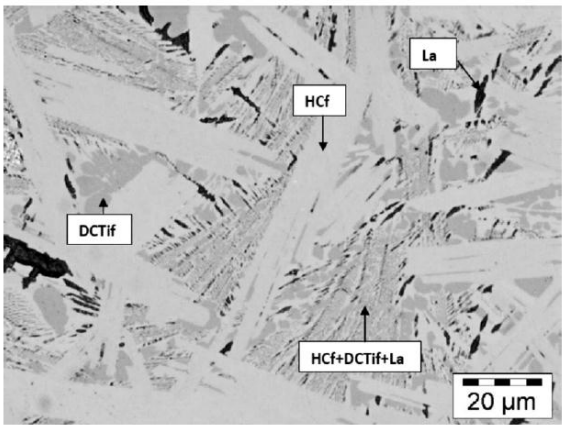

Figure 7: A typical phase association of the test sinter matrix

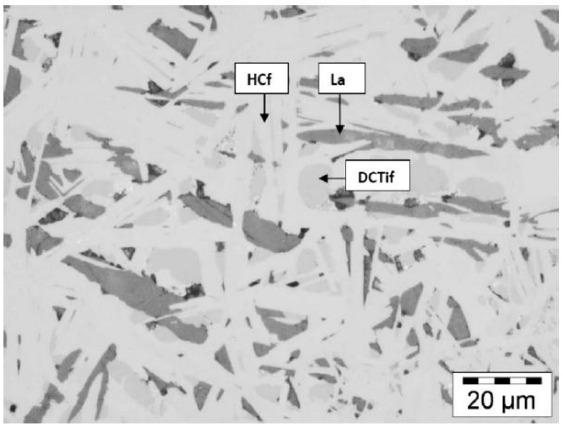

Figure 8: Another typical phase association of the test sinter matrix

Optical microscopy revealed the differences between the production and test sinters. It seems most obvious, that the main reason for the difference in the mineralogy and structure was the sintering temperature. The lower sintering temperature in the pot sintering process created a lower reacting and melting degree for the material. Because about half of the magnetite grains were not involved in the reactions, the reacting material was lower in Fe and higher in CaO and SiO_2. This caused that primary crystallization started from the hemicalcium ferrite phase field instead of the magnetite field of the Fe-richer system taking part in the sintering reactions in the production sinter.

Mineral Chemistry

Typical chemical compositions of the production and test sinter phases are presented in Tables 2 and 3 respectively. Numbers of the first column in Table 2 refers to phases: magnetite/matrix (1 and 2), magnetite/relict (3), olivine/relict (4), hematite/secondary (5), hematite/ternary (6), dicalcium silicate (7), siliceous dicalcium titanoferrite (8 and 9), vitreous slag (10), and SFCA phase (11). In Table 3 the numbers refer to phases: hemicalcium ferrite (1 and 2), magnetite/relict (3), olivine/relict (4), hematite/secondary (5), dicalcium silicate (6), siliceous dicalcium titanoferrite (7 and 8). All Fe is calculated as total FeO (FeO_t).

SUPPLEMENT VI

TANSKANEN P, KINNUNEN K & PAANANEN T: SIGNIFICANT MINERALOGICAL DIFFERENCES BETWEEN BASIC TEST AND PRODUCTION IRON ORE SINTERS WITH EQUAL CHEMICAL COMPOSITION, MOLTEN SLAGS FLUXES AND SALTS, SANTIAGO 2009, PP. 947 - 956.

In general, magnetite and olivine relicts of different sister types were quite comparable in chemical composition. The same was true for the hematite oxidation lamellas, secondary hematite grains and dicalcium silicate. The matrix magnetite of the production sinters had always clearly increased CaO and MgO contents.

Table 2: Typical chemical compositions of the phases existing in the test sinters

No.	MgO	Al_2O_3	SiO_2	CaO	TiO_2	V_2O_5	MnO	FeO_t
1	5,52	0,00	0,00	3,57	0,00	0,00	1,08	77,21
2	1,92	0,00	0,00	2,12	0,00	0,00	0,00	85,01
3	0,00	0,00	0,00	0,00	0,00	0,00	0,00	85,08
4	47,60	0,00	39,01	0,00	0,00	0,00	0,00	8,72
5	0,00	0,78	0,00	0,97	1,68	0,00	0,00	83,57
6	0,00	0,70	0,00	1,51	2,07	0,00	0,00	79,21
7	0,00	0,00	31,63	62,17	0,00	2,08	0,00	1,93
8	0,00	0,44	10,03	40,88	23,18	0,00	0,00	18,13
9	0,00	0,00	10,57	41,46	6,29	1,06	0,00	30,73
10	0,00	0,53	30,94	39,68	5,01	5,45	0,00	10,32
11	0,00	2,21	7,62	16,35	1,68	0,00	0,00	62,59

Table 3: Typical chemical compositions of the phases existing in the test sinters

No.	MgO	Al_2O_3	SiO_2	CaO	TiO_2	V_2O_5	MnO	FeO_t
1	0,00	0,93	1,94	14,55	0,00	0,00	0,00	70,16
2	1,50	0,53	0,00	9,75	0,00	0,00	0,00	75,52
3	0,00	0,39	0,00	0,00	0,00	0,00	0,00	87,28
4	50,64	0,00	40,11	0,00	0,00	0,00	0,00	7,62
5	0,00	0,53	0,00	0,43	0,50	0,00	0,00	84,37
6	0,00	0,00	30,63	59,84	0,00	1,81	0,00	1,97
7	0,00	0,56	8,75	40,13	11,01	0,00	0,00	31,01
8	0,00	0,00	10,11	39,60	1,73	0,81	0,00	38,04

Composition of the calcium ferrites of the production sinters and test sinters are compared in Figure 9. Although there was some overlapping in the compositions, production sinters usually contained the higher SiO_2 containing SFCA phase. In the test sinters the calcium ferrite was typically a hemicalcium ferrite with lower SiO_2 content.

Composition of the siliceous dicalcium titanoferrite is clarified on the basis of 92 SEM assays in Figure 10. This phase had quite stable CaO and SiO_2 contents and variable TiO_2 and FeO contents. TiO_2 content in the production and test sinters varied from 6.3% to 23.2 % and from 1.6% to 11.0% respectively. It was obvious, that Ti is replacing Fe in the siliceous dicalcium titanoferrite structure. Despite of numerous mineralogical characterizations made for different test and production sinters [1, 2, 3, 7], this kind of siliceous dicalcium titanoferrite has not been reported earlier for iron ore sinters.

SUPPLEMENT VI

TANSKANEN P, KINNUNEN K & PAANANEN T: SIGNIFICANT MINERALOGICAL DIFFERENCES BETWEEN BASIC TEST AND PRODUCTION IRON ORE SINTERS WITH EQUAL CHEMICAL COMPOSITION, MOLTEN SLAGS FLUXES AND SALTS, SANTIAGO 2009, PP. 947 - 956.

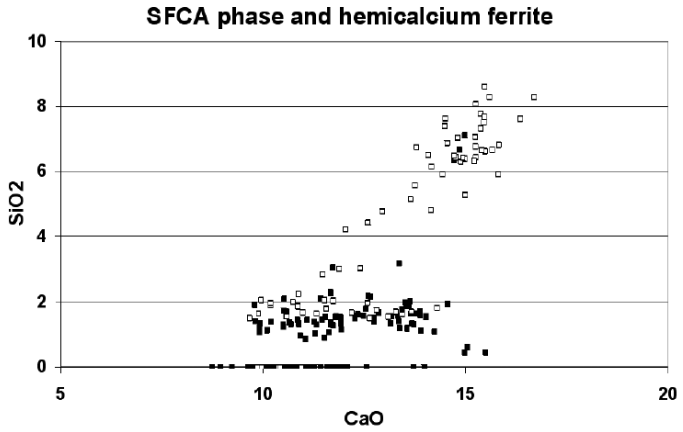

Figure 9: Composition variation of the SFCA phase and hemicalcium ferrite from production sinters (black open squares) and test sinters (black full squares). Scales are in oxide w-%

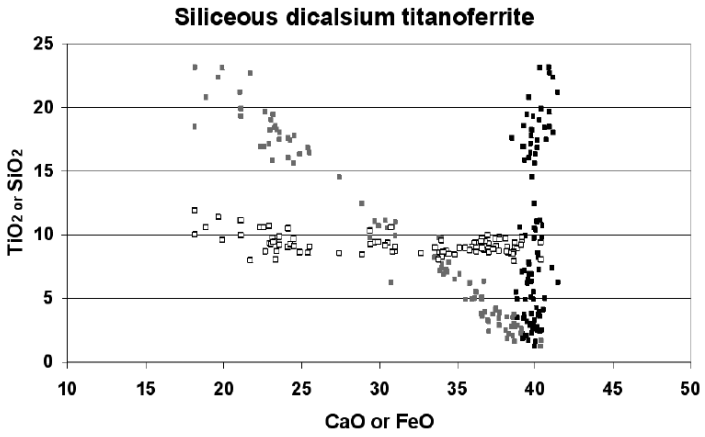

Figure 10: Composition variation of the siliceous dicalcium titanoferrite expressed as CaO vs. TiO_2 (black full squares), FeO vs. SiO_2 (black open squares), and FeO vs. TiO_2 (full gray squeres). Scales are in oxide w-%

Part of the variation in the composition is analytical error due to the very fine grain size of the phase, especially in the case of the production sinters. This generates increased variation in the CaO and SiO_2 content especially for the high TiO_2 (low FeO) compositions.

CONCLUSIONS

RDI values of test sinters made using a pot sintering equipment has been observed to predict quite well the RDI values of the production sinter made from the same mix. Mineralogy and structure of the test sinter-production sinter pairs with basicity of 2.1 and 2.3 was made using optical and scanning electron microscopy.

Results revealed that mineralogy and texture of the test and production sinter made from mix was totally different. The structure and phase composition of the production sinters were dominated by newly formed magnetite matrix with some magnetite relicts, while in the test sinters were dominated by hemicalcium ferrite rich matrix with a great amount of magnetite relicts. In both sinters a new type of dicalcium ferrites was

identified. It was a siliceous dicalcium titanoferrite with constant SiO_2 and CaO contents and varied TiO_2 contents up to 23%.

It is proposed that the reason for the mineralogical difference is the different melting or reaction degree of the production and test sinters, in turn caused by differences in the sintering temperature between the pot and production sintering processes.

ACKNOWLEDGEMENTS

The results reported in this paper were obtained in a research project: Stabilized iron making production - Control and optimization of efficiency and energy consumption by burden material. Rautaruukki Oyj, Ruukki Production and Finnish Technological Agency, Tekes are acknowledged for financing the project. Ruukki Production also enabled the research by making and delivering the research samples. We thank Ph.D Kyösti Heinänen for many scientific discussions and guidance.

REFERENCES

Chaigneau, R. (1994). *Complex Calcium Ferrites in the Blast Furnace Process*. Ph.D. Thesis, Delft University of Technology, The Netherlands. p. 120. [1]

Heinänen, K. (1993). *Mineralogy and Metallurgical Properties of Iron Ore Sinters Based on Magnetite Fines*. Ph.D. Thesis, University of Helsinki, Helsinki, Finland. p. 114. [2]

Hooey, P. L. (1999). *Reduction and High Temperature Behaviour of Iron Ore Sinter Made From Magnetite Fines*. Ph. D. Thesis, University of Oulu, Department of Process and Environmental Engineering, Oulu, Finland. p. 93. [3]

Hsieh, L. H. & Whiteman, J. A. (1989). *Sintering Conditions for Simulating Formation of Mineral Phases in the Industrial lron Ore Sinter*. ISIJ Int., 29, pp. 24-32. [4]

Loo, C. E. & Wong, D. J. (2005). *Fundamental Factors Determining Laboratory Sintering Result*. ISIJ International, 45(4), pp. 449-458. [5]

Lu, L. & Holmes, R. J. (2008). *CSIRO Pilot-scale Sintering Facility and Important Factors Influencing the Sintering Performance of Iron ore Blends*. Proceedings of the Scanmet III, The 3rd International Conference on Process Development in Iron and Steelmaking, 8-11 June, Luleå, Sweden. pp. 87-96. [6]

Pimenta, H. P. & Seshadri, V. (2002). *Characterisation of Structure of Iron Ore Sinter and its Behaviour during Reduction at Low Temperatures*. Ironmaking Steelmaking, 29 (3), pp. 169-174. [7]

ISBN 978-952-93-1814-8 (nid.)

ISBN 978-952-93-1815-5 (PDF)

Printed by Erweko Oy

OULU 2013